Lawrence Berkeley National Laboratory

Recent Work

Title

Microstructual and Phase Stability Studies of Nanometer Period Metal/Carbon Multilayer Stuctures for X-Ray Optics

Permalink

https://escholarship.org/uc/item/0x48k2m9

Author

Nguyen, T.D.

Publication Date

1990-05-01

eScholarship.org Powered by the California Digital Library
University of California

LBL-29206

Lawrence Berkeley Laboratory

UNIVERSITY OF CALIFORNIA

Accelerator & Fusion Research Division

Microstructural and Phase Stability Studies of Nanometer Period Metal/Carbon Multilayer Structures for X-Ray Optics

T.D. Nguyen
(M.S. Thesis)

May 1990

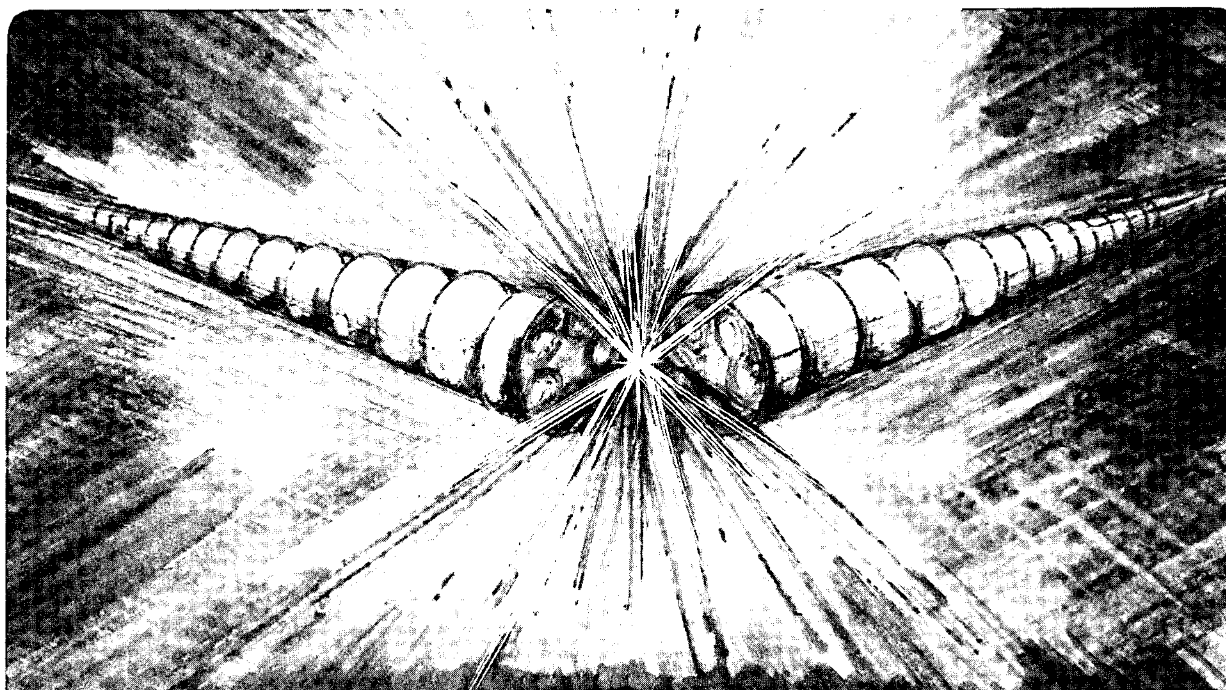

LOAN COPY
Circulates
for 2 weeks
Bldg. 50 Library.
LBL-29206
Copy 2

Prepared for the U.S. Department of Energy under Contract Number DE-AC03-76SF00098.

DISCLAIMER

This document was prepared as an account of work sponsored by the United States Government. While this document is believed to contain correct information, neither the United States Government nor any agency thereof, nor the Regents of the University of California, nor any of their employees, makes any warranty, express or implied, or assumes any legal responsibility for the accuracy, completeness, or usefulness of any information, apparatus, product, or process disclosed, or represents that its use would not infringe privately owned rights. Reference herein to any specific commercial product, process, or service by its trade name, trademark, manufacturer, or otherwise, does not necessarily constitute or imply its endorsement, recommendation, or favoring by the United States Government or any agency thereof, or the Regents of the University of California. The views and opinions of authors expressed herein do not necessarily state or reflect those of the United States Government or any agency thereof or the Regents of the University of California.

MICROSTRUCTURAL AND PHASE STABILITY STUDIES OF NANOMETER PERIOD METAL/CARBON MULTILAYER STRUCTURES FOR X-RAY OPTICS

By

Tai D. Nguyen
(M.S. Thesis)

Department of Materials Science and Mineral Engineering
University of California at Berkeley

and

Center for X-Ray Optics
Accelerator and Fusion Research Division
Lawrence Berkeley Laboratory
Berkeley, California 94720

May 1990

This work was supported by the Director, Office of Energy Research, Office of Basic Sciences, Materials Sciences Division, of the U.S. Department of Energy under Contract No. DE-AC03-76SF00098 and by the Air Force Office of Scientific Research, of the U.S. Department of Defense under Contract No. F49620-87-K-0001.

Microstructural and Phase Stability Studies of Nanometer Period Metal/Carbon Multilayer Structures for X-Ray Optics

by

Tai D. Nguyen

ABSTRACT

Multilayer structures of W/C, WC/C, and Ru/C, of various periods were prepared by magnetron sputtering and studied by x-ray diffraction and high-resolution transmission electron microscopy. Studies of microstructures and phases present inside the layers, interfaces, and stability of layered structures and period, of both as-prepared and annealed samples were made. Both as-prepared and annealed WC/C multilayers are predominantly amorphous, while the phases in the W/C depend on the periods. The 2 nm period W/C multilayer remains amorphous after annealing, and the longer periods recrystallize to form W_2C. The layered structures of both W/C and WC/C systems are stable on annealing for periods equal to or larger than 2 nm, while the amorphous Ru-rich layers in the 2 nm period Ru/C multilayer agglomerate upon annealing to form elemental Ru crystallites. Annealing of 1 nm period W/C multilayer also leads to destruction of the layered structures. Longer period Ru/C multilayers show stable layered structures on annealing, and indicate elemental Ru in the Ru-rich layers. Crystalline planes extending into the amorphous layers and grain boundaries in the crystalline layers roughens the interfaces. X-ray measurements show that the multilayer periods expand on annealing for all metal/C multilayers studied. Mechanisms for this expansion is not known, although it seems to be linked to the amorphous C-rich layers.

TABLE OF CONTENTS

I. INTRODUCTION 1

I.1 Motivation 1

I.2 Goals 2

II. REVIEW OF LITERATURE ON METAL/C MULTILAYERS 4

III. EXPERIMENTAL TECHNIQUES 7

III.1 Multilayer Fabrication 7

III.2 Annealing conditions 8

III.3 X-ray diffraction 8

III.4 Electron Microscopy: 9

III.4.1 Specimen preparation: 9

III.4.1.a Cross-sectional samples 9

III.4.1.b Plan-view samples 12

III.4.2 Transmission Electron Microscopy 13

III.4.3 Image Interpretation 13

IV. RESULTS 15

IV.1 Absolute reflectance: 15

IV.1.1 Expansion of period on annealing 15

IV.1.2 Substrate dependence 16

IV.1.3 Comparison between W/C and WC/C multilayers 16

IV.2 Transmission Electron Microscopy: 17

IV.2.1 W/C system 17

IV.2.2 WC/C system 21

IV.2.3 Ru/C system 21

V. DISCUSSIONS 25

V.1 Microstructures and phases: 25

V.1.1 W/C and WC/C systems 25

V.1.2 Ru/C system 31

V.2 Layer uniformity 32

V.3 Structures and roughness at interfaces 34

V.4 Layered structure stabiltity on annealing 38

V.5 Expansion of multilayer period on annealing 39

VI. SUMMARY AND CONCLUSIONS 42

VII. SUGGESTIONS FOR FURTHER STUDIES 44

VIII. ACKNOWLEDGEMENTS 46

IX. REFERENCES 47

X. TABLES 50

XI. FIGURE CAPTIONS 53

XII. FIGURES 56

I. INTRODUCTION

Certain nanometer period multilayer structures of alternating layers of high and low Z materials have proved to be effective dispersing elements at wavelengths ranging from extreme-ultraviolet to x-ray regions. These structures have been applied in many applications such as x-ray spectroscopy, imaging, laser and synchrotron radiation research.[1] Many other uses of multilayer structures, and their interests, were discussed extensively at a conference on applications of thin-film multilayer structures to figured x-ray optics.[2]

Multilayer structures with appropriate periods have been found to provide highest normal reflectivity in the ultraviolet and extreme-ultraviolet regions of the spectrum. They also have demonstrated many advantages over other means of obtaining high reflectivity. As compared to total reflection, multilayers offer the advantage of reflectance at angles closer to the optic axis. This is a great advantage since geometrical aberrations, which are strong function of angle from the optic axis, are significantly reduced, as the incidence angles approach the normal of the plane, thus provides better point to point resolution in microscopy applications. In addition to improved imaging capabilities, they offer larger collection angles and modest bandpass selectivity. In addition, multilayers can be fabricated onto curved surfaces for many interesting x-ray experiments.

I.1 Motivation

Multilayer structures must show high stabilities over time and under intense radiation in practical applications. These requirements have prompted the studies of the multilayer stability upon thermal annealing,

similar to the conditions that the multilayers are subjected to intense radiation. Recent studies of the materials science aspects of multilayer structures may help to achieve higher reflectivity and better stability of these multilayers. In general, the efficiency of the multilayers depends on a choice of materials that have sufficiently different x-ray scattering powers, on the number of bilayer periods, and on the relative thicknesses of the component layers in a period. Uniformity of the layers and the sharpness of their interfaces are additional criteria for high performance and order control. Localized microstructures and second phases present in the layers, and their transformations after thermal or radiation loadings, have also been found to be important characteristics of the structure stability.

Studies of the layered microstructures, their phases, and their stability during annealing, may lead to more complete understanding of the multilayer systems. It is this understanding, from the materials scientists' important contributions in determination of the effects of interfacial structures, phase transformations, layer interdiffusion, and thermal stability, that enables the optical physicists to design better interference coatings for high performance x-ray optical applications.

I.2 Goals:

The goal of this work is to achieve a better understanding of the microstructures and phases present in the layers, the multilayer stability on annealing, and their relationships to the performance and quality of the multilayers.

A systematic and comparative study on the microstructures and the phases present for the layered structures of W/C, WC/C, and Ru/C multilayer

structures, using low-angle x-ray diffraction and High Resolution Transmission Electron Microscopy (HRTEM), is presented. The identification of the structures and phases inside the layers is determined by cross-sectional HRTEM, and by plan-view TEM of larger areas. The formation of new phases, uniformity of the layers, and stability of the layered structures, including the thickness of the multilayer period during annealing, are discussed. Some of these characteristics are found to affect significantly the quality and performance of the multilayer structures. The stability of the multilayers of various periods is studied upon annealing at 500°C for 4 hours.

Multilayer structures having W and C as their components were chosen because they were some of the first to demonstrate utility in x-ray optical applications. Observation of wide miscible gap between WC and C at low temperatures in the W-C phase diagram motivated the extension of the studies of W/C system to WC/C system. Ru/C multilayers were studied because of their potential applications as normal incident reflectors for soft x-rays with wavelengths between 4.5 and 12.5 nm, and because they have a phase diagram that is distinctly different from that of the W-C.

II. REVIEW OF LITERATURE ON METAL/C MULTILAYERS

A variety of multilayer structures of different combinations have been fabricated and characterized. The higher-Z materials in the x-ray optical multilayers are usually elemental W, Mo, a transition metal, or a metallic alloy, while the low-Z materials are often Si or C. Many techniques have been applied to characterize the multilayer structures. X-ray scattering[3-5] and Extended X-ray Absorption Fine Structure (EXAFS)[6-7] give information on the average interatomic structures within the layers and at their interfaces, and transmission electron microscopy (TEM)[8-14] reveals the quality of the layering and the localized nature of the phases within the layers.

Understanding of interdiffusion and reactions between the metals and the carbon, solid state amorphization or formation of crystalline metal carbides inside the layers is still not well established for any metal/carbon system. This lack of understanding is in part due to the absence of systematic and comparative studies of metal/carbon systems.

Most of the metal/carbon systems studied are those which have applications or potential applications in x-ray optics. The most extensively studied system is W/C, which was one of the first such system used to demonstrate the utility of multilayer structures as x-ray diffracting elements. Significant contrast in atomic numbers and scattering powers of W and C provide efficient x-ray dispersing elements, and their high melting points ensure high stability in power intensive applications. Significant differences in understanding the W/C system exist despite the fact that it is the most well studied multilayer system. In general, the C-rich layers in the W/C multilayers, as well as in other metal/carbon systems, are observed to have an amorphous structure. The structures of the W-rich layers have been observed

to range from amorphous, microcrystalline, to polycrystalline, of elemental W or tungsten carbide phases. The W-rich layers in the as-prepared multilayers are predominantly amorphous within short periods, and exhibit crystalline elemental W within longer periods.[3,13] It has been observed that they remain amorphous in multilayers of W-layer thickness up to 4 nm,[14] although microcrystalline WC has also been reported at above 1 nm W-layer thickness.[10] EXAFS studies reveal that the W in the W-rich layers are in a local environment of substantially rich carbon content, suggesting interdiffusion during deposition.[7] Evidence of intermixing of W and C in as-prepared amorphous W/C multilayers has also been reported.[3]

Moderate annealing of the multilayers leads to dramatic changes in the W-rich layer structures, while the layers still remain somewhat intact. Crystallization of the amorphous phase or recrystallization of the bcc W to form W_2C upon annealing has generally been observed,[3-4,7,13] while observation of crystalline W in a 3.2 nm W-layer thickness W/C multilayer after annealing at 770°C has also been reported.[8] Formation of the crystalline carbide phases during annealing seems to depend on the initial W layer thickness and the W to C layer thickness ratio.[4,6-7] Expansion of the multilayer periods after moderate annealing has also been reported for many metal/carbon systems, independent of crystallization of the initial W-rich layers. Lamble et al.,[6] however, reported a slight decrease in the period of the sample as a result of annealing.

The layers in the multilayers and their interfaces are more uniform and well defined at larger periods than at low periods. It has been proposed that the limit for the W layers to retain their continuity is approximately 1 nm.[15] In multilayers having a W-layer thickness of less than 1 nm, discontinuity of

the layers has been observed in the W-rich layers.[14] High-Resolution TEM (HRTEM) studies[13] however, have demonstrated that the layered structures remain continuous and quite uniform in a 2 nm period W/C multilayer, or effectively 0.8 nm nominal thickness of the W-rich layers, after annealing at 500°C for 4 hours.

The layer roughness in the as-prepared samples has been observed to decrease away from the substrates,[5,15-16] and amorphous carbon was proposed to be responsible for such smoothing of the layers.[15] The effect of intentional roughness on a GaAs substrate was removed after about 10 layers of the multilayer,[14] although it has also been reported that roughness in W/C increases with each successive layer away from substrate.[17]

Intermixing between the constituents in the layers at the interfaces has been observed in many metal/carbon systems, as well as in the W/C system. Data fitting of measured x-ray reflectance with calculated profiles indicated a mean interfacial roughness of 5 Å at each interface in the W/C system.[5] Ruterana et al.[14] suggested that amorphous layers have a lower interfacial roughness than crystalline layers which results in higher reflectivity. An observation of reduction of reflectivity by more than a factor of 10 after annealing at 400°C for 4 hours in Fe, Ni, Co/C multilayers was proposed to be associated with the roughening of the layer boundaries produced by the microcrystallites resulting from a transition from an amorphous to a polycrystalline state during annealing.[18] Peak reflectivity in Ru/C multilayers, which have mean roughness of 3.5 Å at the interfaces, in the same study, however, remained unchanged after annealing.

III. EXPERIMENTAL TECHNIQUES

III.1 Multilayer Fabrication:

Multilayers were prepared by DC magnetron sputtering at the Center for X-ray Optics. In this sputtering technique, the positions of the sources are fixed while the substrates are moving during deposition. The sources and their targets are mounted in the same radius as the circular path of the substrates. During deposition, the substrates rotate in turn over two elemental targets at substrate floating temperature. One multilayer period is deposited during one single revolution of the substrates. The substrate table is about 100 mm above the targets, and the argon sputter gas pressure is 0.002 torr.

Multilayers of different nominal periods were prepared for this study. Different thicknesses of the multilayer periods of the samples were controlled by keeping the target sputtering rates fixed and varying only the rotation velocity of the substrates. The nominal relative thicknesses of the metal-rich and the carbon-rich layers based on the sputtering rates of the individual targets, were the same for all the samples, such that the metal-rich layer would make up 40%, and the carbon-rich layer make up 60% of the period. This layer thickness percentile has been calculated to yield optimum reflection[19] and is typical of that in multilayers used in x-ray optical applications.

Multilayers were prepared on two types of substrates: 3-inch semiconductor-grade (111) Si wafers provide samples for cross-sectional TEM observation, and TEM copper grids provide samples for plan-view TEM characterization. In addition, some multilayers were also prepared on superpolished optical flat substrates for reflectivity measurements and x-ray diffraction studies. For each run, the substrates were first coated with an amorphous carbon buffer layer of approximately 10 nm. The multilayers were

then deposited to yield total multilayer thicknesses ranging from 150 to 350 nm. Each deposition run spans about 2.5 hours.

III.2 Annealing conditions:

One sample from each of the multilayers prepared was annealed in a tube furnace at 500°C for 4 hours in a vacuum of 10^{-6} torr. The vacuum system contains a mechanical roughing pump, and a turbo molecular pump that can provide a vacuum of 10^{-7} in the vacuum tube at room temperature. The samples were heated by an electric coil furnace, which was calibrated by a thermalcouple meter, and gives an accurate reading of ±10°C about 500°C. The samples were subsequently cooled under vacuum, and usually reach room temperature in about 4 hours.

III.3 X-ray diffraction:

X-ray measurements were used to determine the periodicity of the multilayers and the absolute reflectance profile. The low-angle region spanning the total reflection regime and the first few multilayer Bragg peaks were measured in a two crystal, Bragg geometry diffractometer utilizing Cu $K\alpha_1$ radiation with the multilayers in the position of the second crystal. During reflectance measurements, both the detector and the sample move in steps by motors, such that the detector moves twice as fast as the sample, to establish the θ - 2θ relationship. Absolute reflectance profiles were measured in step of 0.010° over durations of 30 seconds. Bragg peaks from the multilayers were used to determine the period of the multilayers, using Bragg's law $n\lambda = 2d \sin\theta$. A high number of Bragg peaks was measured to increase the accuracy of period determination.[20]

III.4 Electron Microscopy:

III.4.1 Specimen preparation:

III.4.1.a Cross-sectional samples:

As-prepared and annealed multilayer samples on Si substrates were prepared for cross-sectional TEM observation by the conventional mechanical thinning and ion beam milling technique.[21-24] The specimen preparation procedure follows from figure 1a). First, two slabs of the silicon substrate sample, 10 mm long by 3 mm wide, were cut, with the longer side of the slabs parallel to the flat edge of the Si wafer, using a diamond-ball pen. The orientation of the cut was chosen to yield the <110> direction parallel to the electron beam when viewed in the microscope. Next, the two slabs were glued together using Devon 2-ton epoxy, with the deposited films facing each other, as shown in figure 1b). This provides mutual protection for the multilayer thin films against breakage and fracture during thinning. The Devon 2-ton epoxy was then cured by thermosetting at a temperature of about 90°C for 30 minutes, or by remaining at room temperature over night.

The glued sample was then mechanically thinned using sandpaper on a rotating grinding wheel, and polished using alumina powder on polishing cloths. To start, the sandwiched sample was mounted on a 1 inch-diameter 5/8 inch-thick piece of Pyrex glass, using Crystal Bond 509 wax by Aremco Products, Inc. The glass piece, with a small volume of the Crystal Bond, was placed on top of a hot plate set at about 300°C. The wax usually melted within about 5 minutes. The sample was then carefully mounted on top of the glass, ensuring that the film surfaces were perpendicular to the surface of the glass, so that the sample was mechanically thinned perpendicular to the <110> direction.

The sample was first thinned using 600-grit paper (20µm silicon carbide particles) on a rotating grinding wheel, as illustrated in figure 1c). During grinding, ample water was made to run over the sandpaper so that the wax does not heat up and melt. The top surface of the sandwich-like sample was kept as parallel to the glass surface as possible. Throughout all the thinning and polishing steps, the motion of the sample relative to the paper was controlled to keep the movement parallel to the films or the interfaces, so that less fracture or artifacts formed due to mechanical stresses.

On one side, the sample was not thinned, but only ground and polished to a flat surface parallel to the glass surface. Leaving the sample thick at this point made for easier handling. A pre-polishing step was added to expedite the polishing procedure. In this step, the sample was polished by moving back and forth on 2400-grit paper (5 µm), with little distilled water to keep it cool. The polishing motion again was also parallel to the films or the interfaces. This step does not thin the sample as much as it smooths the surface before subsequent polishing. At this point, the surface was observed to have a specular finish. The sample was then polished using 1 µm alumina, and followed by 0.05 µm alumina, on a polishing cloth and rotating wheel (figure 1d)).

After polishing the first side, the sample was turned over, so that the polished side was facing toward the glass piece. Following the same steps as before, the unpolished side was thinned and polished, using 600-grit paper, 2400-grit paper, 1 µm alumina, and 0.05 µm alumina. However, the sample was now thinned to about 20 µm before being polished. Care was taken so that the sample was not broken or ground away since the sample becomes more fragile the more it is thinned. The use of a glass support for mechanical thinning

enabled the observation of the sample condition, e.g. its thickness, during the thinning operation. In general, the specimen was usually thinned until the edges start to regress. This was a sign that the specimen is ready for polishing.

Pre-polishing and polishing steps were carried out as before, but with even more care now that the specimen was extremely thin and delicate. The 20 μm-thick sample is next mounted on a TEM grid to be ion milled. The grids were cemented onto the sample to create a support for the sample before removing it from the glass base, for easy control and less chance of breakage during handling. Two small drops of the epoxy were placed on the sample at about the length of a grid apart, using a pointed wooden stick. The 0.5 mm-width oval-slot TEM grids were then placed on top of the thinned sample, such that the film surfaces or interfaces were parallel to the longer side of the slot, and the sample covered the entire slot, as shown in figure 1e). The epoxy was then cured at 90°C for 30 minutes, or over night at room temperature.

After curing, the specimens were separated by carefully using a pair of tweezers to break off excess sample around the 3 mm-diameter grids. Removal of the specimens from the glass base was done by placing it on a hot plate to soften the wax, sliding the sample grids in the direction parallel to the films until they overhang the glass base, removing them with tweezers, and soaking in warm acetone for about 15 minutes to remove the remaining wax.

The sample was ion-milled in a cold stage Gatan "Dual Ion Mill" Model 600, with argon ion guns bombarding on both sides of the specimen, schematically shown in figure 1f). The argon ions were first accelerated with a voltage of 5 kV, drawing a specimen current of 0.5 milliamps, at a specimen tilt angle of 13°, under 10^{-4} torr pressure during milling. By employing a laser auto-terminator, the specimen was left in the ion milling machine until

the ion source is automatically switched off when perforation was achieved. This usually took about 4 to 6 hours, depending on the final thickness of the sample and the lifetime of the ion guns. Once perforation was achieved, the sample was ion milled for about an hour more, with the tilt angle reduced to 11°, in order for the sample to have a shallower thickness gradient for TEM observation. After the ions created a hole along the epoxy about 1 mm long, as illustrated in figure 1g), it was exposed again to an ion beam of 3.0 kV potential, 0.3 milli-amp current, for another 15 to 30 minutes. This last step did not thin the sample any further but was used to remove any "overlayers" of damaged, amorphous material on the specimen which built up as a result of ion bombardment.

III.4.1.b Plan-view samples:

Multilayers were prepared for TEM plan-view observation to complement the cross-sectional studies. Figure 2 shows the steps in preparing plan-view samples for TEM observation.[25] The substrates on which the multilayers were grown consisted of 3 mm-diameter 300-mesh copper microscope grids, mounted on glass slide with Crystalbond vacuum adhesive, as shown in figure 2a). Multilayers were then deposited on the grids and the glass slide (figure 2b)). After a deposition of a few bilayers of the multilayers, to make up total multilayer thickness of about 30 nm, the glass slide holding the samples was soaked in acetone to dissolve the Crystalbond (figure 2c)), leaving the multilayer spanning the holes of the copper grids, as shown in figure 2d). One of the copper grid samples was annealed along with the Si-substrate sample at 500°C for 4 hours.

III.4.2 Transmission Electron Microscopy:

Cross-sectional transmission electron microscopy was performed in a double-tilt top-entry high-resolution JOEL JEM 200CX microscope, equipped with high resolution goniometer, at the National Center for Electron Microscopy. The operating voltage was 200 kV which yields a nominal point-to-point resolution of better than 2.4 Å. The specimens were aligned so that the electron beam was parallel to the <110> direction of the Si substrate, so that the {111} planes (d_{111} = 0.3135 nm) were resolved in high-resolution electron microscopy and used for image calibration. Image observation and acquisition under the electron beam was carried out quickly, and carefully, to ensure that minimum exposure to the beam was achieved, and little or no radiation damage occurred. When a thin region was identified, the sample wass tilted to a [110] Si pole while the beam was on the silicon substrate, not the multilayers. The beam was then defocused, and moved to the multilayer region. The multilayer was then focused and adjusted for astigmatism at as low a defocused beam as possible, to reduce radiation exposure from the electron beam. A through-focus-series of images was then recorded.

Plan-view samples were studied in a Philips 301 operating at 100 kV. The area of observation in the plan-view samples was much larger than that of the cross-sectional samples, hence providing more conclusive information than the cross-sectional samples about larger-scale microstructural features.

II.4.3 Image interpretation:

Image interpretation in electron microscopy is an important step in providing information of the samples. Artifacts induced during specimen preparation process, or under the electron beam during TEM observation, can

lead to erroneous interpretation of the images. Consequently, care in preventing and identifying these artifacts was carried out systematically.[24] The thicknesses of the layers can not be determined precisely due to the possible projection errors in the transmission image, or due to the presence of interfacial layers between the layers. Interpretation of the microstructures inside the layers and at their interfaces is also complicated by the great difference in contrast between the metal-rich and the carbon-rich layers imaged in the micrographs, and by the differences in images taken at different defocus values arising from Fresnel Fringe effects at interfaces between two high contrast layers.[26-27] In this study, the images of different samples were taken at approximately the same defocus value for uniformity, and attention was paid to all sources of artifacts during interpretation of results.

IV. RESULTS

IV.1 Absolute reflectance:

A typical x-ray reflectance profile of a multilayer structure is presented in figure 3. It is a θ - 2θ x-ray diffraction scan of an as-prepared 50 bilayer 7 nm period W/C multilayer prepared on a superpolished optical flat. Shown in this figure are the incident beam, the total reflection region, and five low order Bragg peaks of the multilayer. The total reflection 2θ for W/C multilayers is at approximately 0.6°. Nine low order Bragg peaks in this sample were used to determine its period. The high number of Bragg peaks measured is an indication of the high quality of the multilayer. Typical peak reflectance of W/C multilayers is about 70%.[3] A high number of Bragg peaks was usually measured to increase the accuracy of the determination of the period of the multilayer.[28]

IV.1.1 Expansion of period on annealing:

After annealing, the period of the multilayer is observed to increase by 2.4%, as signified by the shift of the Bragg peaks to lower angles. The log reflectivity plots in figure 4 show the comparison between the reflectance profile of the as-prepared 7 nanometer W/C multilayer with an annealed multilayer. Absolute peak reflectances of the multilayer are observed to remain unchanged or increase after annealing, as also observed in other studies under similar annealing conditions.[8,29] The second order Bragg peak in this sample, however, has disappeared after annealing. It is observed that even order peaks have lower peak reflectance than odd order peaks, and this observation in the as-prepared sample is more pronounced than in the annealed sample.

IV.1.2 Substrate dependence:

Peak reflectance of multilayers prepared on silicon substrates is known to be sufficiently lower than that of multilayers prepared on superpolished optical flat substrates. This reduction is illustrated in figure 5, in which the reflectance profile of a multilayer prepared on Si substrate is compared with that prepared on the optical flat. Peak reflectance of the sample on Si is approximately 35% lower than that of the sample prepared on optical flat. This reduction in peak reflectance value is probably due to higher surface roughness of the Si substrate, as compared to that of the optical flat. Higher order peaks of both samples appear almost identical, although calculation to determine peak reflectance was not made to study higher order Bragg peak reduction.

IV.1.3 Comparison between W/C and WC/C multilayers:

Figure 6 shows the reflectance profile of 7 nm period as-prepared and annealed WC/C multilayers. The presence of the secondary harmonic peaks in the region between the specular reflection and the first order Bragg peak indicates high periodicity of the multilayer. The high number of pronounced Bragg peaks observed also indicates high quality of the multilayers. Large shifts in the Bragg peaks of the annealed sample to lower angles indicate higher expansion of the period as compared to the W/C multilayer. Indeed, the relative expansion of this multilayer was determined to be 6.6%, which is almost three times greater than that of the W/C multilayer of the same period.

Peak reflectances of the Bragg peaks are observed to increase on annealing in the WC/C sample. Peak reflectance of this multilayer is also

observed to be slightly higher than that of the W/C multilayer of comparable period. The trend that the peak reflectance of the even order Bragg peaks are lower than that of the odd order peaks is not observed in the WC/C multilayer profile. Observation of this trend in the W/C profile suggests that the W-rich layers and the C-rich layers are approximately of the same thickness.

IV.2 Transmission Electron Microscopy:

Figure 7 shows a cross-sectional image of a full 7 nm W/C multilayer structure. It consists of the Si substrate, the C buffer layer, 50 bilayers of W and C, with W as the last deposited layer, and the epoxy layer holding the multilayer sandwich together during TEM specimen preparation. This image was taken in the JOEL JEM 200CX operating at 200 kV. The high contrast layers are the W layers, and the low contrast ones are the C layers. The field of view of the thin area under observation in this image is more than 350 nm wide. At this magnification, the layers appear to be smooth, and flat across the interfaces. Much more information of the multilayer structures, however, are obtained from high magnification phase contrast HRTEM images.

IV.2.1 W/C system:

A summary of the structural and phase characteristics of the W/C multilayers is presented in Table 1. The first four columns indicate the measured periods of the multilayers, determined from x-ray measurements, and the predominant phases present in the W-rich layers, for both as-prepared and annealed W/C multilayers. The last column gives the relative change in period on annealing, as observed from x-ray measurements.

A multilayer of approximately 1 nm was prepared on a Si substrate to study the stability of layered structures in the sub-nanometer period range. The bright field image, along with its electron diffraction pattern, of this multilayer is shown in figure 8. The effective thicknesses of the individual W and C layer are roughly 4 and 6 Å, respectively, which correspond to about 1.5 atomic planes of the W and 2 atomic planes of the C. The layered micro-structures are apparent, and show well defined spots in the electron diffraction pattern. Discontinuity in the W-rich layers, however, are frequently observed. X-ray profile of this nanometer period multilayer shows that the first order Bragg peak is visible, but higher order peaks are not observed. The presence of only first peak suggests that the transition between the W-rich and the C-rich layers is not abrupt but of sinusoidal shape. This argument is reasonable since at this period, the thickness of the transition layers between the W-rich and the C-rich layers are comparable to the individual layer thickness in the multilayer. The peak is quite broad, and has two distinct maxima, which correspond to 9.81 and 10.27 Å periods, with the higher and sharper peak at the shorter period. The peak reflectance of this multilayer is in the order of 10^{-3}. Upon annealing, the constituents in the layers have diffused into each other to form microcrystallites of tungsten carbides and have destroyed the layered structures of the multilayer, as shown in figure 9. The microcrystallites are seen across the whole sample and in the range of a few nm in size. The exact carbide phase identification of these microcrystallites however can not be determined from the spots and diffuse ring in its diffraction pattern.

Figures 10 - 13 show the cross-sectional bright field images of as-prepared and annealed 2, 4, 7, and 12 nm period multilayers, respectively, and

figures 14 - 17 show the plan-view images of the corresponding periods, along with the Selected Area Diffraction (SAD) patterns corresponding to these images. In all of the figures showing as-prepared and annealed images, figures a) in these figures show the images of the as-prepared samples, and figures b) are of the annealed samples. In cross-sectional images, the lattice images of the (111) planes of the Si substrates are clearly visible, which are used for image calibration. The cross-sectional electron diffraction patterns show the [110] zone axis along which the Si substrate was imaged, and the finely spaced diffraction spots arising from the periodicity of the multilayer. The multilayers are inclined from approximately 4.5° from exact (111) epitaxy of the substrate. Apparent variations of the layer thicknesses within one multilayer may be observed in these micrographs due to the possible bending of the specimen under the electron beam. Although the as-prepared and annealed images of one multilayer sample were enlarged at the same magnification, apparent decrease in the periods on annealing, as noted in the 7 and 12 nm period sample images, is not real and is only an artifact from preparation of these images.

As-prepared W/C multilayers have predominantly amorphous structure at short periods, as can be seen clearly in both cross-sectional and plan-view images. Close examination of the as-prepared 7 nm period images in figures 12a) and 16a) indicates some microcrystallinity present in the W-rich layers along with an amorphous phase. Images of the as-prepared 12 nm period show the predominant occupance of a crystalline phase. Because of high contrast in imaging of W and C layers in the cross-sectional images, crystallinity inside the W-rich layers and at their interfaces is difficult to observe. The lattice images of the crystalline phase are clearly visible, however, at thinner

regions of the specimen, as shown in the enlarged images of the as-prepared 12 nm period multilayer, in figure 18. The enlarged area is indicated in the figure, and the rings in the electron diffraction pattern are identified as elemental W, consistent with the identification of the rings in the plan-view pattern in figure 17a). Figure 18 also indicates the presence of a minor amorphous phase present along with the crystalline phase.

The layered microstructures of the periods 2 to 12 nm remain intact after annealing. The W-rich layers in the 2 and 4 nm period samples remain amorphous, while those in longer period structures crystallize on annealing. The bright field images of the annealed 4 nm period in figure 11b) may indicate some small crystallites at the interfaces. The W-rich layers, however, are predominantly amorphous. The ring pattern in the annealed 12 nm period plan-view sample in figure 17b) is consistent with the identification of W_2C, with a minor trace of elemental W indicated by the weaker rings. The rings in the plan-view diffraction patterns suggest that there is no preferred orientation of the crystallites in the plane of the layers. Figure 16b) shows that the microcrystallites in the annealed 7 nm period sample are of nanometer size. Single crystallites in the annealed 12 nm period multilayer are observed to extend for more than 100 nm in lateral direction in the W-rich layers, which are in the same order as the crystallites measured from the plan-view images. The smallest rings present in the annealed plan-view diffraction patterns are not identified with a carbide phase, and probably result from presence of oxygen or oxide phases, as also observed by pronounced peaks in EXAFS studies of the same multilayer system.[6,30]

IV.2.2 WC/C system:

Figures 19 - 21 show the cross-sectional images of as-prepared and annealed 2, 7, and 12 nm period WC/C multilayers, and figures 22 - 24 show the corresponding plan-view images of the same periods. The microstructures of all periods studied are amorphous or predominantly amorphous for both as-prepared and annealed samples. Observation of larger areas in the plan-view samples and their corresponding electron diffraction patterns is consistent with amorphous structure. Close examination of the cross-sectional annealed 12 nm period in figure 21b) reveals signs of microcrystallites in the WC-rich layers, though not conclusive. The corresponding diffraction pattern definitely shows no signs of crystallinity in this sample. The cross-sectional images show that the layered structures are stable after annealing. Figures 20 and 21 of the 7 and 10 nm period multilayer, repectively, show highly defined interfaces in both as-prepared and annealed samples.

Annealing also leads to expansion in the multilayer period, with higher relative expansion at shorter period, similar to that observed in the W/C system. The microstructures of the WC-rich layers, the thicknesses of the measured periods, and their relative period expansions on annealing, are summarized in Table 2.

IV.2.3 Ru/C system:

The microstructures and layered stability of the Ru/C system are distinctly different from those of the W/C and WC/C systems. A summary of the results from the Ru/C multilayers is presented in Table 3. The crystalline phases are identified by the electron diffraction patterns of both cross-sectional and plan-view samples. The periods of all samples are observed to

expand from 4 to 12% on annealing, with larger relative expansions at shorter periods.

Figure 25 shows the cross-sectional TEM images of the as-prepared and annealed 2 nm period Ru/C multilayers. The as-prepared layered micro-structures in figure 25a) are amorphous, as also evidenced by the lack of any indication of crystallinity in the corresponding diffraction pattern. Strong vertical textures in the electron diffraction pattern perpendicular to the layer plane are rod-shape effects arising from reciprocal transformation of ultra-thin layers of the multilayer; and texture signifying preferred orientation parallel to the plane of the layers suggests that the microstructures may contain some very small microscrystallites in the Ru-rich layers having a preferred orientation.

Upon annealing, the Ru in the 2 nm period sample has agglomerated to form almost spherical crystallites of about 2 nm, as seen in figure 25b). The layered structures are almost destroyed, in contrast to the behavior of the W/C and WC/C multilayers at same period. Observation of a larger area of the annealed sample at lower magnification in figure 26, however, shows that signs of layered structure are still apparent, although the layers and their interfaces are not as well defined as in the as-prepared sample. X-ray diffraction of this annealed sample indicates almost a 10^2 fold decrease in peak reflectance from that in the as-prepared sample. Only the first two Bragg peaks were observed in the annealed reflectance profile, and a large shift in the Bragg peaks to lower angles indicating expansion of the period is also observed. The low number of Bragg peaks detected in the annealed sample, and poor performance of peak reflectance, are strong indications of the low

quality of the multilayer, consistent with the observation of the cross-sectional TEM image.

For larger periods, both as-prepared and annealed Ru/C samples have stable layered microstructures, and show presence of a crystalline phase in the Ru-rich layers. Figure 27 shows cross-sectional bright field images of as-prepared and annealed 5 nm Ru/C multilayers. Lattice images can be seen in the Ru-rich layers at thinner regions of the specimen in figure 27a), although the exact structure could not be identified. Its electron diffraction pattern shows diffuse rings having six-fold symmetry, which indicates that the layers may contain very small crystallites of hexagonal structures. Even at 4.3 nm period, or effectively about 1.7 nm Ru layer thickness, the Ru-rich layers already show the presence of microscrystallites of similar symmetry, as can be seen in figure 28, which shows enlarged images of as-prepared 4.3 nm period Ru/C multilayer sample. The microstructures in the Ru-rich layers in the 5 nm period annealed sample are identified as elemental Ru by the ring pattern in its electron diffraction pattern. Figure 29 shows the cross-sectional images of as-prepared and annealed 10 nm period Ru/C multilayers. The crystalline fringes are clearly visible in the Ru-rich layers at thinner regions in both figures 9 a) and b). Electron diffraction patterns of both as-prepared and annealed sample coincide with ring patterns of elemental Ru.

All cross-sectional TEM diffraction patterns of the elemental Ru show a strong texture in [101] direction perpendicular to the layer interfaces.

Plan-view images of the corresponding periods reveal more conclusive information on phase identification and crystallite size determination. Figures 30 - 32 show the plan-view bright field images of as-prepared and annealed 2, 5, and 10 nm period Ru/C multilayers, respectively. The electron

diffraction patterns in the as-prepared 10 nm period sample and in all the annealed samples clearly indicate the presence of elemental Ru, and show no signs of preferred orientation in the plan of the layers. The crystallites in the plan-view annealed 2 nm period are of few nanometers, in agreement with those observed in its cross-sectional counterpart. The size of the crystallites in the as-prepared 10 nm period are also in the order of few nanometers. Upon annealing, however, these crystallites have grown to sizes of tens of nanometers in lateral direction, which are of the same order as the Ru-rich layer thickness in the multilayer.

V. DISCUSSIONS

The quality and stability of the multilayers depend on many factors: microstructures and phases present inside the layers, layer uniformity, microstructures at the interfaces, and layered structure stability. All these factors are interrelated that one may affect the behavior of the others, and they all play important roles in improving the quality and performance of the multilayers. Although the W/C, WC/C, and Ru/C multilayers may serve different specific purposes in multilayer optics, they all share common materials science characteristics of modulated thin film structures.

V.1 Microstructures and phases:

V.1.1 W/C and WC/C systems:

Formations of the amorphous and crystalline phases in the metal-rich layers on annealing are quite different for W/C, WC/C, and Ru/C multilayer systems, as also are their phase diagrams. The W-C phase diagram in figure 33, taken from reference 31, shows low temperature carbide phases, WC and W_2C. Thus significant intermixing of W and C in W/C multilayers, as observed by various studies,[3,7,13] in both as-prepared and annealed samples, is not surprising. WC and C, however, remain separated in the wide immiscible gap from 50 to 100 atomic percent C in the equilibrium phase diagram. This observation motivated the investigation of WC/C multilayers, since upon deposition and annealing, the layers in these multilayers would expect to be separated and have more defined interfaces between the layers.

Microstructures and phases of the W/C and WC/C multilayers are summarized in the electron diffraction patterns of their plan-view samples shown in figures 34 and 35, respectively. Consistency in phase identification

between the cross-sectional and plan-view patterns indicates that the plan-view samples, containing of only few bilayers prepared spanning the TEM grids, have similar microstructures as the multilayers prepared on Si substrates. Although there may be differences in internal stresses in the structures, the microstructures and phases in the plan-view samples are representative of those in cross-sectional samples, and provide significant complementary tools for positive identification of the phases.

The C layers in all multilayers studied have amorphous structure and remain amorphous after annealing. This is typical for sputtered C films. Short period as-prepared W/C multilayers show predominant amorphous structure, while longer periods show the presence of elemental W microcrystallites in the W-rich layers. The exact nature of the amorphous structure in the short period multilayers could not be conclusively determined by TEM technique. It could be amorphous W, or a W_xC_{1-x} mixture resulted from interdiffusion of the C into the W-rich layers. Quantitative analysis of EXAFS studies by Lamble et al., however, deduced that the coordination number of C neighbors for each W in the W-rich layers is one in as-prepared multilayers, which indicates diffusion leading to high C content in the W-rich layers.[7]

It is unclear if solid-state amorphization reactions (SSAR) have occurred in the W/C and WC/C systems. In a SSAR process, an amorphous alloy is formed during a solid-state reaction from crystalline elemental constituents. It has been observed in amorphization of alternating thin film layers of elemental crystallites.[32] Important criteria for SSAR are: 1) one of the constituents is a fast diffuser in the other, and 2) large negative heat of mixing between the constituents, which provides a thermodynamical driving force for the reactions.[33] The amorphous transition layers between the

polycrystalline W-rich and the C-rich layers in the as-prepared 12 nm W/C multilayer, as seen in figure 18, may have been formed by SSAR from a few atomic planes of the crystalline W layers during C deposition. These layers are observed both on top, e.g, they are formed between the deposition of the W-rich and C-rich layers, in that order, and bottom, e.g., they are formed between the depostion of the C-rich and W-rich layers, of the W-rich layers. After the formation of the polycrystalline W in the W-rich layer, it is possible that interactions between the W atoms of this layer and the sputtered C atoms from the next deposited layer leads to the formation of the amorphous structure to accomodate for the lattice mismatch between the crystalline W and amorphous C structures, and to minimize the interfacial energy between these layers.

Formation of a critical nucleus of a crystalline phase requires the collective diffusive motions of both constituents.[34-35] In the as-prepared 12 nm period WC/C multilayer, a crystalline phase is not formed probably because the slow diffusing W atoms in the WC-rich layers suppress the formation of tungsten carbide nuclei, while the fast diffusing C atoms promote intermixing to form an amorphous phase. High C content in the WC-rich layers hence is responsible for the amorphous formation in these layers. With the presence of the fast diffuser species, SSAR can occur at temperatures below the crystallization temperature of the amorphous phase. Formation of the amorphous phase is associated with a decrease in Gibbs free energy, which results in lower free energy than that of the crystalline phases. Calculation of the free energies of the crystalline and amorphous phases may provide explanation for the formation of the amorphous phases in these multilayers.

Crystallization of elemental W in the W-rich layers in as-prepared samples appears to depend only on the thickness of the W-rich layers, and is

independent of the W to C layer thickness ratio. Observation of elemental W in the W-rich layers of 12 nm period W/C multilayer, or effectively 4.8 nm W and 7.2 nm C layer thicknesses, is consistent with results of other studies.[3-4,7,13] Nucleation of elemental W crystallites in larger W layer thickness samples is possible due to low C concentration in the W-rich layer. It suggests that the C has not diffused into the entire thickness of the W-rich layer. As a result, there is a thin layer of pure W at the center of the W-rich layer.[3] As the W layer thickness increases, it is shown below that the diffusion length of C into the W layer increases only with the square root of the increase of the W layer thickness. When the thickness of the pure W layer in the multilayer is greater than the critical nucleation layer thickness for crystallization, nucleation of a stable crystalline phase occurs at the expense of the decreasing growth rate of the compound amorphous phase. Observation of the crystalline W in these layers also suggests that the nucleation and growth rate of the crystalline W is faster than the diffusion rate of the C. The diffusion length of C into the W-rich layer during deposition, or initial C-content in the metal-rich layers, hence is important to the formation of the microstructures in the metal-rich layers.

There are two types of diffusion of C atoms during deposition: thermal diffusion at the floating temperature of the substrate, and kinetic diffusion from bombardment of energetic atoms from sputtering. Neglecting surface diffusion, and using Fick's law of non steady-state diffusion,[36] the diffusion length for C from the thermal source is expressed as:

$$x=\sqrt{Dt}$$

where x is the diffusion length, D is the diffusion coefficient which depends on the temperature, and t is the time of diffusion. Diffusion of C into the W

layers, at the same temperature, thus is found to increase not linearly with period thickness but only to its power of 1/2.

Consider two W layers of different thicknesses, the ratio of diffusion length x_1 / x_2 is proportional to the square root of the ratio of their diffusion time t_1 / t_2, under the same conditions. Since the time for deposition of one layer of the multilayers is linearly proportional to the layer period, then x_1 / x_2 is also proportional to the square root of the ratio of the layer thicknesses d_1 / d_2. The picture of C diffusion into crystalline W, however, is different from that into amorphous W. Once a crystalline W layer has been formed, C atoms from the next deposited layer can diffuse interstitially into the crystalline W, but may not disturb the already existing crystalline structure. Thus for multilayer of period d_1 that is 3 times of period d_2, for example, the diffusion length x_1 of C into the W layer is only $\sqrt{3}$ or 1.7 times x_2. Applying these numbers to the W/C system, assume that the C diffuses completely through the W-rich layer in the 4 nm period multilayer, or a distance of about 1.6 nm of the W layer thickness. The diffusion length of C in the W-rich layer in the 12 nm period thus is only approximately (1.6 nm x 1.7) or 2.7 nm. Since the nominal thickness of the W-rich layer in this sample is 4.8 nm, the "pure" W layer, that can nucleate to form the crystalline phase before deposition of the next C layer, is 2.1 nm. Although this value is a low limit of the diffusion length, it still illustrates the mechanism for formation of the structures inside the W-rich layer.

Interdiffusion during deposition probably results from energetic bombardment of the sputtered atoms. Preliminary calculation of the diffusion length x during deposition of one W-rich layer in the 12 nm period W/C

multilayer, assuming at maximum substrate deposition temperature of 150°C, using

$$D=D_o e^{-Q/RT}$$

where D_o is the frequency factor, Q is the activation energy for diffusion, and R and T are the gas constant and the absolute temperature in °K, and

$$D_o=3.15 \times 10^{-3} \text{ cm}^2/\text{sec}$$

$$Q = 172 \text{ Kcal/mole}$$

for the temperature range 100-400°C,[37] yields a value of the diffusion length of C into W of only 10^{-38} nm. Thus kinetic-source interdiffusion from atom bombardment, instead of thermal interdiffusion, is probably the dominant process in intermixing of the layers during deposition. The average energies of the atoms reaching the substrate in sputtering processes could be as high as 30eV.[38] This argument suggests that the W-rich layers in the short period as-prepared W/C multilayers contain sufficiently high C content, and there is a interfacial layer of intermetalic alloy at each interface in longer period samples. The images of as-prepared 12 nm W/C multilayer in figure 18 indeed do show the presence of interfacial layers, which may be interpreted as intermixing layers resulting from bombardment of energetic atoms onto the existing layers.

Formation of the W_2C phase on annealing, as a result of C diffusion into the W-rich layers, appears to depend on both the W layer thickness, and the W to C layer thickness ratio. This is illustrated by comparison among annealing results of this study and other previous studies. Annealing of multilayers having W to C layer thickness ratio of 0.66 with the W layer thickness of 2.8 nm (7 nm period) or greater in this study results in formation of W_2C. Similarly, multilayer having 4 nm W layer thickness and W to C ratio of 4.0 in

annealing studies by Takagi et al. resulted in formation also of the same crystalline phase.[4] Lamble et al.,[7] however, prepared a W/C multilayer of W layer thickness 3.7 nm, and W to C ratio of approximately 0.29, and found that the structure remained amorphous after moderate annealing. Thus a high ratio of W to C layer thickness is required for formation of W_2C on annealing. The 4 nm period multilayer, having 1.6 nm W layer thickness and 0.66 ratio, in this study, however, does not crystallize on annealing. The initial thickness of the W layer hence is also a criterion for W_2C crystallization.

If it were assumed that crystallization of W_2C during annealing results partially from C diffusion into the W-rich layers, it is surprising to observe that the short period W-rich layers, in which more diffusion takes place, do not crystallize, whereas the longer period layers do. In the short period layers, higher C content, as compared to that in longer period layers, probably is reponsible for the suppression of the crystalline phase formation. Similarly, high initial C content, or low W to C ratio, in the metal-rich layers of the WC/C multilayers, which stabilizes the amorphous structure against crystallization, is responsible for the retation of the amorphous structures in these multilayers upon annealing.

V.1.2 Ru/C system:

The phase diagram of the Ru-C system is shown in figure 36, which shows characteristics distinct from those of the W-C system. It is of simple eutectic type, with Ru and C immiscible at low mutual solubilities at low temperatures.[31] A RuC phase has been reported, but has not been reconfirmed by other groups, so no equilibrium carbide phase is recorded in the solid state region.[39] This suggests that components of Ru and C should yield multilayers

of highly defined interfaces and less interdiffusion between the layers upon annealing. Formation of a crystalline phase at 4.3 nm period multilayer, or effectively about 1.7 nm Ru layer thickness, as compared to greater than 2.8 nm W layer thickness in W/C multilayer system, suggests that there is more defined separation between the Ru and C layers at their interfaces, which promotes the formation of the crystalline Ru phase at such thin layer. Summaries of the microstructures and phases present in Ru/C multilayer system are presented in their cross-sectional and plan-view electron diffraction images in figures 37 and 38. The Ru-rich layers in longer period as-prepared and in all annealed multilayers show structures of elemental Ru. Annealing of the 2 nm period multilayer leads to agglomeration of the Ru-rich layers, and also formation of elemental Ru crystallites. No carbide phases are found in these layers, which is consistent with that shown in the Ru-C equilibrium phase diagram.

V.2 Layer Uniformity:

Cross-sectional TEM images of the multilayers show that the layers appear relatively uniform and flat for all as-prepared multilayers of periods 2nm or greater, and for those annealed samples that retain their layered structures after annealing. Disruption in the W-rich layers and the broad x-ray Bragg peak in the as-prepared 1 nm period W/C multilayer suggest that layer uniformity in the W/C system begins to decrease dramatically at a period somewhere between 1 and 2 nm, or effectively at W layer thickness between 0.4 and 0.8 nm, in agreement with the value of 0.6 nm reported by Ruterana et al.,[14] and a little shorter than the value reported by Lepetre et al.[9] Differences in deposition techniques and conditions may explain the different

qualities of the multilayers. At 2 nm period, however, the layers appear relatively uniform for all as-prepared W/C, WC/C, and Ru/C multilayers studied. Sub-nanometer period multilayers of WC/C and Ru/C multilayers have not been attempted, but from their behaviors at longer periods, it is expected that the layers in these as-prepared sub-nanometer period multilayers would behave similar or better than those in the W/C multilayer of the same period.

The cross-sectional images also reveal that the relative compositional distinction between the W-rich and the C-rich layers to be greater for multilayers with longer periods, consistent with intermixing of W and C at the interfaces inferred from x-ray scattering[3] and TEM[10,13] techniques. The average thickness of the multilayer period can be determined to high accuracy from x-ray measurements of high order Bragg peaks, or from the spacings of the multilayer diffraction spots in the electron diffraction patterns, using the Si diffraction spots as calibration. Thicknesses of the individual layers, however, can not be determined accurately but are only inferred from visual inspection of the cross-sectional TEM bright field images. Inaccuracy in determining these thicknesses by TEM technique arises due to high imaging contrast between the metal-rich and the C-rich layers and possible bending of the specimen under the electron beam, which can falsely increase the apparent thickness of the W-rich layers, and due to the difficulty in defining the exact interface between the metal-rich and the C-rich layers. Analysis of the x-ray reflectance of high order Bragg peaks may provide accurate determination of the individual layer thicknesses.

Uniformity of the layers and quality of the multilayers also depend on the surface roughness of the substrate. Multilayers prepared on optical flat substrates, which have a surface roughness of approximately a few angstroms,

have distinctly higher peak reflectance than multilayers prepared on Si substrates, which have surface roughness of about few atomic planes. Deposition of an amorphous C buffer layer between the substrate and the multilayer is intended to smooth out the substrate roughness; its effects, however, have not been observed conclusively from cross-sectional TEM images.

"Wavy" structures in the layers are occasionally observed at the thinner edge of the wedge-shaped specimen in shorter period samples, as seen in figures 10, 19, and 25, of 2 nm period multilayers. They are observed near the thinner edges of the specimens but not at thicker areas near the substrates, in the cross-sectional TEM images. In addition, they are not observed in images of longer period samples. This observation indicates that these structures appear in the images as a result of ion milling during specimen preparation process, and are not related to internal stresses, as suggested by Vidal et al.[5] They argued that these internal stresses have been formed during the cooling period after uncooled deposition, and their presence in the multilayer effectively reduces the reflectivity of the multilayer. The drastic decrease in reflectivity of W/C multilayer period below 2 nm,[3] is probably due to the higher ratio of interfacial roughness layer to period thickness in short periods, as compared to that in longer periods, rather than to internal stresses.

V.3 Structures and roughness at interfaces:

Studies of reactions at interfaces are important to improvement of multilayer quality. Compositional gradients or intermixing at the interfaces disturbs the definition of sharp interfaces, and the interfacial roughness

induces local scattering of the incident beam. X-ray diffraction in some cases may provide information on atomic arrangements of the constituents at interfaces.[6] Interpretation of the structures and layer thickness at these interfaces from TEM images, however, is more difficult, because of the differences in the images taken at different defocus values resulting from Fresnel fringe effects at high contrast potential boundaries,[27] and because of possible tilting of the layer interfaces from exact edge-on orientation when imaged in the microscope.[14,24] Nevertheless, general observations of the interfaces in the systems can be made without any danger of erroneous interpretations.

In general, interfaces in longer period W/C, WC/C, and Ru/C multilayers appear sharper than those in shorter periods. Interfaces in 2 nm period W/C, WC/C, and Ru/C multilayers show no appreciable difference from each other, while they appear more defined in the WC/C and Ru/C than in the W/C multilayers for longer periods. High C content and amorphous WC mixture are probably responsible for the sharp interfaces in WC/C multilayers. Sharp interfaces in Ru/C multilayers suggests phase separation between the Ru and C layers during deposition, consistent with immiscibility in the solid state region of the Ru-C phase diagram.

There are indications of the presence of an interfacial layer between the layers, where intermixing of the constituents occurred during deposition. This intermixing at interfaces is best observed in the enlarged cross-sectional images in figure 18. In these images, crystalline lattice images of elemental W are clearly visible inside the W-rich layers. At the boundaries of the layers, however, an amorphous layer of decreasing contrast from the W-rich layer to the C-rich layer, indicating a decrease in W-density across the interface,

suggests the presence of a tungsten carbide layer at these interfaces, as also reported by Petford-Long et al. in their studies.[10] In multilayers where the layers are predominantly amorphous, the presence of an interfacial layer is also observed. The structures of these interfacial layers appear to be amorphous, in contrast to the report of crystalline WC by Petford-Long et al. The exact thicknesses of the interfacial layers are difficult to determine from the TEM images, and are not attempted in this study. Data fitting of x-ray diffraction with dynamical theory approximation by Debye-Waller factor suggested an interfacial roughness of 0.5 nm at each interface;[5] however, the thickness of the interfacial layers from intermixing and diffusion of the atoms are generally greater than that value.

X-ray peak reflectance profiles of W/C and WC/C multilayers indicate that interdiffusion between the layers in the W/C is greater than that in the WC/C multilayers. Reduction in peak reflectance of even order Bragg peaks observed in W/C multilayers, as shown in figure 4, suggests that the W-rich layers and the C-rich layers have strictly almost equal thicknesses, similar to the structure of a quaterwave stack at longer wavelengths. Since the intended nominal relative thicknesses for the W and the C layers were 40 and 60%, respectively, it suggests that the interdiffusion between the W and C layers, which roughens the interfaces, and effectively increases the apparent thickness of the W-rich layers, has occurred. Interfaces in the WC/C multilayers, on the contrary, remain quite sharp and x-ray reflectance profile in figure 6 does not show a trend of reduction in peak reflectance in even order Bragg peaks.

Microstructures inside the layers also have effects on the definition of the interfaces. It has been observed that interfaces between crystalline and

amorphous layers are rougher than those between amorphous and amorphous layers, due to the extension of the crystalline planes into the amorphous layers. This observation is illustrated in figure 39, which shows enlarged images of annealed 12 nm W/C and WC/C multilayers. The W-rich layers in the W/C multilayer have recrystallized to form W_2C, while the WC-rich layers in the WC/C multilayer remain amorphous after annealing. Close observation of figure 39b) reveals signs of microcrystallinity in the WC layers, though are not conclusive. Interfaces in the W/C multilayer are significantly rougher than those in the WC/C multilayers, because the crystalline planes in the W-rich layers extend into the C-rich layers. These crystalline planes can be observed to extend 4 - 5 atomic planes, and are more severe when they are inclined at an angle from the layer plane.

Another source of interfacial roughness in crystalline - amorphous interfaces is grain boundaries in the crystalline metal-rich layers. Figure 40 shows enlarged images of a few periods of as-prepared and annealed 10 nm Ru/C multilayers. Both images show polycrystalline structures in the Ru-rich layers. The size of the microcrystalline grains in the as-prepared multilayers, shown in figure 40a), is approximately 10 times smaller than those in the annealed sample. The arrows in figure 40a) show a smooth grain boundary between two Ru grains in the layer. The two sets of arrows in figure 40b) indicates one Ru grain which has [101] direction perpendicular to the layer plane, as observed in the texture in the cross-sectional electron diffraction patterns. A disruption at the interface between the Ru and C layers is shown at arrows B in figure 40b). At the boundary, mismatch in crystal planes of the grains causes roughening of the boundaries, which extends into the interfaces of the layers. Also shown in this figure are the Ru crystal planes

extending into the amorphous C layer, indicated by arrow A, similar to that observed in the annealed 12nm W/C multilayer.

Roughening of the interfaces resulting from either source above has little or no effects, however, on the reflectivity, or absolute reflectance of the first order Bragg peak, of the multilayer since the magnitude of the interfacial roughness is much smaller than that of the operating wavelength. Local scatterings from such small deviations from ideal interfaces are neglegible and do not affect first order peak reflectance significantly. This interfacial roughness, however, affect the characteristics of higher order Bragg peaks of the reflectance profile.

V.4 Layered structure stability on annealing:

The layered microstructures of W/C and WC/C multilayers at short period are more stable on annealing than those of Ru/C multilayer system. The layers in the 2 nm period annealed W/C and WC/C multilayers remain intact and show relatively uniform structure as compared to those in their as-prepared counterparts. The Ru-rich layers in the Ru/C multilayer of the same period, however, have agglomerated to form almost spherical crystallites of elemental Ru, and have destroyed the layered structures of the multilayers. Although as-prepared Ru/C multilayers have shown superior quality than the W/C multilayers, and comparable to the WC/C multilayers, their uses at short wavelength application may not be as good due to their degradation of the layered structures from intensive x-radiation.

Annealing of the 1 nm period W/C multilayer also leads to destruction of the layered structures, and formation of microcrystallites throughout the whole samples. Mechanisms for degradation of the layered structures in the

1 nm period W/C and the 2 nm period Ru/C multilayers on annealing, however, are quite different. Loss of the layered structures in the annealed W/C multilayer results from interdiffusion of the W and C atoms in the ultrathin layers to form tungsten carbide microcrystallites; while in the annealed Ru/C multilayer, it is due to agglomeration of the Ru-rich layers without any reaction with the C atoms. Recrystallization in the W/C multilayer is a nucleation and growth process of an intermetallic compound to form a more stable crystalline phase. Agglomeration of the Ru, however, results from the driving force to lower the ratio of interface to volume energies, which is strongest in this sample. Kinetic factors may also be of importance in the agglomeration of the Ru/C multilayer.

V.5 Expansion of multilayer periods on annealing:

All W/C, WC/C, and Ru/C multilayers of all periods expand on annealing, with larger relative expansion at shorter periods. Absolute expansion seems to increase with initial C content in the multilayers. Takagi et al. reported that expansion of the multilayer period on annealing was not observed in W/C multilayer of 4 nm-W / 1 nm-C, while multilayers having 1.5 nm-W / 1.5 nm-C, and 1 nm-W / 4 nm-C, expanded after annealing under the same conditions.[17] The mechanism for the expansion on annealing in the metal-C multilayers is not well understood, though this expansion appears to be linked to the amorphous C-rich layers, and not result from agglomeration of the W-rich layers as suggested by Lepetre et al.[9]

Figure 41 shows the absolute expansion plots, and figure 42 shows the relative expansion plots, for all W/C, WC/C, and Ru/C multilayers. There appears to be no relationship among the absolute expansions of W/C, WC/C, and

Ru/C systems. Absolute expansion in W/C multilayers is almost constant for all periods, and is roughly 0.2 nm. Absolute expansion in WC/C multilayers, however, seems to increase almost linearly with period in the range of periods studied, ranging from 0.15 nm at 2 nm period to more than 0.6 nm for 12 nm period. There appears to be no pattern in absolute expansion of Ru/C multilayers. Multilayer of 5 nm period expands the most, at about 0.46 nm, while 2 nm period expand the least, at about 0.25 nm, and 10 nm period multilayer expands moderately between the 2 and 5 nm period samples.

Relative expansion plots of W/C, WC/C, and Ru/C multilayers in figure 42 show similar behaviors among themselves. They all show higher relative expansion for shorter periods than for longer periods. The plots of WC/C and Ru/C appear almost linear with period, and are significantly higher than that of the W/C multilayers. Sufficient interdiffusion between the W-rich and the C-rich layers in the W/C multilayers upon annealing, together with assumed expansion of the amorphous C layers, can explain the differences in the values of relative expansion between the W/C and the other systems. A large decrease in relative expansion from the 4 to 7 nm period in the W/C plot is probably related to the crystallization of the W-rich layers in the 7 nm period on annealing, where in the process, some of the C atoms have participated in the formation of the crystalline carbide phase, while the 4 nm period remains amorphous upon annealing. Further systematic annealing studies, or modeling of the multilayers, are required to explain for the similarities and differences in these plots, and to explain the mechanism for multilayer period expansion on annealing.

Peak reflectivities of higher order Bragg peaks depend on the relative thickness of the metal-rich and the C-rich layers in one period. Equal layer

thickness, for example, results in the suppression of all even order peaks. Similarly, preliminary calculations show that a relative thickness of the C-layer in the range of 20-30% or 70-80% of the period yields maxima of the second order peaks. It was observed that peak reflectivities of most even order peaks in the x-ray profiles increase after annealing, while the odd order peaks decrease or remain unchanged. This observation is seen in both W/C and WC/C systems, as illustrated in figures 4 and 6. A thorough study of calculated and experimental peak reflectances of higher order Bragg peaks may provide information on the relative thickness of the layers in one period and the layer reponsible for the expansion of the multilayer period.

Stability of multilayer period on annealing is important to practical applications. The effect of thermal annealing is similar to that of intensive radiation. Experiments employing multilayer structures require that the reflected wavelengths, or the multilayer periods, remain stable over a long time. It is then important to understand the mechanism for this expansion, to be able to design more stable multilayers under thermal or radiation loading. It was observed that multilayer period in metal/Si multilayers, on the contrary, tend to decrease on annealing.[40] Mechanism for this contraction is also not understood, though studies of metal/SiC multilayers would be interesting and may provide stable multilayers against period expansion or contraction under loading.

VI. SUMMARY AND CONCLUSIONS

Results from a systemmatic comparison of microstructural and phase stability of W/C, WC/C, and Ru/C, multilayer structures, using x-ray diffraction and high-resolution transmission electron microscopy, have been presented. Effects of annealing at 500°C for 4 hours on layered structure and multilayer period stability of these multilayers were also studied. Relationship between the structural characterics of the multilayers and their optical performance was discussed.

It was found that the phase stability of the WC/C system is very different from that of the W/C system. The as-prepared WC/C multilayers are predominantly amorphous, and remain amorphous after annealing, at all periods. The short period W/C multilayer remains amorphous upon annealing, while the longer periods recrystallize to form W_2C in the W-rich layers. Nucleation of a crystalline phase in as-prepared W/C multilayers depends only on the thickness of the W-rich layers, and formation of the crystalline phase upon annealing depends on both the thickness of the W-rich layers, and the W to C content ratio. For both systems, the layered structures are stable for annealing at 500°C for 4 hours, and for periods equal to or greater than 2 nm. Discontinuity in the layers were observed in the as-prepared 1 nm W/C multilayer, although diffraction spots from the periodicity of the multilayer are still visible. Annealing of this ultrathin multilayer leads to interdiffusion between the constituents in the layers to form mircrocrystallites, and destruction of the layered structures.

The layered microstructures of the Ru/C multilayers, however, are stable only for longer periods, while 2 nm period sample agglomerates upon annealing. Agglomeration in this thin period multilayer on annealing

probably results from reduction in surface to volume energy of the structure. The phases in the as-prepared Ru/C multilayers depend on the periods, namely amorphous to crystalline as the period increases. Annealing of the Ru/C multilayers leads to formation of elemental Ru. The Ru crystallites in all multilayers show no preferred orientation in plane of the layers, and a strong preferred orientation along [101] perpendicular to the layers. No carbide phases were found, consistent with the Ru-C equilibrium phase diagram.

The periods of the multilayers expand moderately for all metal/C systems studied. Relative expansion is greater at shorter period for all systems. It varies from 1.6 to 6.8% for the W/C, 5.4 to 7.5% for the WC/C, and 4.2 to 12.7 for the Ru/C system. There appears to be a correlation in relative expansion between different periods, and between different systems. Mechanisms for this expansion is still not well understood, although it seems to be linked to the amorphous C-rich layers.

Performance of multilayers depend on many different structural and characteristic factors. Subtrate roughness reduces peak reflectivities of the multilayers, while annealing seems to cause them to increase or remain unchanged. Uniformity of the layers, and sharpness at their interfaces, are important criteria for high reflectivity. Microstructures inside the layers, and roughness at interfaces induced from these microstructures, may also have effects on the performance of the multilayers.

VII. SUGGESTIONS FOR FURTHER STUDIES

Studies of the metal/C multilayer structures have become more and more interesting as they reveal many insights into these systems. At the same time, however, they lead to many new questions, of both optical and materials science aspects, that need further examination. For the continuation of this study, the following studies are suggested:

1) Studies of the theoretical and experimental x-ray reflectance performance of these multilayers, and the relationship of their performance to their microstructures.

2) Experimentations of other combinations of materials that may improve the quality and performance of the multilayers.

3) Studies of the mechanisms of the expansion of the multilayer period on annealing by:

- Quantization of the peak reflectance of higher order Bragg peaks with various relative thickness multilayers.

- Annealing studies of a thin C layer with repect to expansion. Quantitative experimentation could include transformation of the C bonds from sp3 to sp2, for instance, on annealing, and determination of the density of thin layer C by Electron Energy Loss Spectroscopy, and x-ray diffraction.

- Comparison with metal/Si and metal/SiC systems on period expansion.

4) Studies of the critical temparatures and period at which the layered structures remain stable during annealing.

5) Studies of reflectivity and stability of sub-nanometer period metal/C multilayers.

6) Studies of the nucleation and growth of the phases in the layers and their orientation during deposition, and at their interfaces, to understand the formation of the layers and interfaces.

7) Calculations of the free energy for crystalline and amorphous metal-C compounds to study the amorphous and crystalline phase formations in the structures, and to see if SSAR had occurred in these systems.

8) Studies of the interface to volume energies of thin layers of Ru and C and the Rayleigh criterion, to establish a relationship between the layer thickness, temperature, and stability of the Ru layers, and to explain the agglomeration of Ru as observed in the 2 nm period Ru/C multilayer after annealing. Experimental techniques could include direct observation of the transformation by in-situ HRTEM.

9) Studies of the Fresnel Fringe Effects at potential boundaries, or at the interfaces in these multilayers, on the difference between images taken at different defocus values.

VIII. ACKNOWLEDGEMENTS

Through the years it took me to finish this work, I had become friend with many, colleagues of many, and most important of all indebted to many individuals for their helps and encouragements:

I would like to express my appreciations to my two advisors, Professor Ronald Gronsky, and Dr. Jeffrey B. Kortright, for their guidance and support throughout the course of this study. Their advices and counseling were invaluable and educational. Individually, I would like to thank Dr. Kortright for his patient helps in my training of x-ray diffraction and methods, and I would like to thank Prof. Gronsky for his understanding, his whole-hearted support and encouragements, that have lifted me up again many times, during my graduate career.

I would like to thank Prof. Marjorie Olmstead and prof. Dave Attwood for reviewing this thesis. Special thanks to Prof. Attwood for first introducing me to x-ray optics, for giving me an opportunity to conduct research at the Center for X-Ray Optics, and for supporting me in the new Interdisciplinary Program.

I would like to acknowledge NCEM and its managements for allowing me to use the 200CX microscope. I also would like to thank the scientists, staff, and friends, at both CXRO and NCEM, for many insights of all aspects, and for making my years more enjoyable. Many helps and useful discussions, especially in computer, technical supports, from many members of both Centers are greatly appreciated. I would like to thank J. Turner at NCEM for his helps in preparing the photographs in the TEM Specimen Preparation Sections, and I would like to thank the staff at the Photo-Lab for their understanding and patience in doing many rush printing jobs.

My brothers, my relatives, and my friends, I thank you all, for guidance and supports, for helps and encouragements, and for making my life in the last few years more bearable.

And as for any other achievement, I would like to dedicate this work to my parents in Vietnam.

IX. REFERENCES

1. D.T. Attwood, in Proceedings of the Topical Meeting on Free Electron Generation of Extreme Ultraviolet Coherent Radiation, Brookhaven National Lab, Upton, NY (1983).

2. Applications of Thin-Film Multilayered Structures to Figured X-Ray Optics, G.F. Marshall, ed., (Proc. Soc. Photo-Opt. Instrum. Eng. **563**, Bellingham, WA 1985).

3. J.B. Kortright and J.D. Denlinger, in Multilayers: Synthesis, Properties and Non-Electronic Applications, edited by T.W. Barbee, Jr., F. Spaepen, and L. Greer (MRS Proc. **103**, Pittsburgh, PA 1988) p. 95.

4. Y. Takagi, S.A. Flessa, K.L. Hart, D.A. Pawlik, A.M. Kaden, J.L. Wood, J.E. Keem, J.E. Tyler, in Applications of Thin-Film Multilayered Structures to Figured X-Ray Optics, edited by G.F. Marshall (Proc. SPIE **563**, Bellingham, WA 1985) p. 66.

5. B.A. Vidal and J.C. Marfaing, J. Appl. Phys. **65**, 3453 (1989).

6. G.M. Lamble, S.M. Heald, D.E. Sayers, and E. Zeigler, in Multilayers: Synthesis, Properties and Non-Electronic Applications, Proc. MRS **103** (1988).

7. G.M. Lamble, S.M. Heald, D.E. Sayers, E. Ziegler, and P.J. Viccaro, J. Appl. Phys. **65**, 4250 (1989).

8. E. Ziegler, Y. Lepetre, I.K. Schuller, and E. Spiller, Apl. Phys. Let. **48**, 1354 (1986).

9. Y. Lepetre, E. Ziegler, I.K. Schuller, and R. Rivoira, J. Appl. Phys. **64**, 2301 (1986).

10. A.K. Petford-Long, M.b. Stearns, C.-H. Chang, S.R. Nutt, D.G. Stearns, N.M. Ceglio, and A.M. Hawryluk, J. Appl. Phys. **61**, 1422 (1987).

11. S.R. Nutt and J.E. Keem, in Multilayers: Synthesis, Properties and Non-Electronic Applications, p. 87.

12. K. Holloway, K.B. Do, and R. Sinclair, in Multilayers: Synthesis, Properties and Non-Electronic Applications, p. 167.

13. T.D. Nguyen, R. Gronsky, and J.B. Kortright, in High-Resolution Microscopy of Materials, edited by W. Krakow, F.A. Ponce, and D.J. Smith (Mater. Res. Soc. Proc. **139**, Pittburgh, PA 1989) p. 357.

14. R. Ruterana, J.-P. Chevalier, and P. Houdy, J. Appl. Phys. **65**, 3907 (1989).

15. Y. Lepetre, I.K. Schuller, G. Rasigni, R. Rivoira, R. Philip, and P. Dhez, Opt. Eng. **25**, 849 (1986).

16. V. Bodart, Docteur es-Sciences Thesis, Paris VII University, 1987.

17. A.F. Jankowski and D.M. Malowiecki, SPIE **984**, 64 (1988).

18. L. Golub, E. Spiller, R.J. Bartlett, M.P. Hockaday, D.R. Kania, W.J. Trela, and R. Tatchyn, Appl. Opt. **23**, 3529 (1984).

19. A.V. Vinogradov and B.Y. Zeldovich, Appl. Opt. **16**, 89 (1977).

20. A.E. Rosenbluth and J.M. Forsyth, AIP Conf. Proc. **75**, 280 (1981).

21. M.S. Abrahams, and C.J.J. Buiocchi, Appl. Phys. **45**,3315 (1974).

22. C.S. Baxter, and W.M. Stobbs, Ultramicroscopy **16**, 213 (1985).

23. J.C. Bravman, and R. Sinclair, J. Electron. Microsc. Tech. **1**, 53 (1984).

24. T.D. Nguyen, R. Gronsky, and J.B. Kortright (submitted to J. Electron. Microsc. Tech.)

25. T.D. Nguyen, R. Gronsky, and J.B. Kortright, EMSA Proc. (1989).

26. C.S. Baxter and W.M. Stobbs, Appl. Phys. Lett. **48**, 1202 (1986).

27. T.D. Nguyen, R. Gronsky, and J.B. Kortright, ICEM Proc. (1990).

28. A.E. Rosenbluth and P. Lee, Appl. Phys. Lett. **40**, 466 (1977).

29. T.W. Barbee, Jr., AIP Conf. Proc. **75** (1981).

30. D. Roux, A. Rolland, P. Renucci, and J.P. Petrakian, Appl. Surf. Sci. **28**, 93 (1957).

31. W.G. Moffatt, The Handbook of Binary Phase Diagrams, vol. **2** (Genium Pub. Corp., New York 1987).

32. B.M. Clemens, Phys. Rev. **B 33**, 7615 (1986).

33. R.B. Schwarz and W.L. Johnson, Phys. Rev. Lett **51**, 415 (1983).

34. B.M. Clemens and R. Sinclair, MRS Bulletin, vol. **XV**, 2, 19 (1990).

35. W.L. Johnson, Mater. Sci. Eng. **97**, 1 (1985).

36. D.A. Porter and K.E. Easterling, Phase Transformations in Metals and Alloys (Van Nostrand Reinhold, 1988).

37. Diffusion Data, vol. **2**, 2, 156 (1968).

38. W.D. Westwood, MRS Bulletin, vol. **XIII**, 12, 46 (1988).

39. R.A. Shunk, Constitution of Binary Alloys, Second Supplement (McGraw-Hill Book Comp., 1969).

40. J.B.Kortright, S. Joksch, and E. Ziegler, to be published.

Table 1. -- Structural Charateristics of W/C multilayers

As - prepared		Annealed		
d (nm)	phases in W-rich layer	d (nm)	phases in W-rich layer	Δd/d (%)
0.98	amorphous (discontinuous layer)	----	microcrystalline (layered structure detroyed)	----
1.98	amorphous	2.12	amorphous	6.8
3.93	amorphous	4.15	amorphous + crystalline	5.8
7.08	amorphous + crystalline	7.25	crystalline	2.4
12.07	amorphous + bcc W	12.26	$W_2C + W$	1.6

Table 2. -- Structural Charateristics of WC/C multilayers

As - prepared		Annealed		
d (nm)	phases in WC-rich layer	d (nm)	phases in WC-rich layer	Δd/d (%)
1.95	amorphous	2.09	amorphous	7.5
6.41	amorphous	6.84	amorphous	6.6
11.23	amorphous	11.85	amorphous	5.4

Table 3. -- Structural Characteristics of Ru/C multilayers

As - prepared		Annealed		
d (nm)	phases in Ru-rich layer	d (nm)	phases in Ru-rich layer	Δd/d (%)
1.94	amorphous + microcrystalline	2.19	Ru (agglomerated)	12.7
4.98	crystalline	5.44	Ru	9.3
10.12	elemental Ru	10.55	Ru	4.2

XI. FIGURE CAPTIONS

Figure 1.--- Specimen preparation of cross-sectional TEM samples: a) obtaining sample, b) sandwich of slabs, c) mechanical grinding, d) polishing, e) place on TEM grids, f) ion milled,

Figure 2.--- Plan-view TEM specimen preparation: a) place grids on glass slide by wax, b) sputtered samples, c) soaked in acetone to dissolved the wax, d) multilayer spanning the holes of the grids.

Figure 3.--- X-ray reflectance profile of a 7 nm as-prepared W/C multilayer, showing the incidence beam, the total reflection region, and low order Bragg peaks.

Figure 4.--- Comparison between as-prepared and annealed x-ray profile. Shifts of the Bragg peaks to lower angles indicate expansion of the period after annealing.

Figure 5.--- X-ray profiles of multilayers prepared on optical flat and Si substrate, showing the effects of the substrate on peak reflectance.

Figure 6.--- X-ray profiles of as-prepared and annealed 7 nm WC/C multilayers.

Figure 7.--- Full cross-sectional image of a 7 nm period W/C multilayer.

Figure 8.--- Cross-sectional HRTEM images of 1 nm W/C. Diffraction spots of the multilayer period are seen in the diffraction pattern.

Figure 9.-- Cross-sectional HRTEM images of annealed 1 nm W/C.

Figure 10.-- Cross-sectional HRTEM images and SAD patterns of a) as-prepared and b) annealed 2 nm W/C.

Figure 11.-- Cross-sectional HRTEM images of 4 nm W/C.

Figure 12.-- Cross-sectional HRTEM images of 7 nm W/C.

Figure 13.-- Cross-sectional HRTEM images of 12 nm W/C.

Figure 14.-- Plan-view TEM images of a) as-prepared and b) annealed 2 nm W/C.

Figure 15.-- Plan-view TEM images of 4 nm W/C.

Figure 16.-- Plan-view TEM images of 7 nm W/C.

Figure 17.-- Plan-view TEM images of 12 nm W/C, showing a) bcc W, b) crystalline W_2C.

Figure 18.-- Close up images of cross-sectional HRTEM of as-prepared 12 nm W/C, showing crystalline fringes inside the W-rich layers.

Figure 19.-- Cross-sectional HRTEM images of a) as-prepared and b) annealed 2 nm WC/C.

Figure 20.-- Cross-sectional HRTEM images of 7 nm WC/C.

Figure 21.-- Cross-sectional HRTEM images of 12 nm WC/C.

Figure 22.-- Plan-view TEM images of a) as-prepared and b) annealed 2 nm WC/C.

Figure 23.-- Plan-view TEM images of 7 nm WC/C.

Figure 24.-- Plan-view TEM images of 12 nm WC/C.

Figure 25.-- Cross-sectional HRTEM images of a)as-prepared and b) annealed 2 nm Ru/C. The Ru layers in the as-prepared sample agglomerated to form elemental Ru crytallites after annealing.

Figure 26.-- Low magnification cross-sctional HRTEM images of annealed 2 nm Ru/C. The layered structures are still apparent at this magnification.

Figure 27.-- Cross-sectional HRTEM images of 5 nm Ru/C.

Figure 28.-- High magnification cross-sectional HRTEM image of an as-prepared 4.3 nm period Ru/C multilayer, showing the polycrystalline structure ins the Ru-rich layers and the same symmetry in the diffraction pattern as in the as-prepared 5 nm multilayer.

Figure 29.-- Cross-sectional HRTEM images of 10 nm Ru/C.

Figure 30.-- Plan-view TEM images of a) as-prepared and b) annealed 2 nm Ru/C.

Figure 31.-- Plan-view TEM images of 5 nm Ru/C.

Figure 32.-- Plan-view TEM imagesof 10 nm Ru/C.

Figure 33.-- W-C phase diagram.

Figure 34.-- Plan-view TEM SAD patterns of 2, 4, 7, and 12 nm a) as-prepared and b) annealed W/C samples, which summarizes the microstructures in the layers.

Figure 35.-- Plan view SAD patterns of 2, 7, and 12 nm WC/C.

Figure 36. -- Ru-C phase diagram.

Figure 37.-- Cross-sectional TEM SAD patterns of 2, 5, and 10 nm a) as-prepared and b) annealed Ru/C multilayers, showing the microstructures of the Ru-rich layers.

Figure 38.-- Plan-view SAD patterns of Ru/C multilayers.

Figure 39.-- Enlarged cross-sectional HRTEM images of annealed 12 nm a) W/C and b) WC/C multilayers, showing the difference between crystalline-amorphous and amorphous-amorphous interfaces.

Figure 40.-- Enlarged HRTEM cross-sectional images of a) as-prepared and b) annealed 10 nm Ru/C multilayers. Arrows B show a grain boundary of Ru crystallites causing roughness at the interface.

Figure 41.-- Abolute expansion plots of W/C, WC/C, and Ru/C multilayers on annealing.

Figure 42.-- Relative expansion plots of W/C, WC/C, and Ru/C multilayers on annealing.

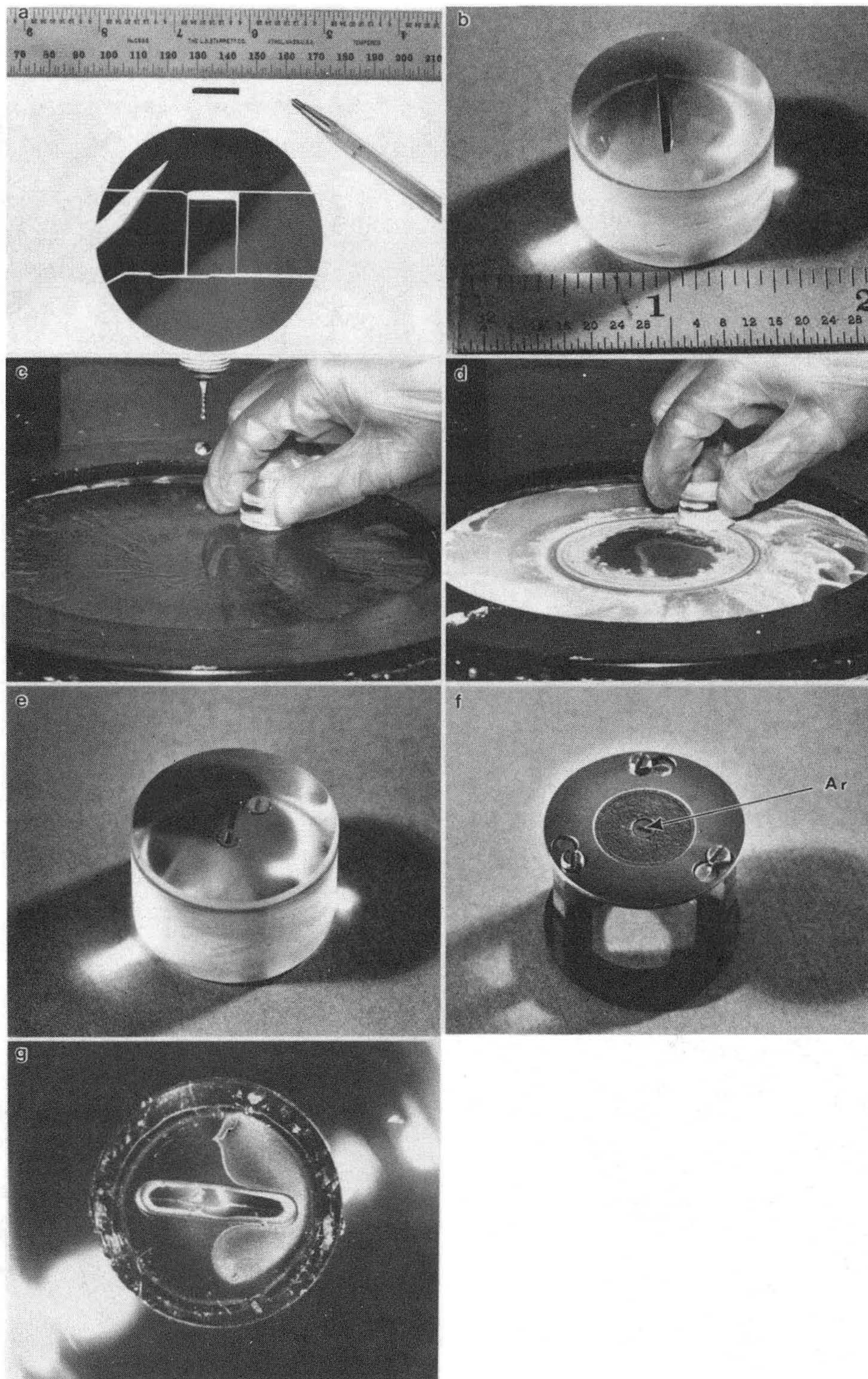

Figure 1 XBB890-10823A

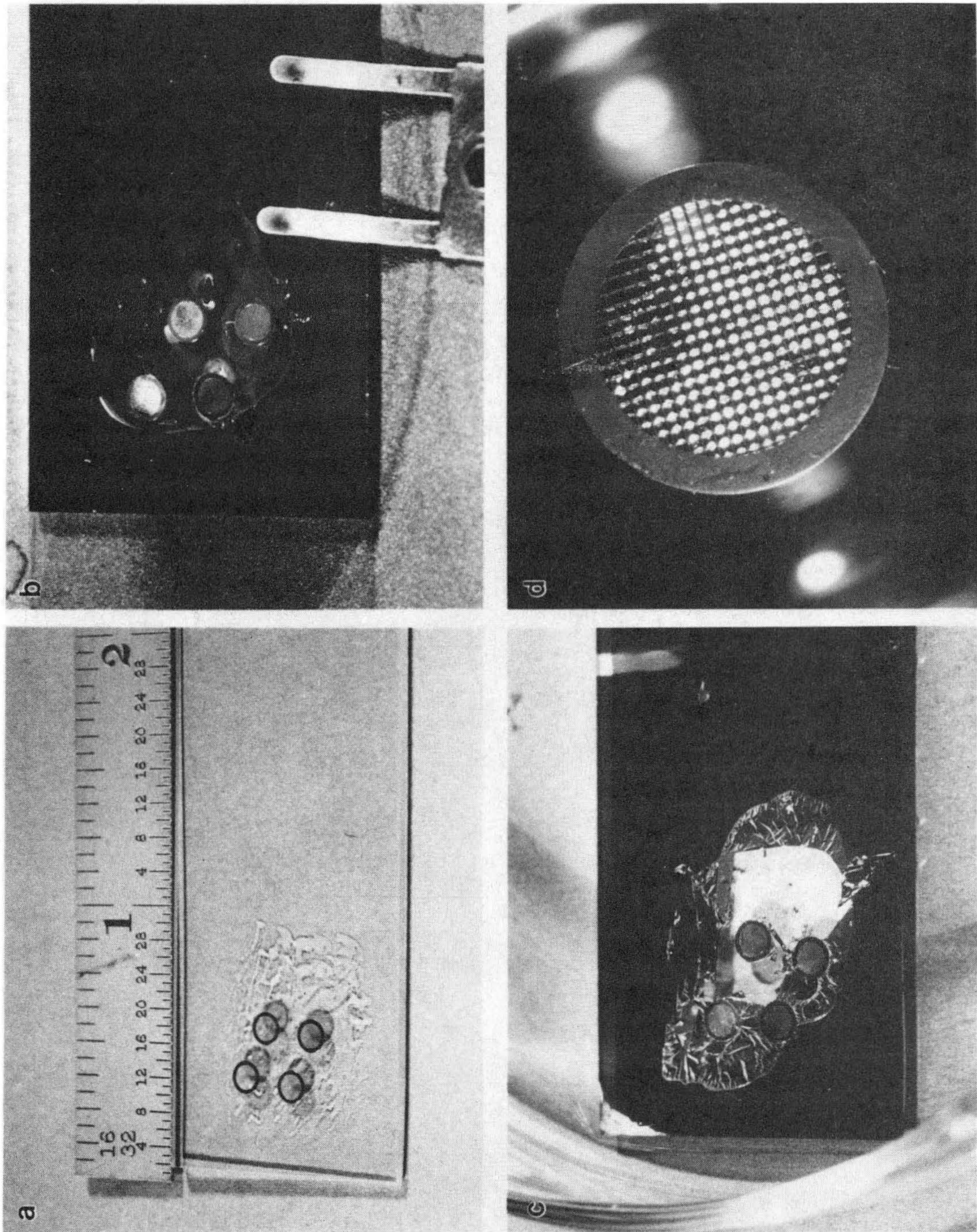

Figure 2

XBB902-1207A

Reflectance profile of 7 nm W/C

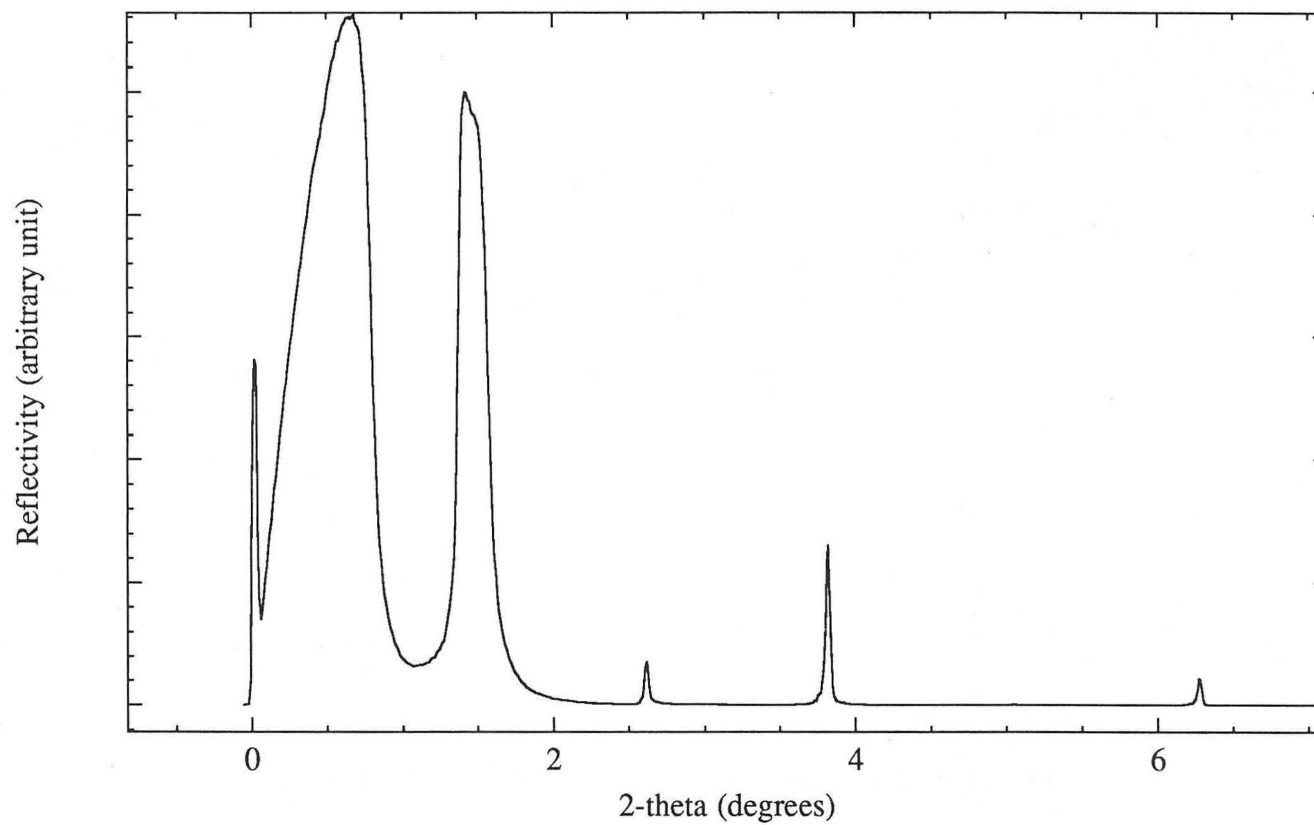

Figure 3

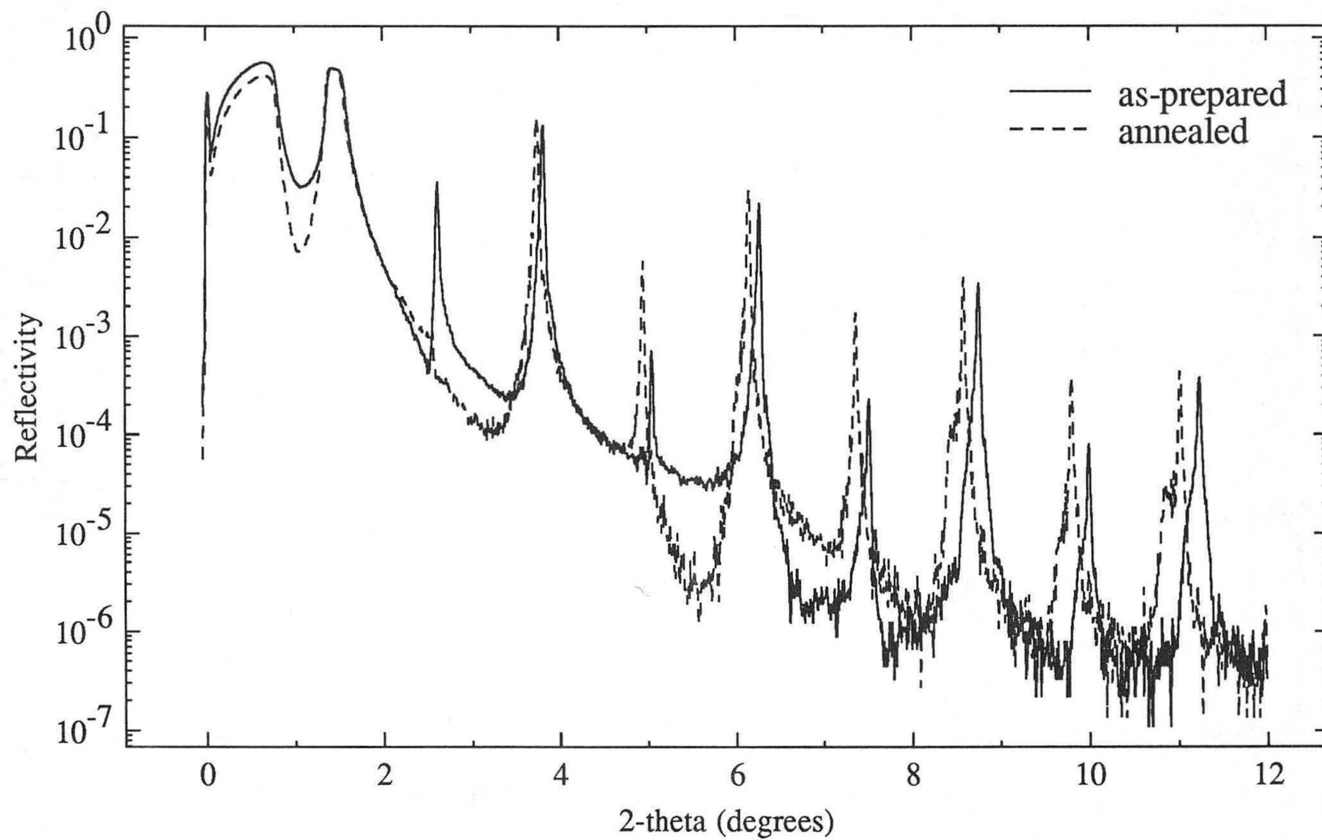

Figure 4

Peak reflectances from different substrates

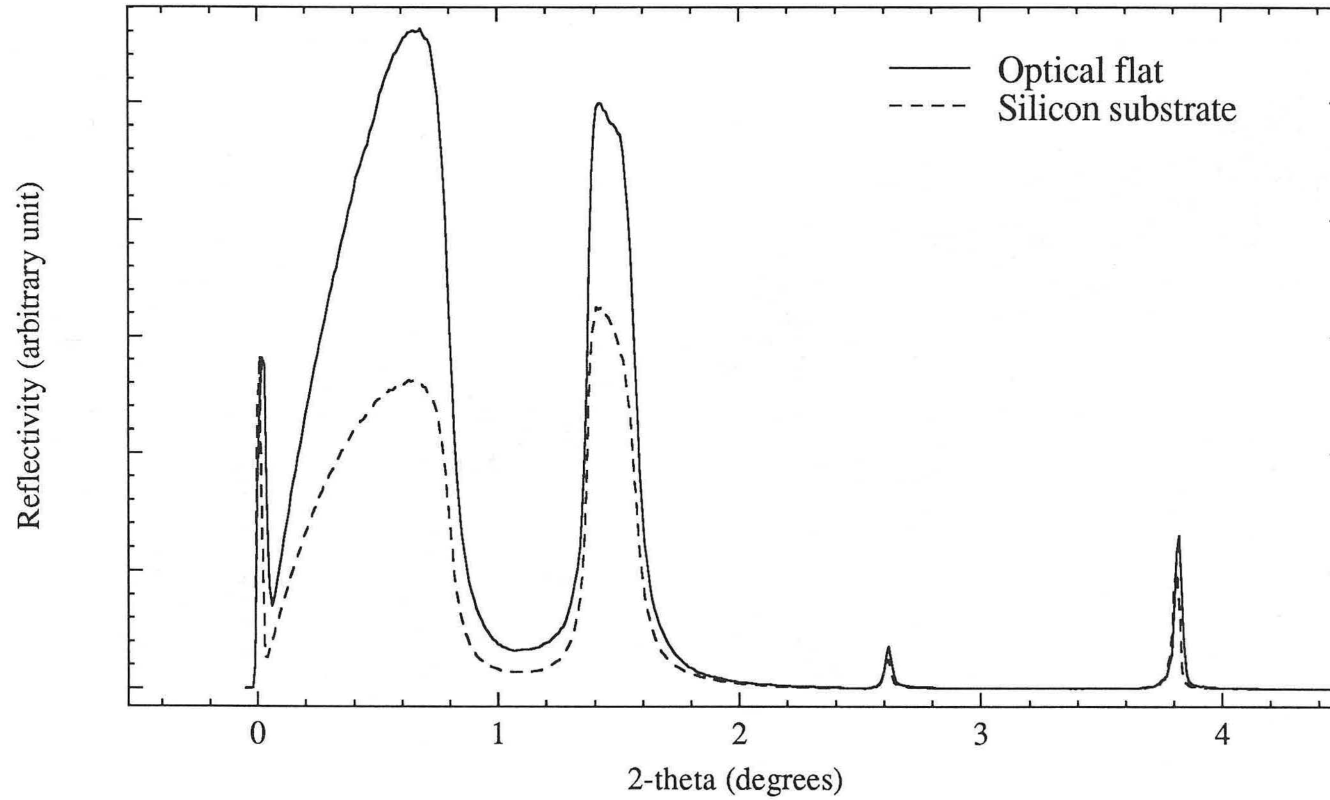

Figure 5

Reflectance profiles of 7 nm WC/C multilayers

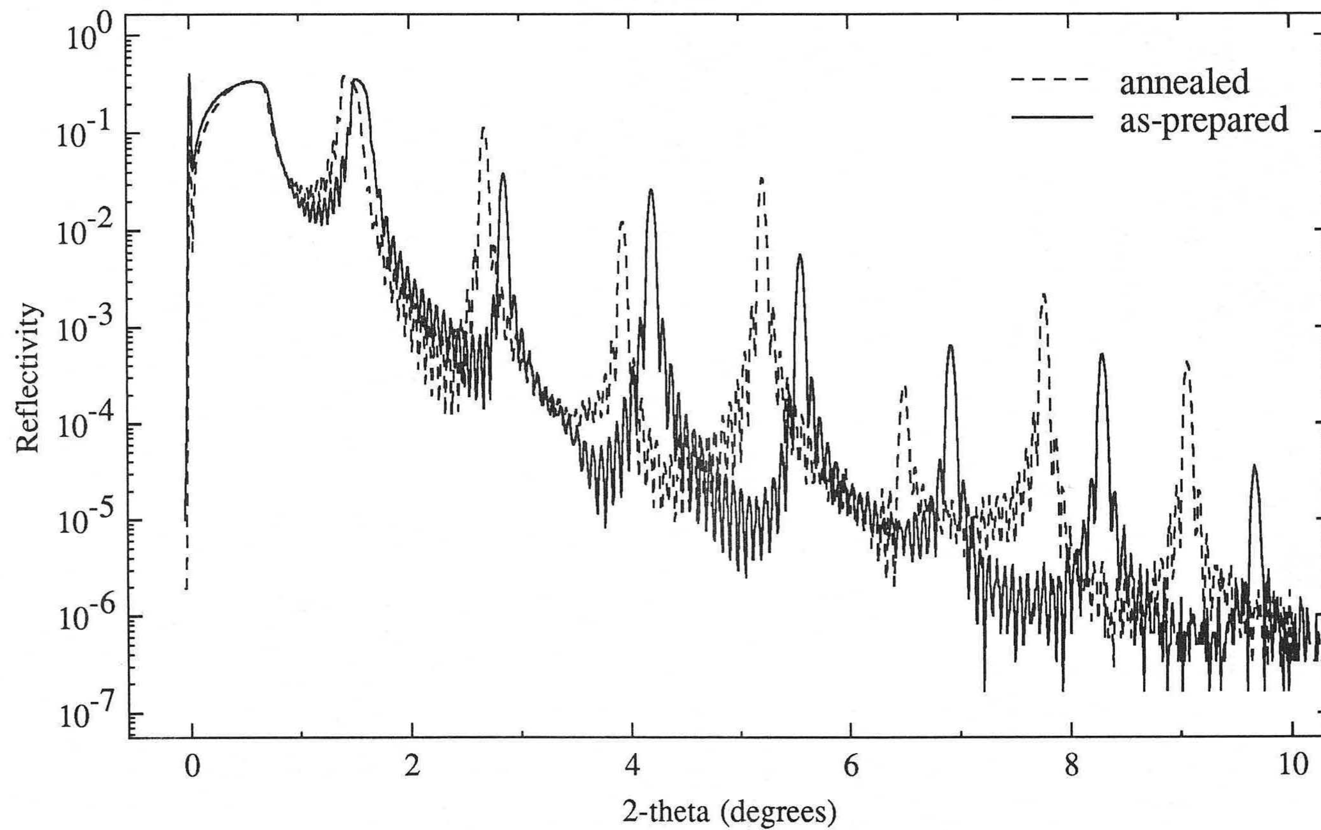

Figure 6

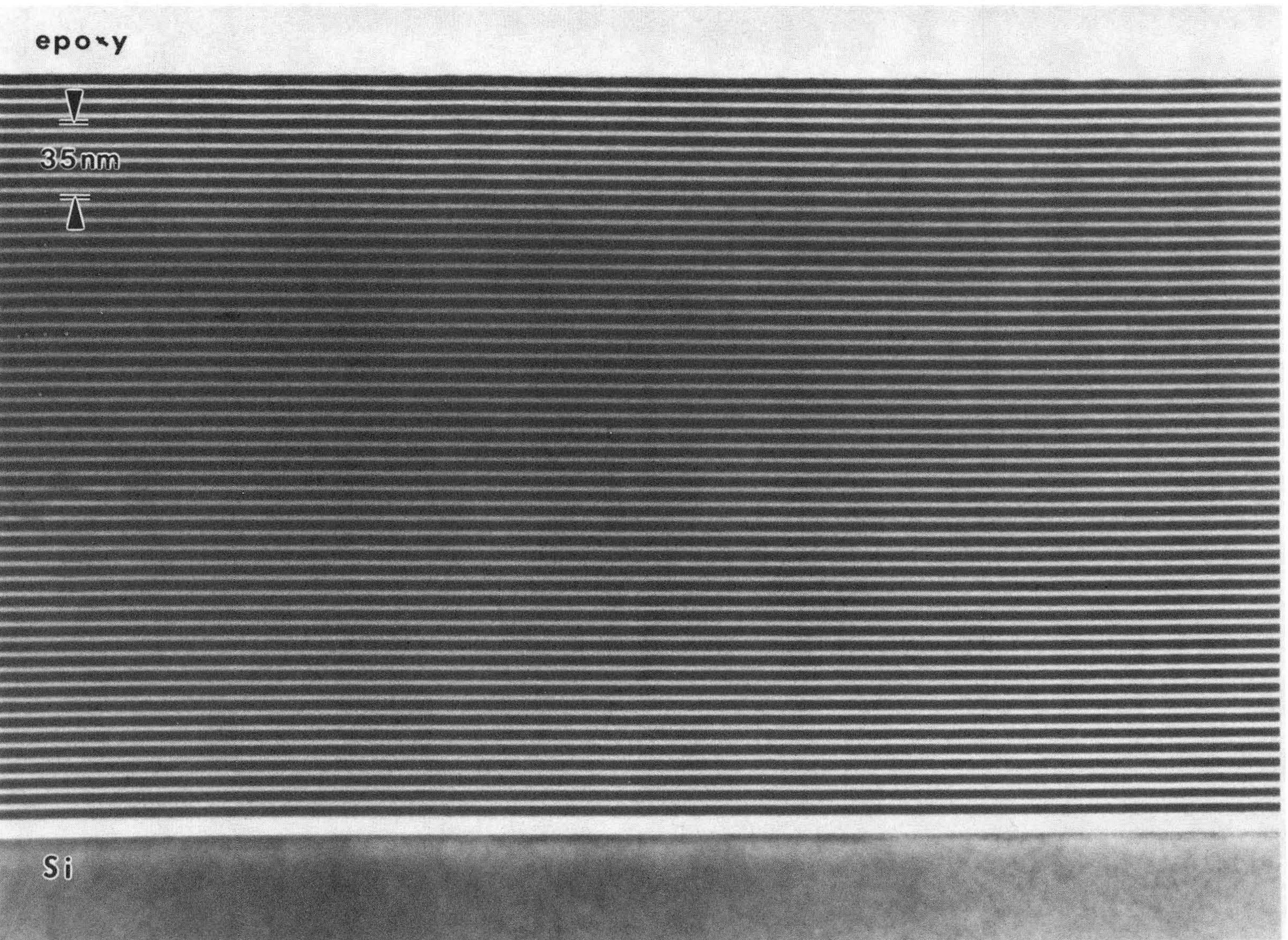

XBB904-3492

Figure 7

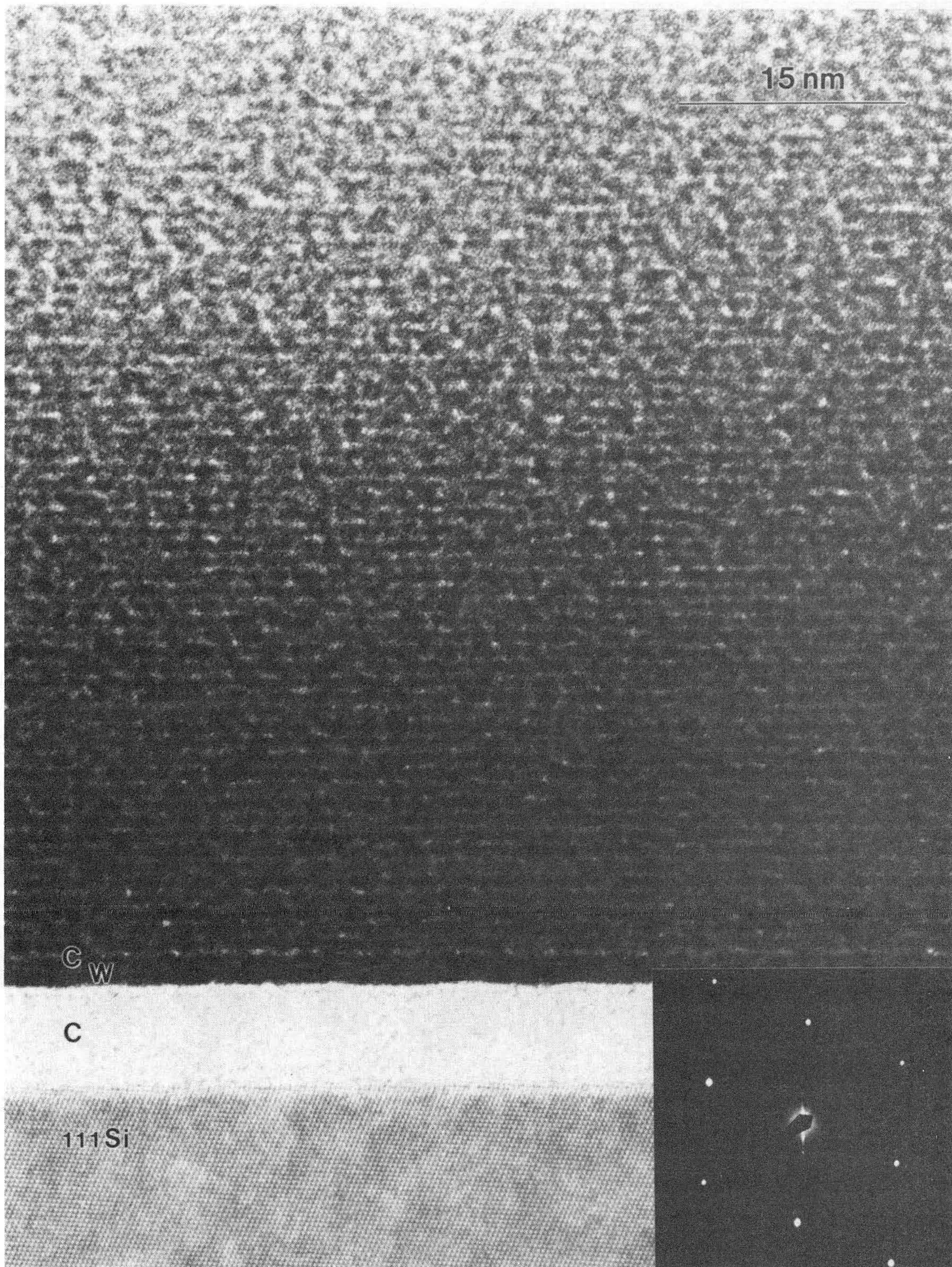

XBB904-3406

Figure 8

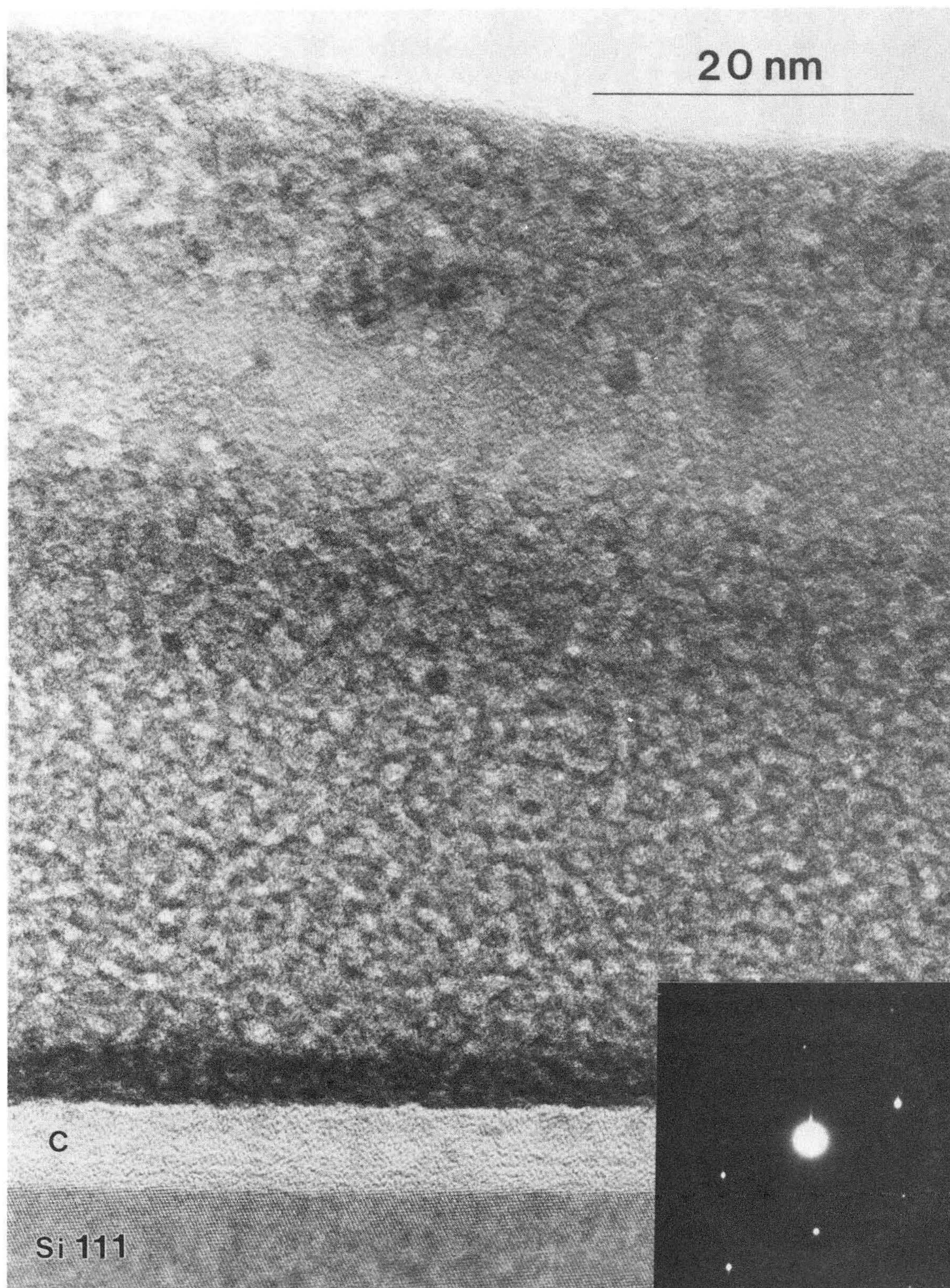

Figure 9

XBB902-1223

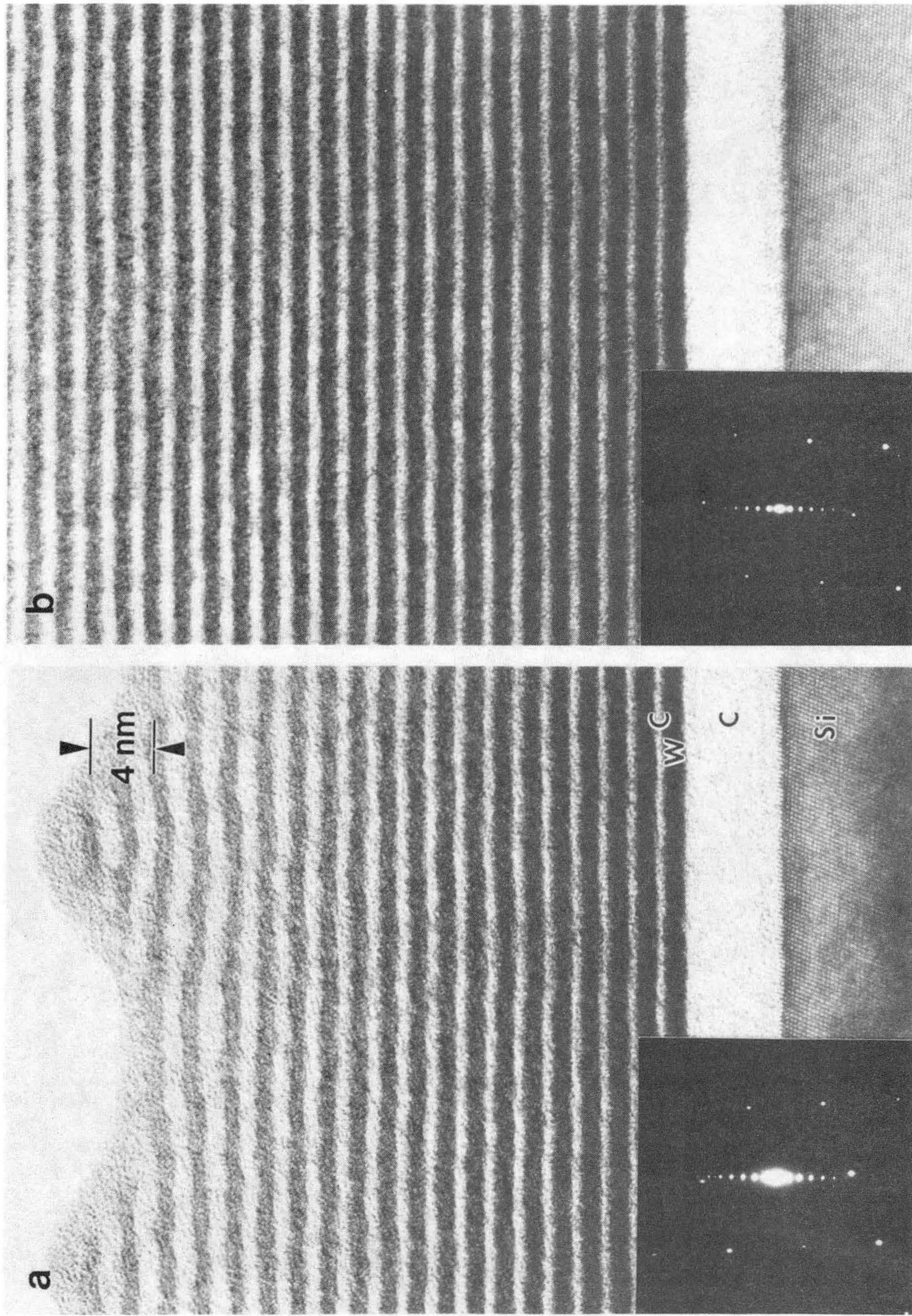

Figure 10

XBB904-2888

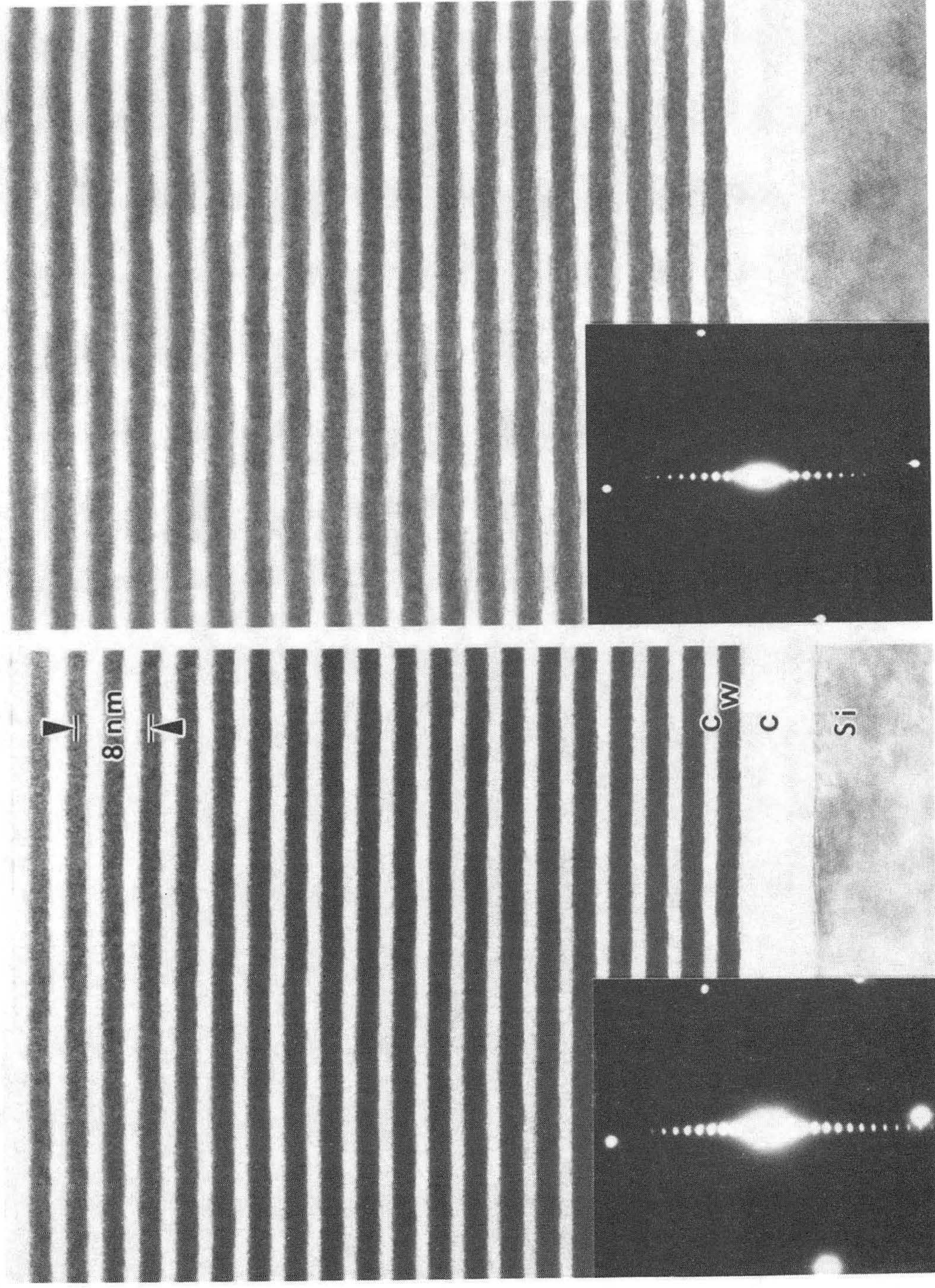

Figure 11

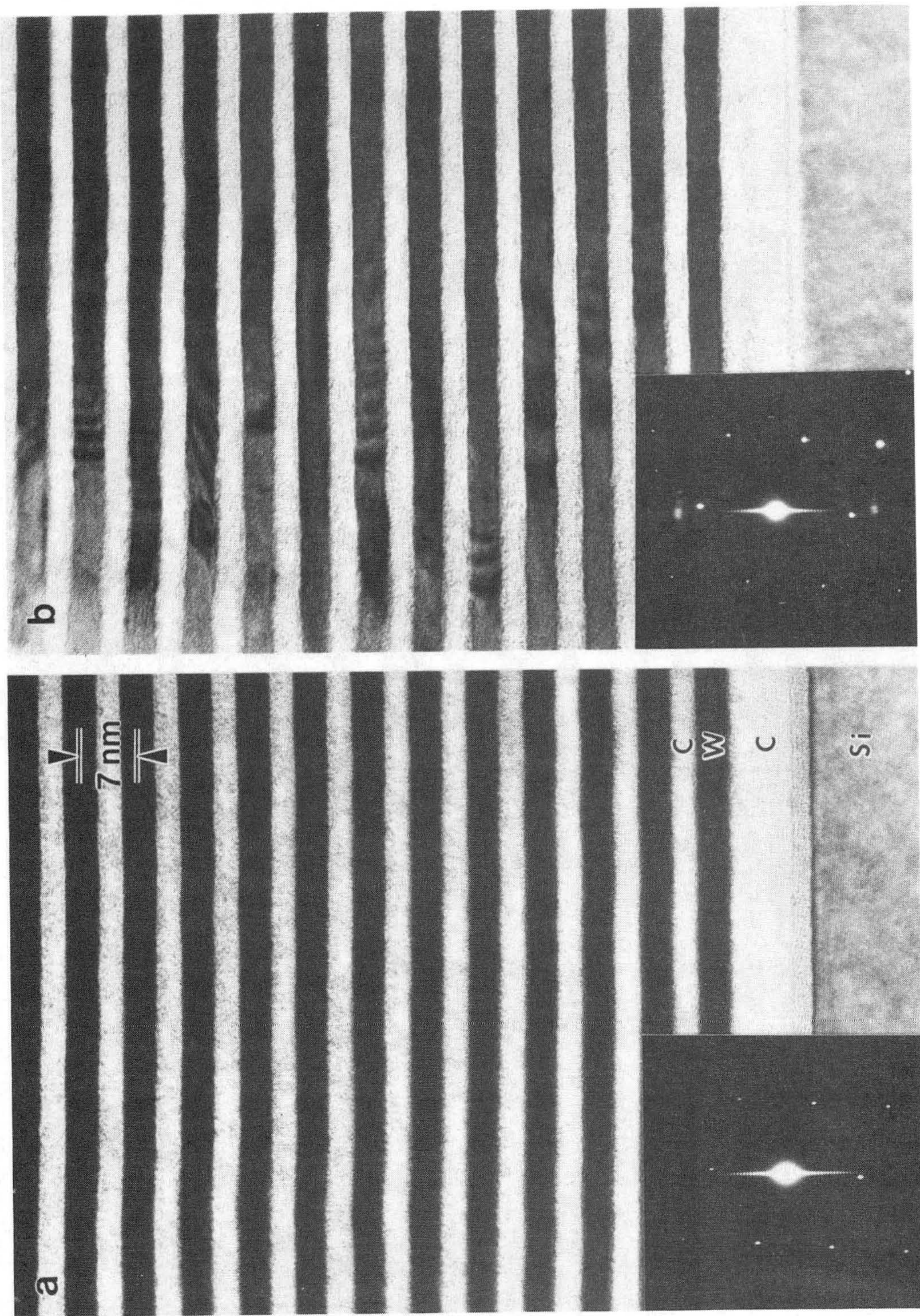

Figure 12

XBB904-2887

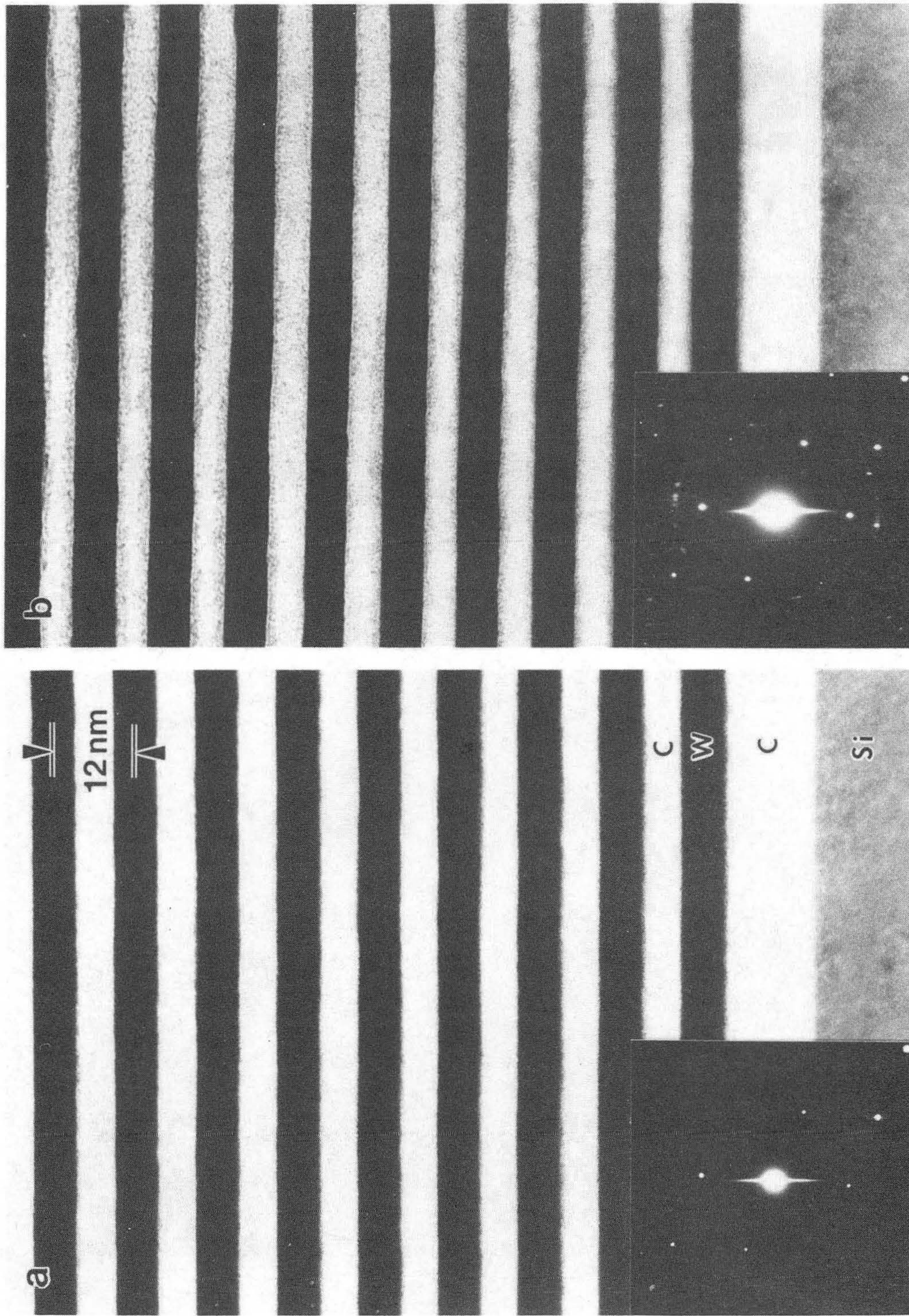

Figure 13

XBB904-2886

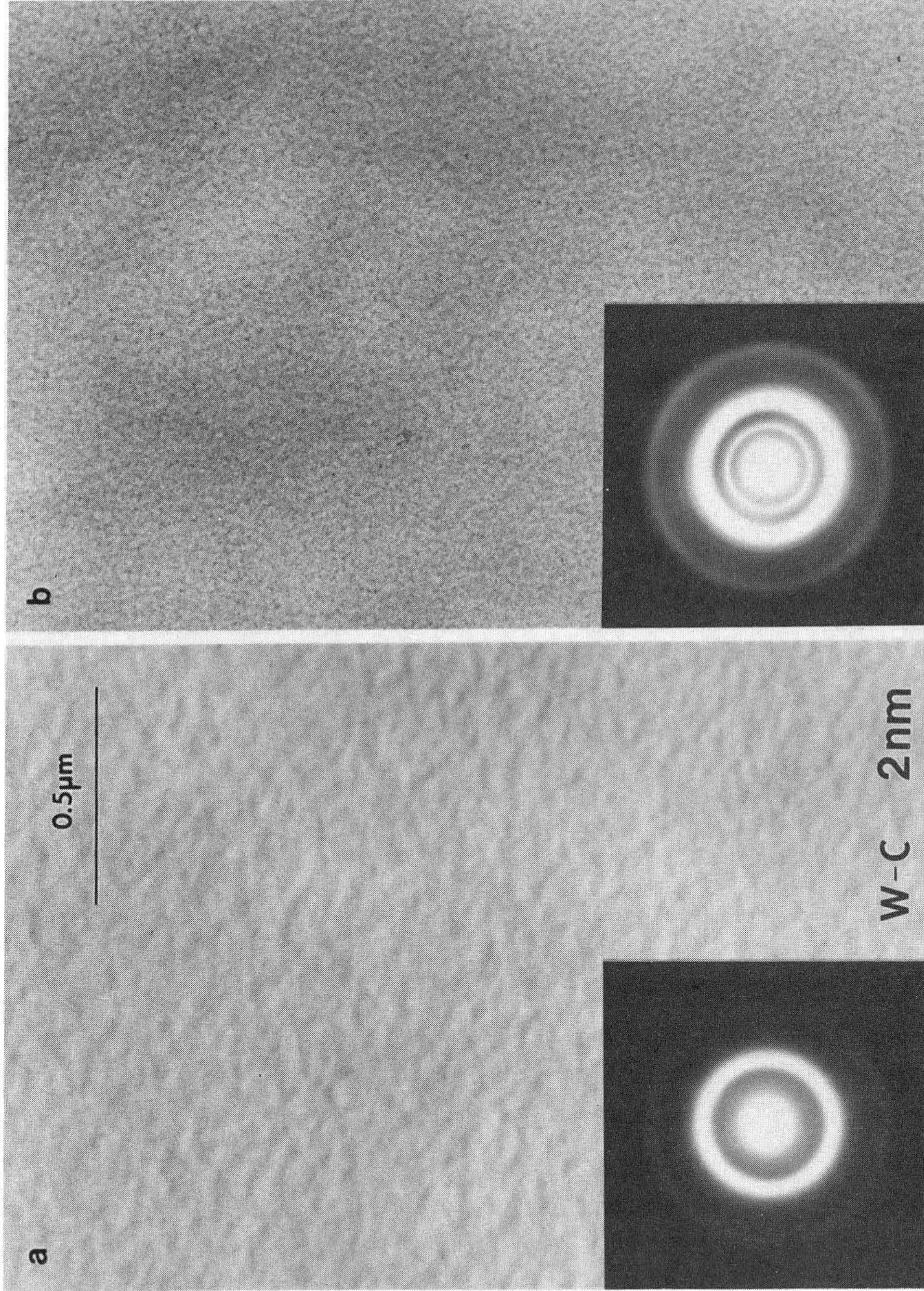

Figure 14

XBB904-3498

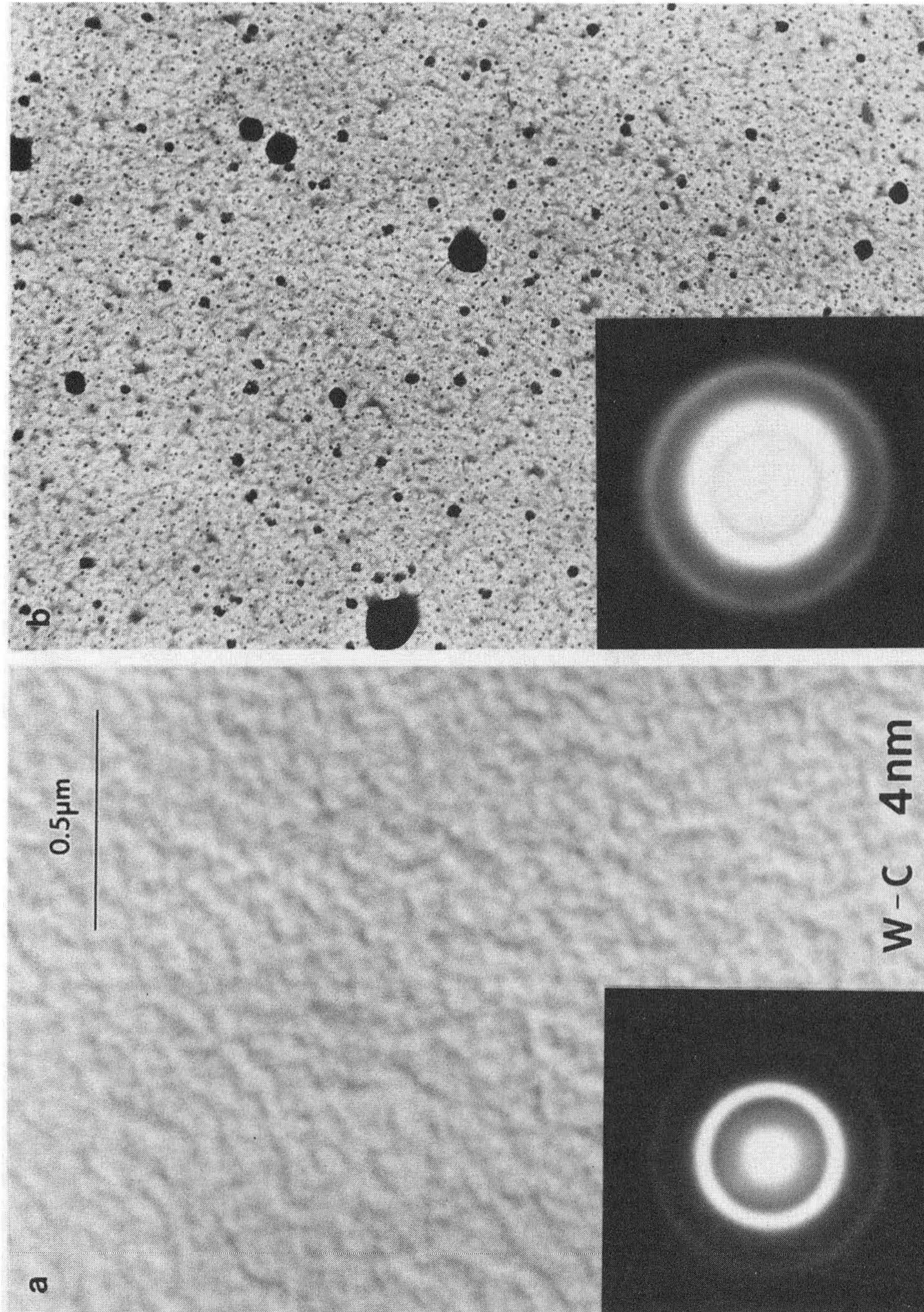

Figure 15

XBB904-3497

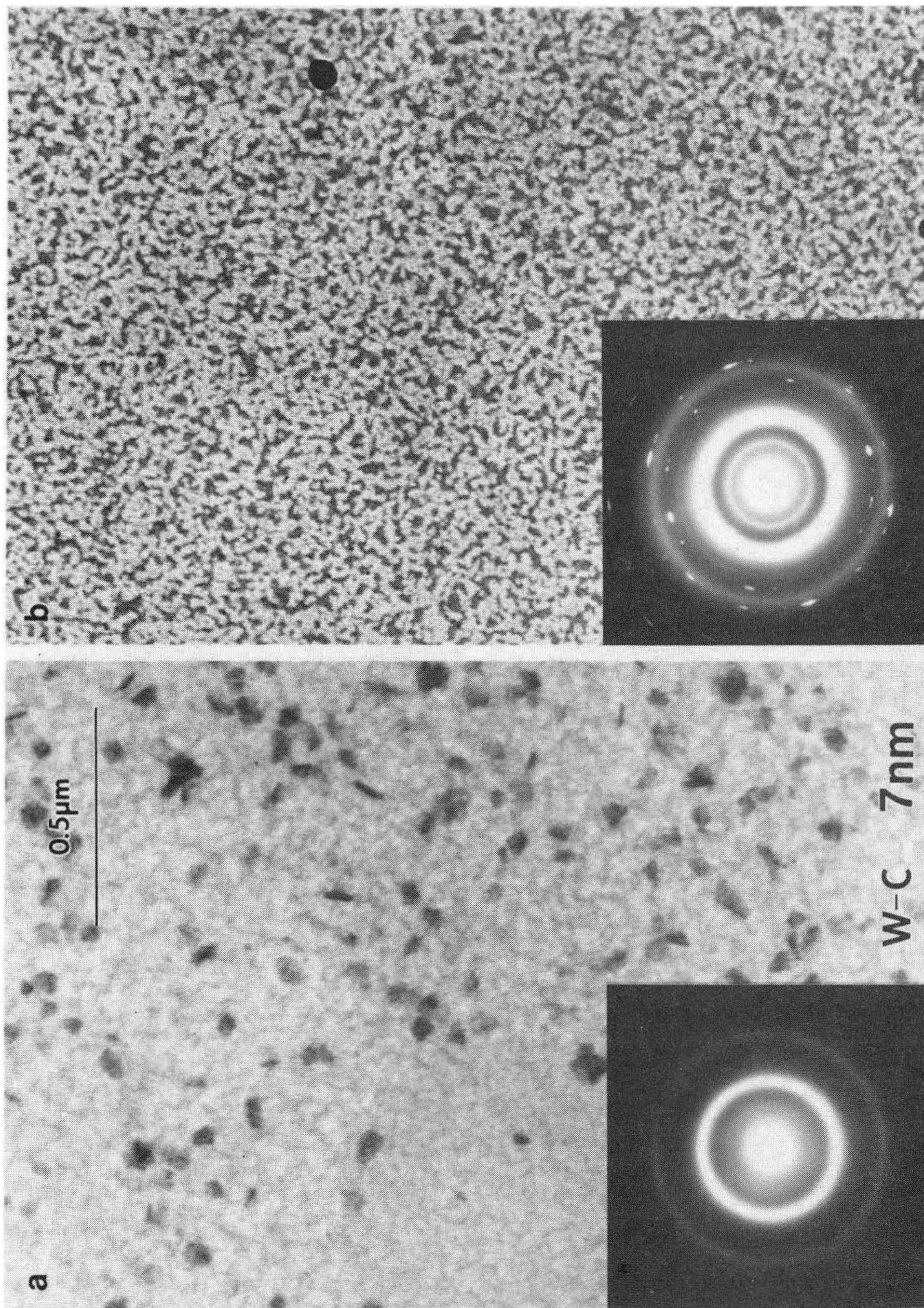

Figure 16

XBB904-3496

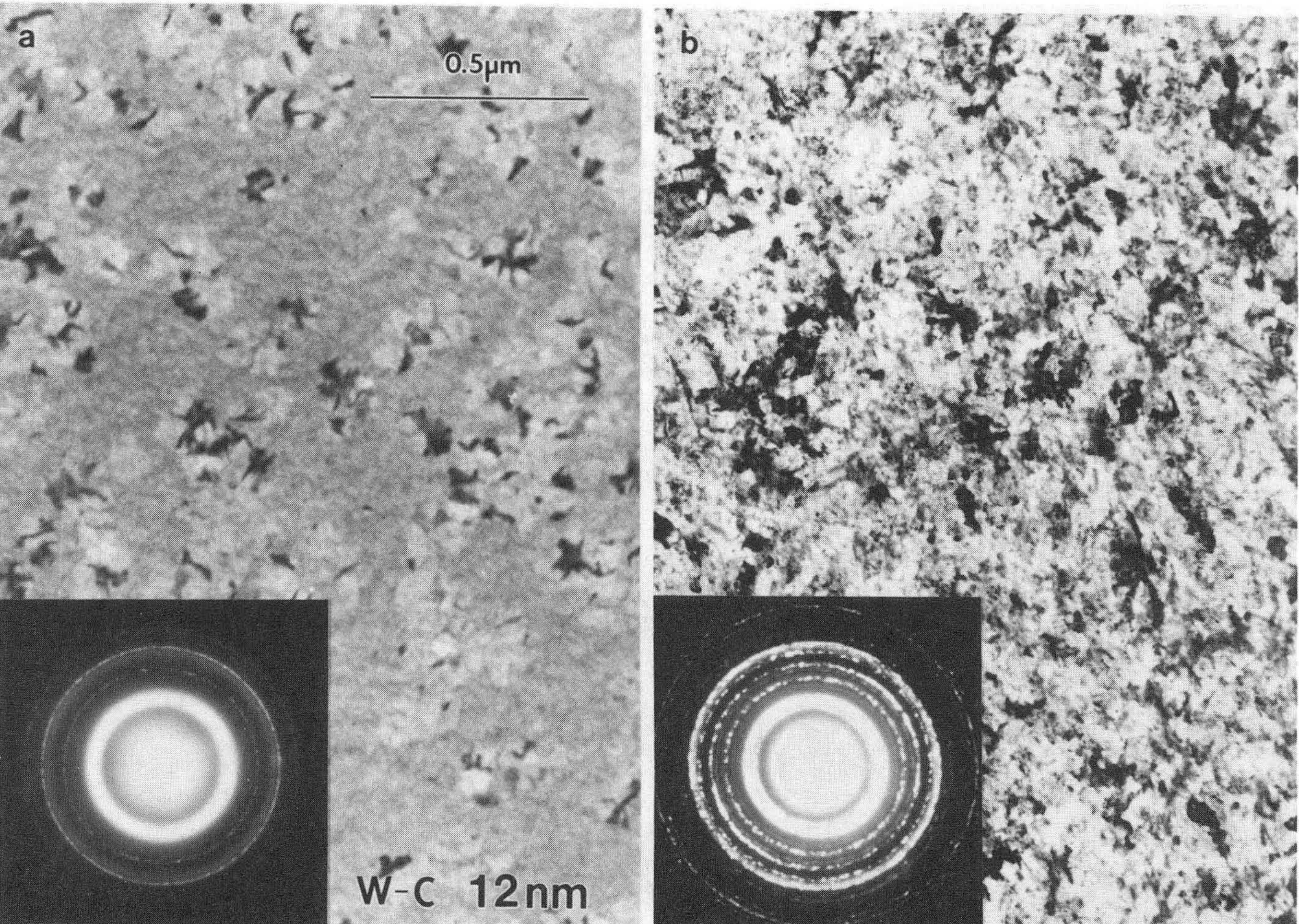

Figure 17

XBB904-3495

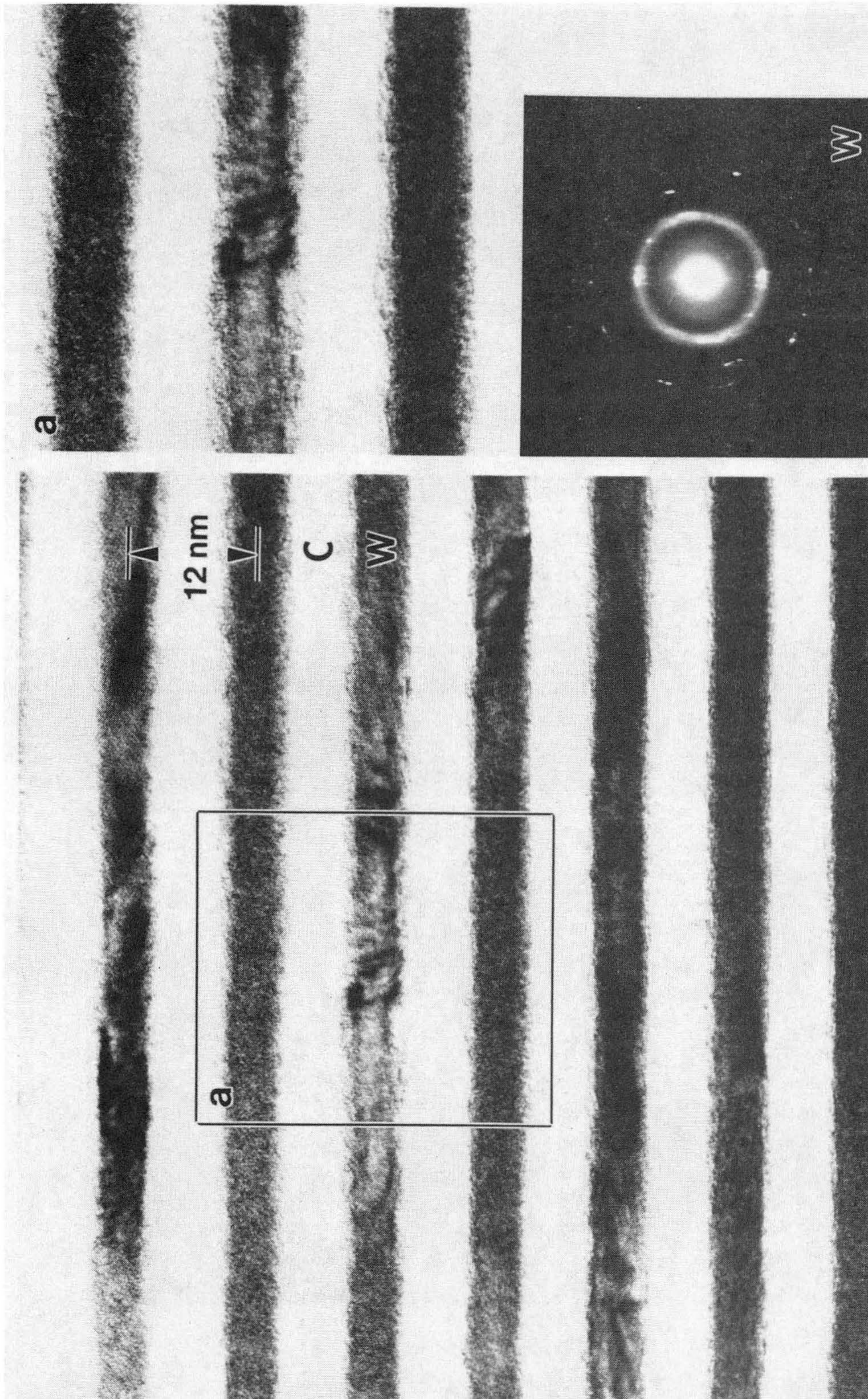

XBB904-2880

Figure 18

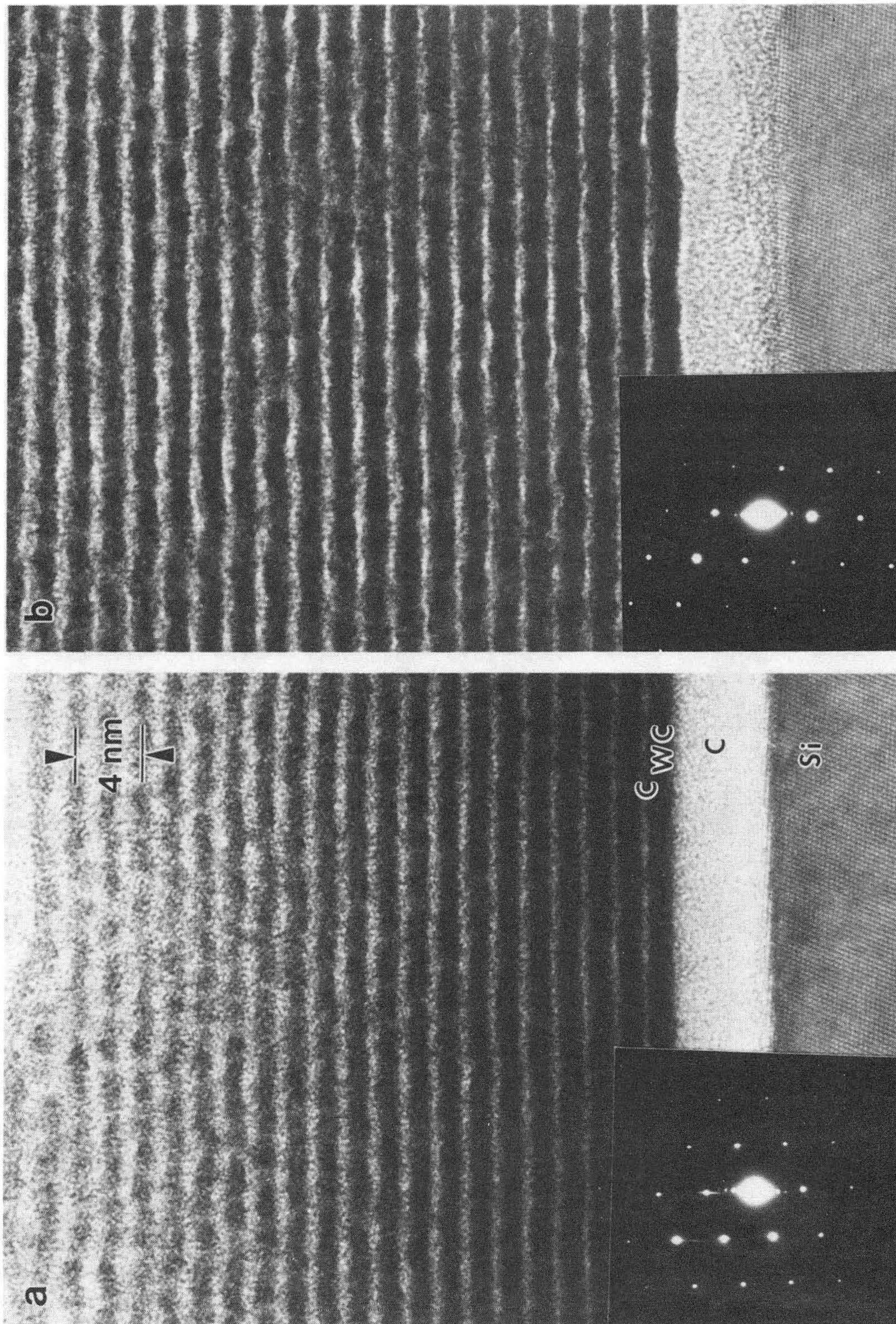

Figure 19

XBB904-2885

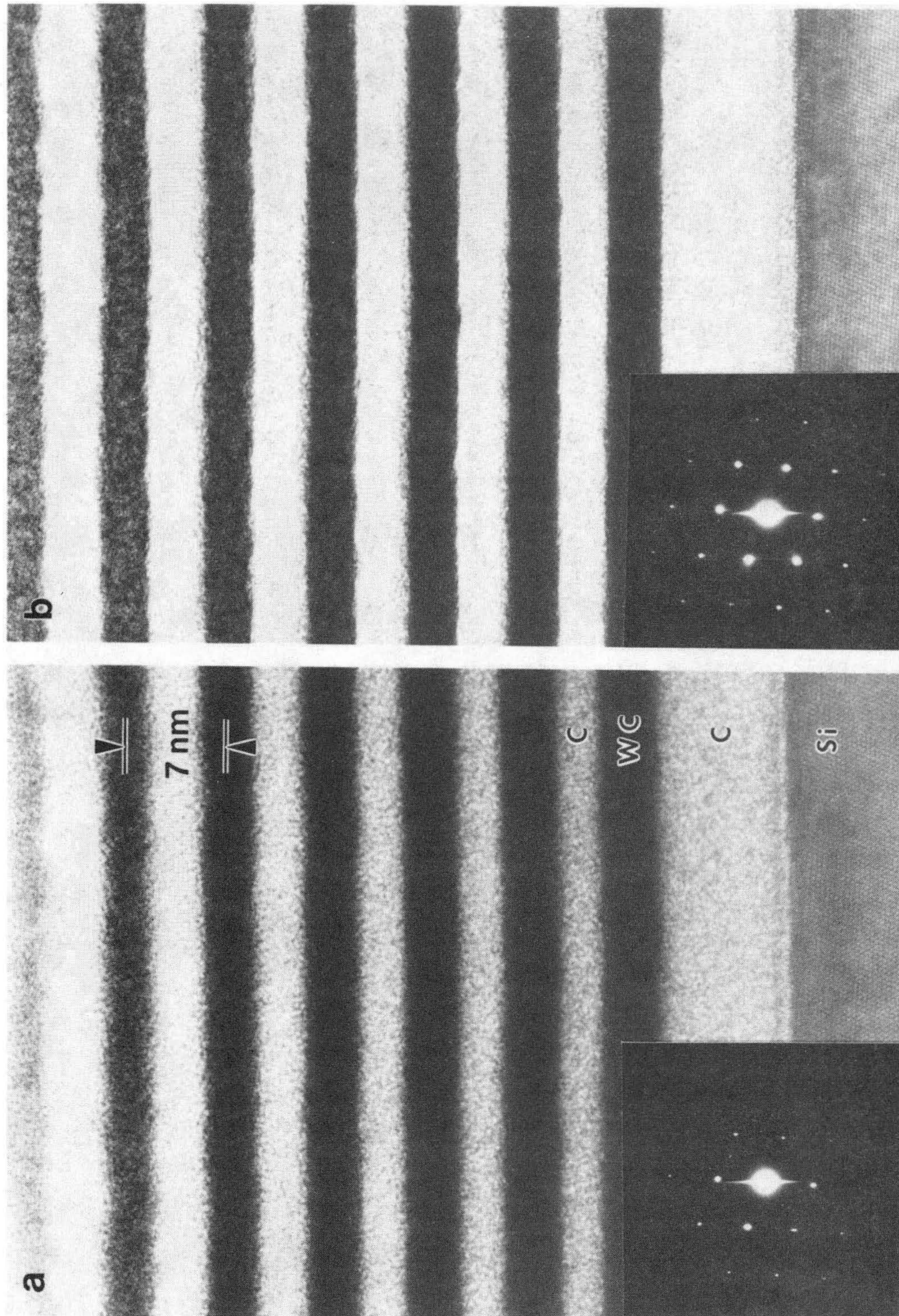

Figure 20

XBB904-2884

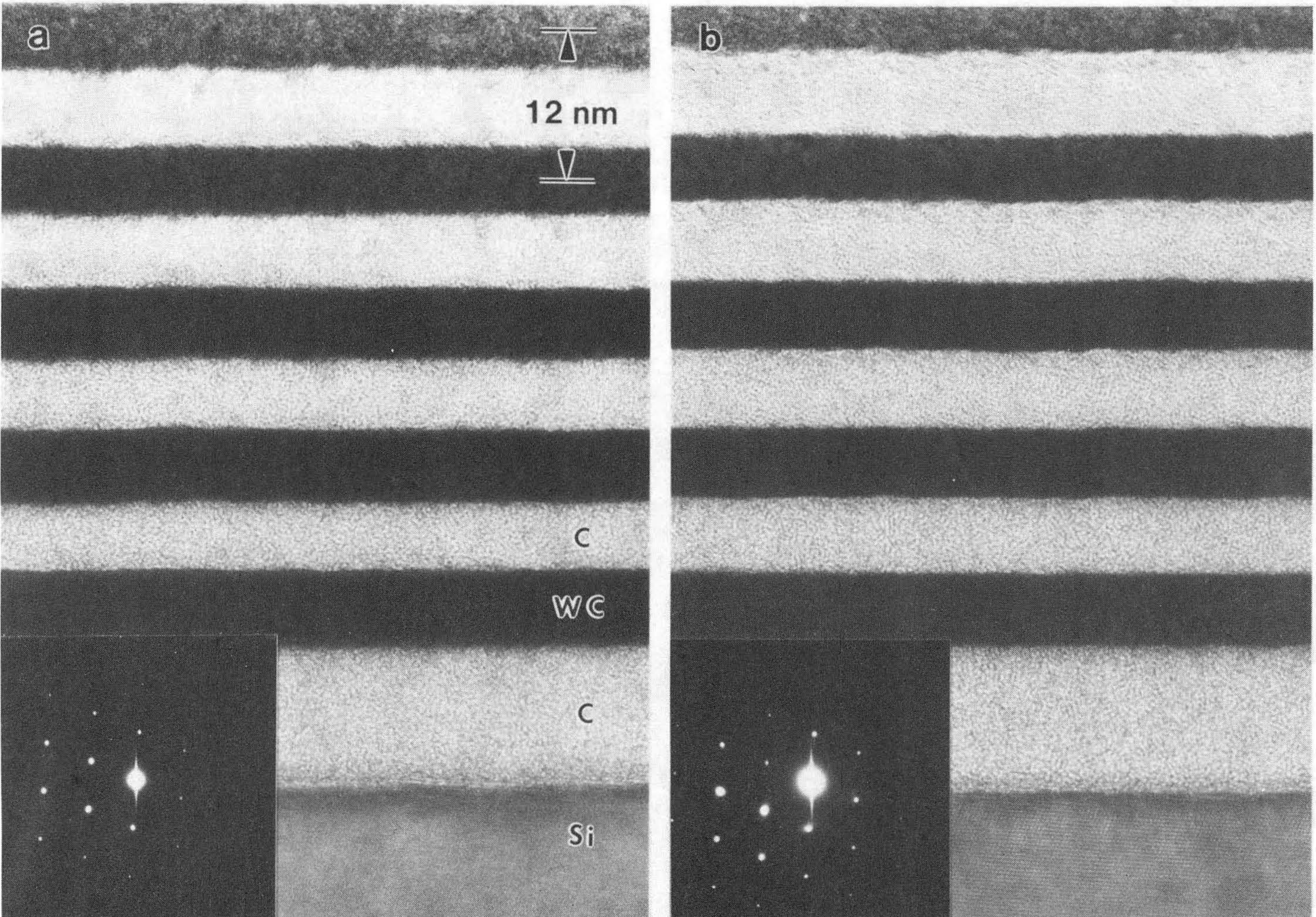

Figure 21

XBB904-2881

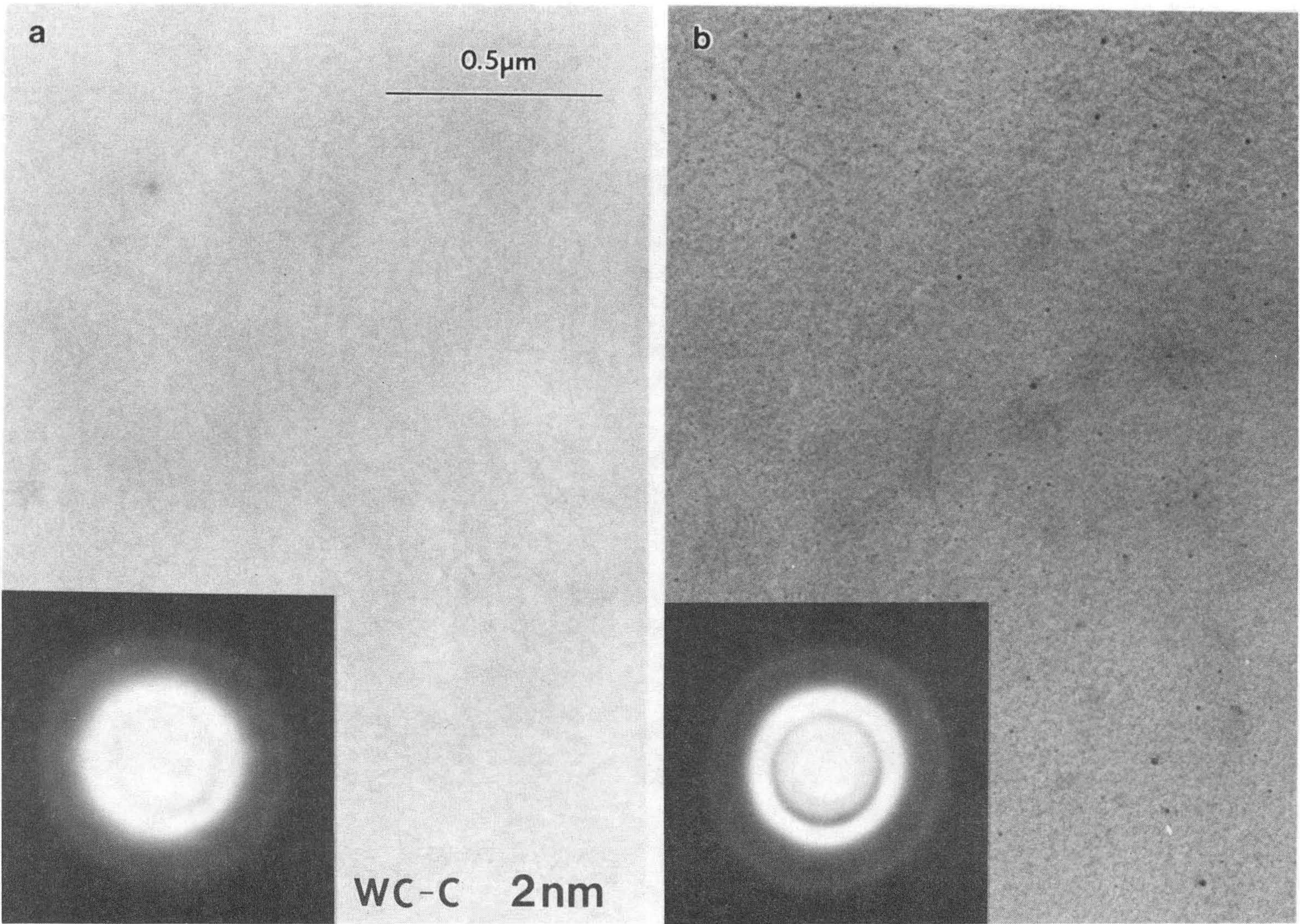

Figure 22

XBB904-3500

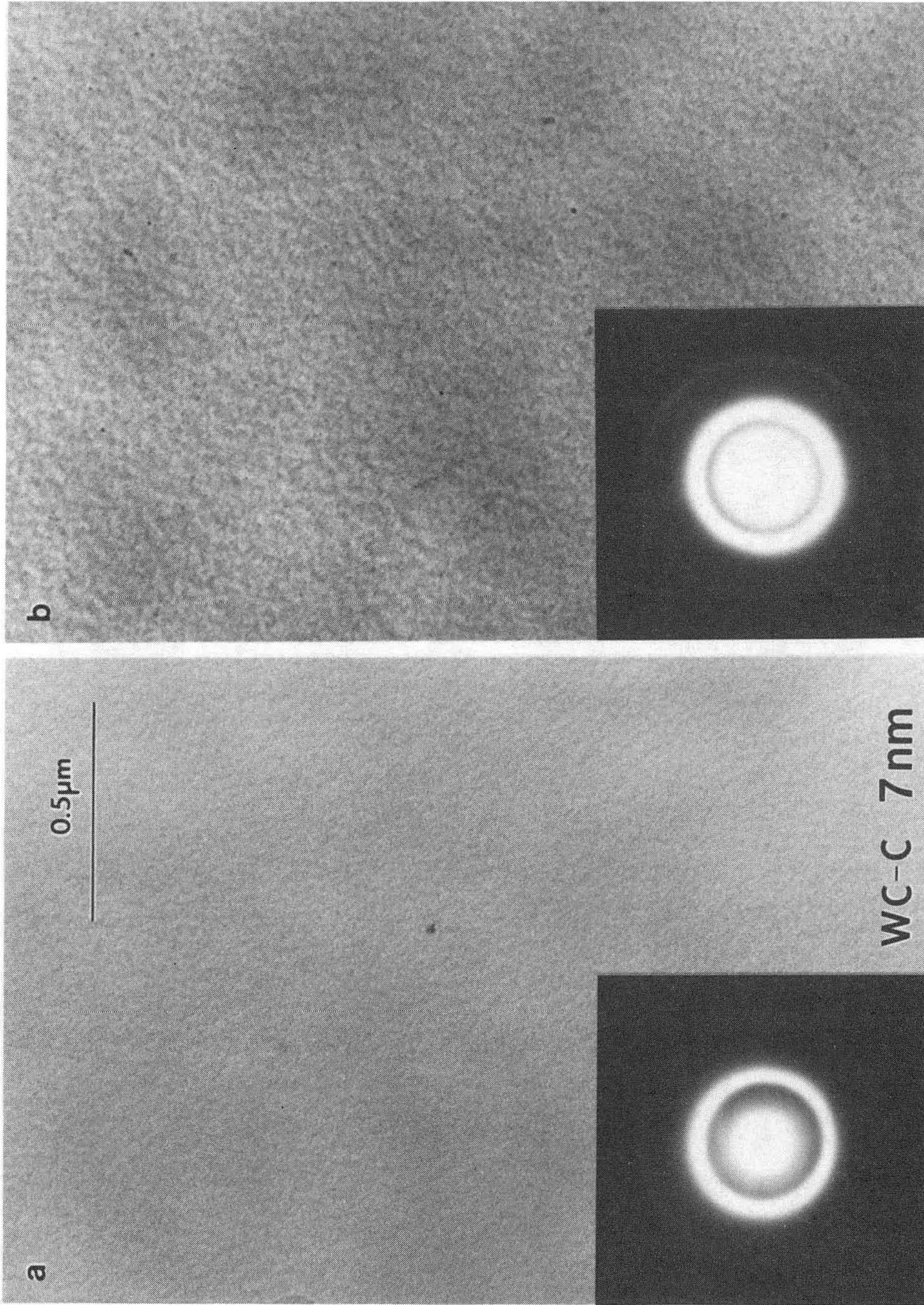

Figure 23

XBB904-3499

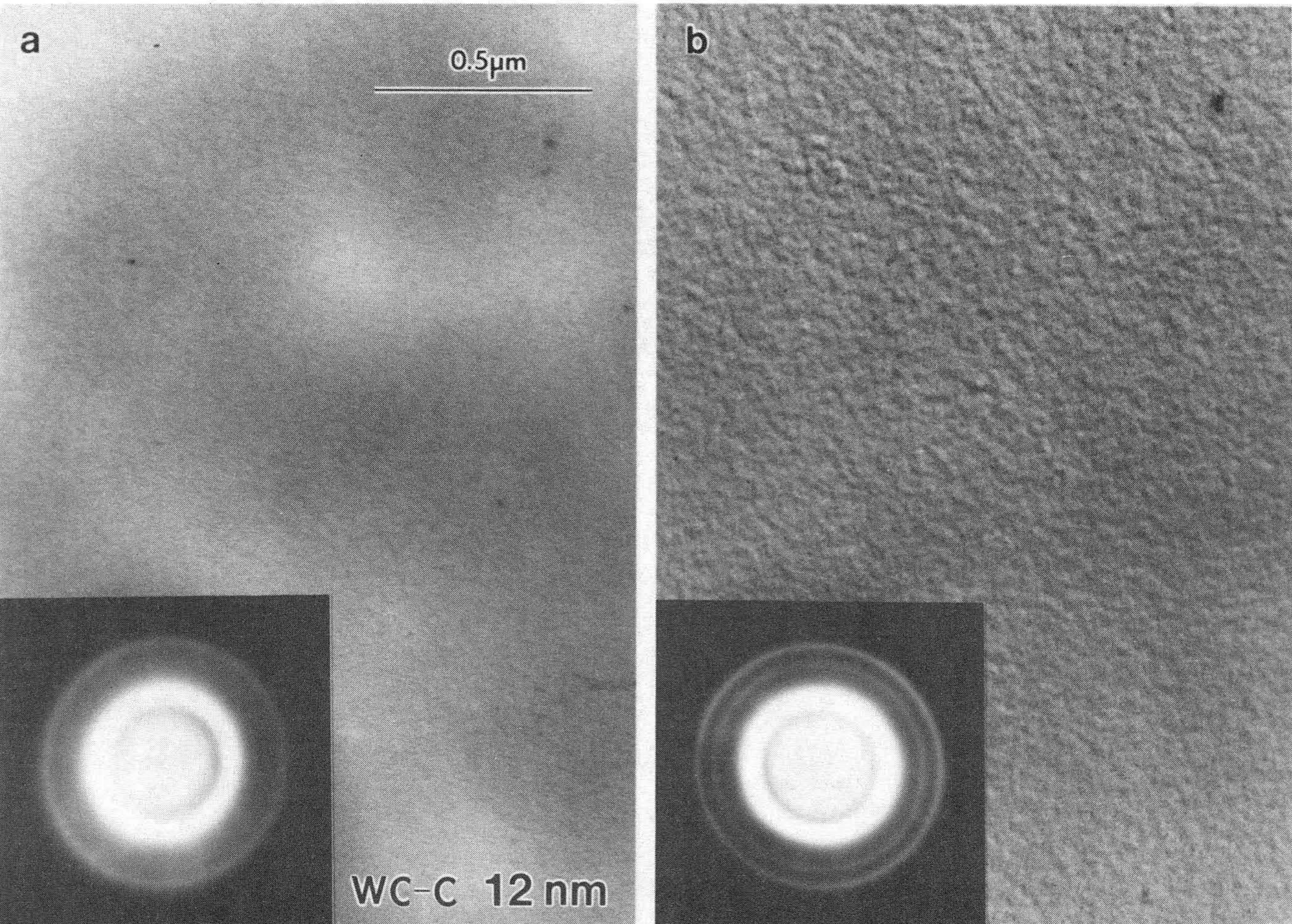

Figure 24

XBB904-2988A

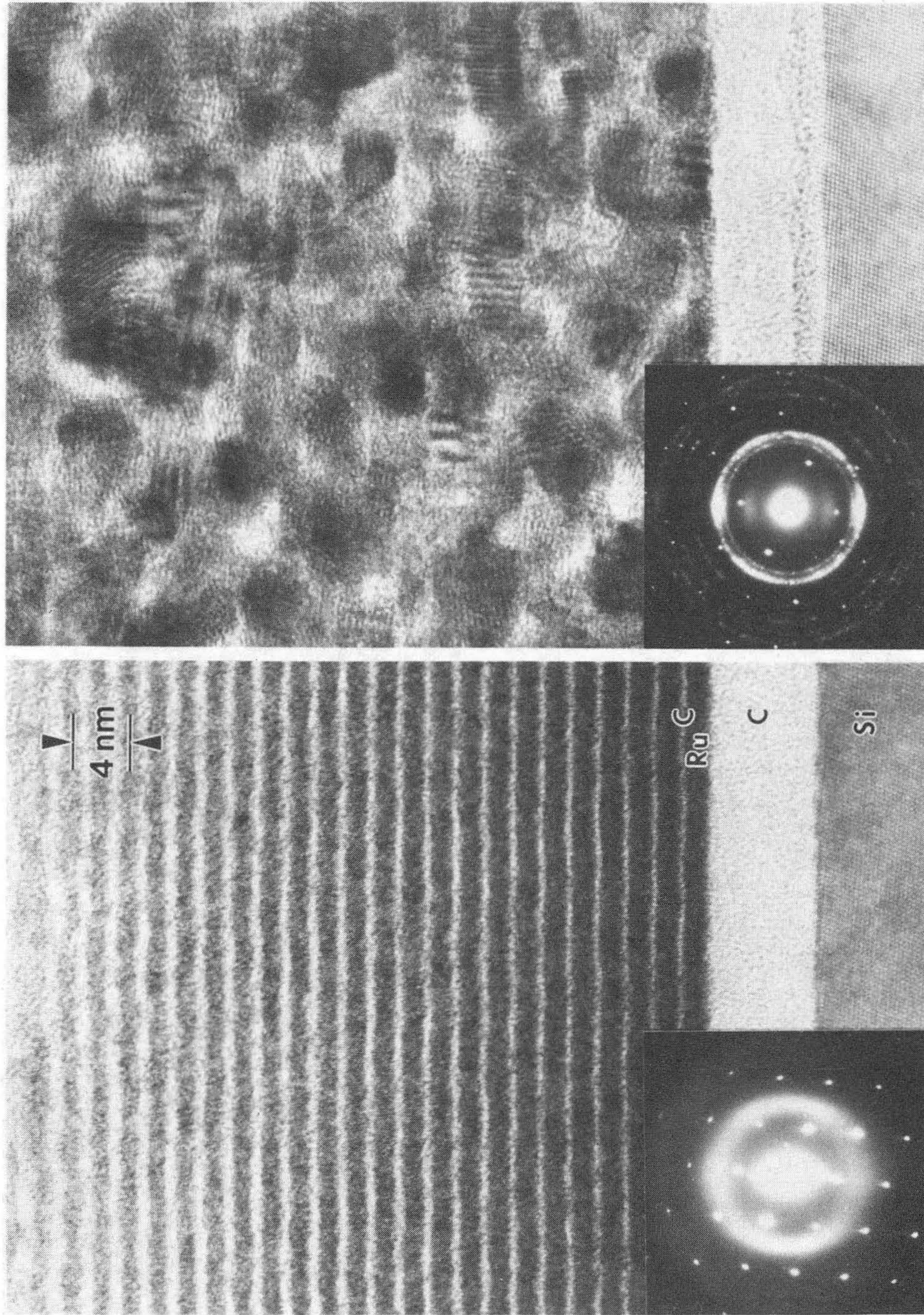

Figure 25

XBB904-3494

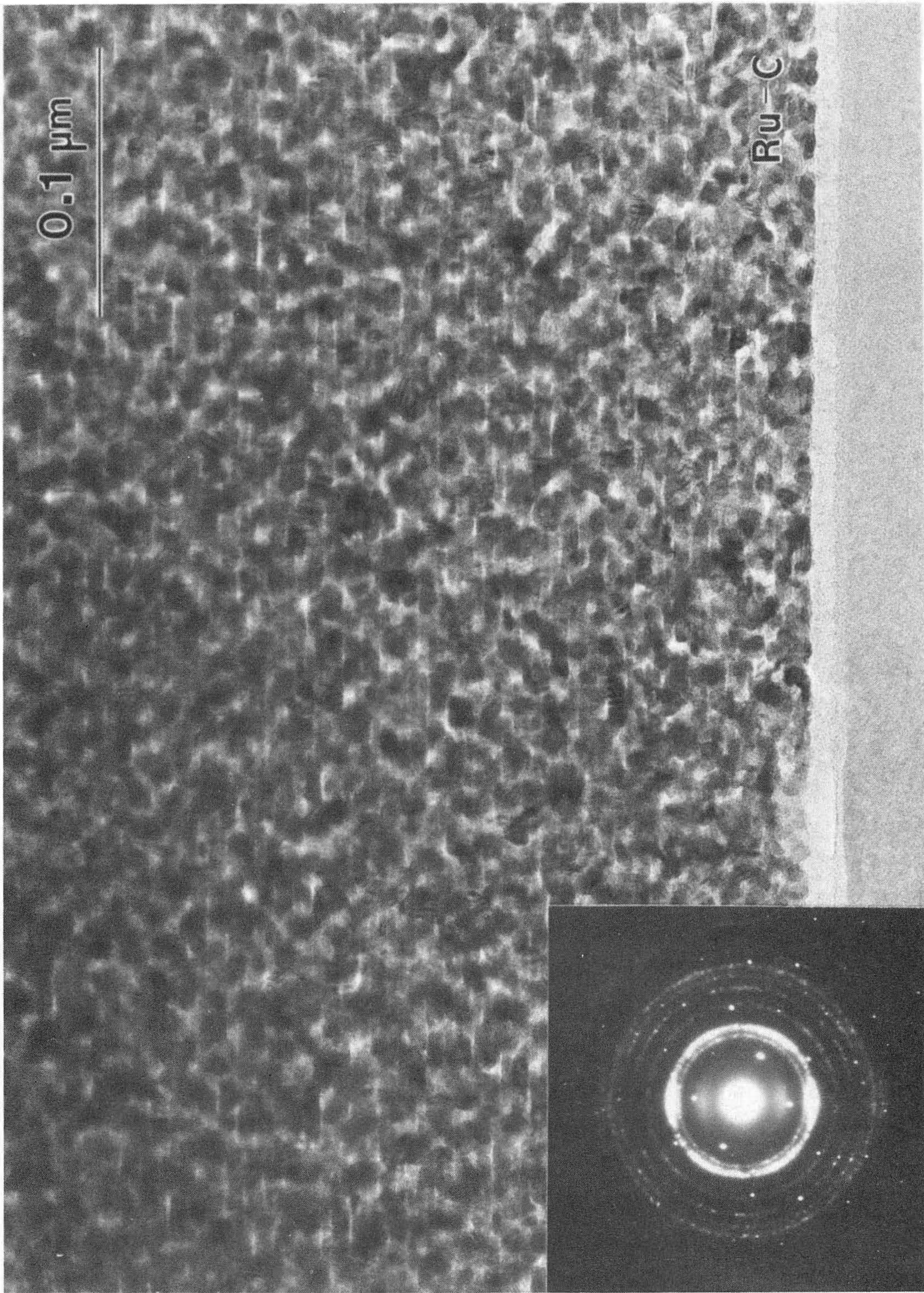

Figure 26

XBB904-2889

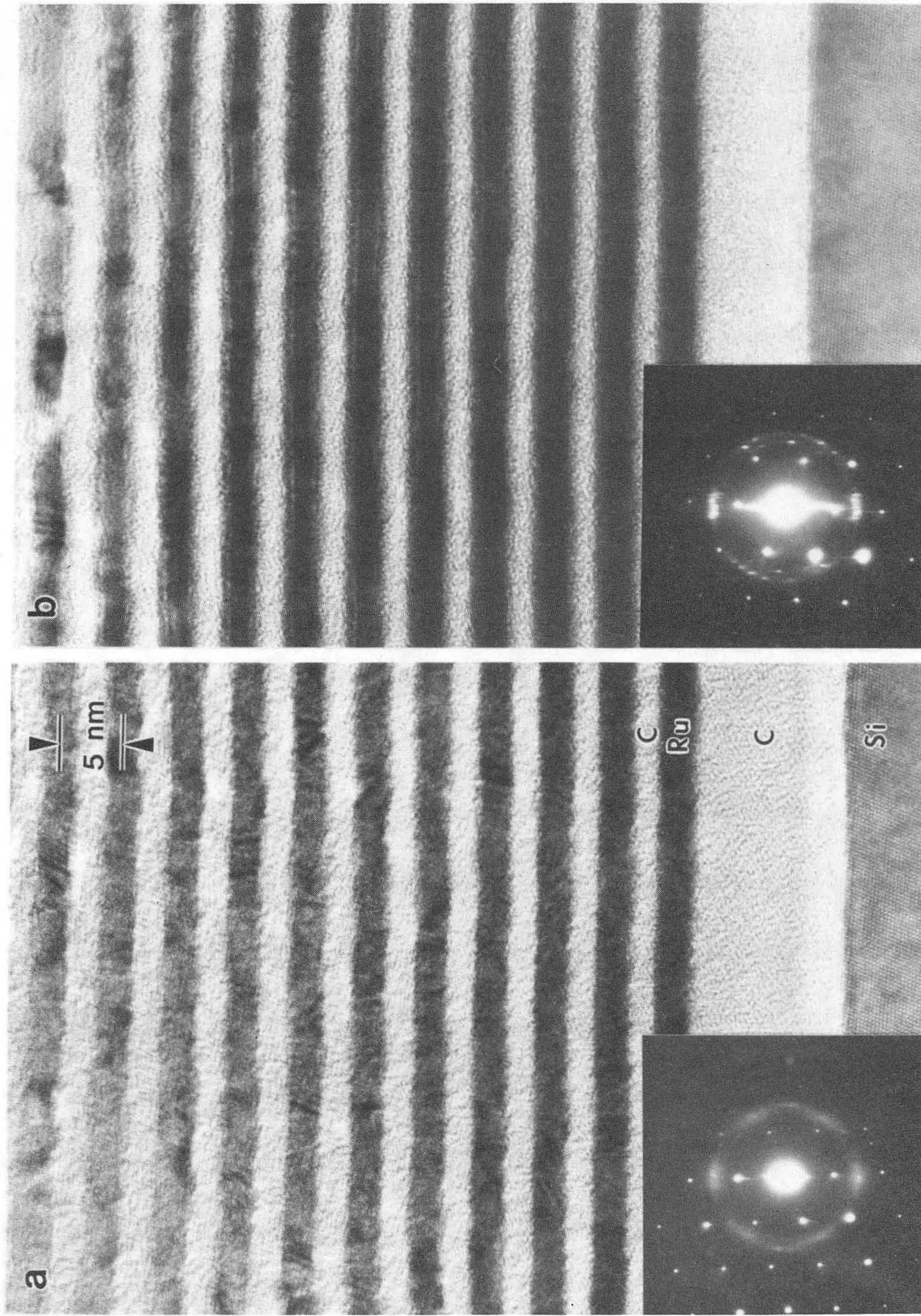

Figure 27

XBB904-2855

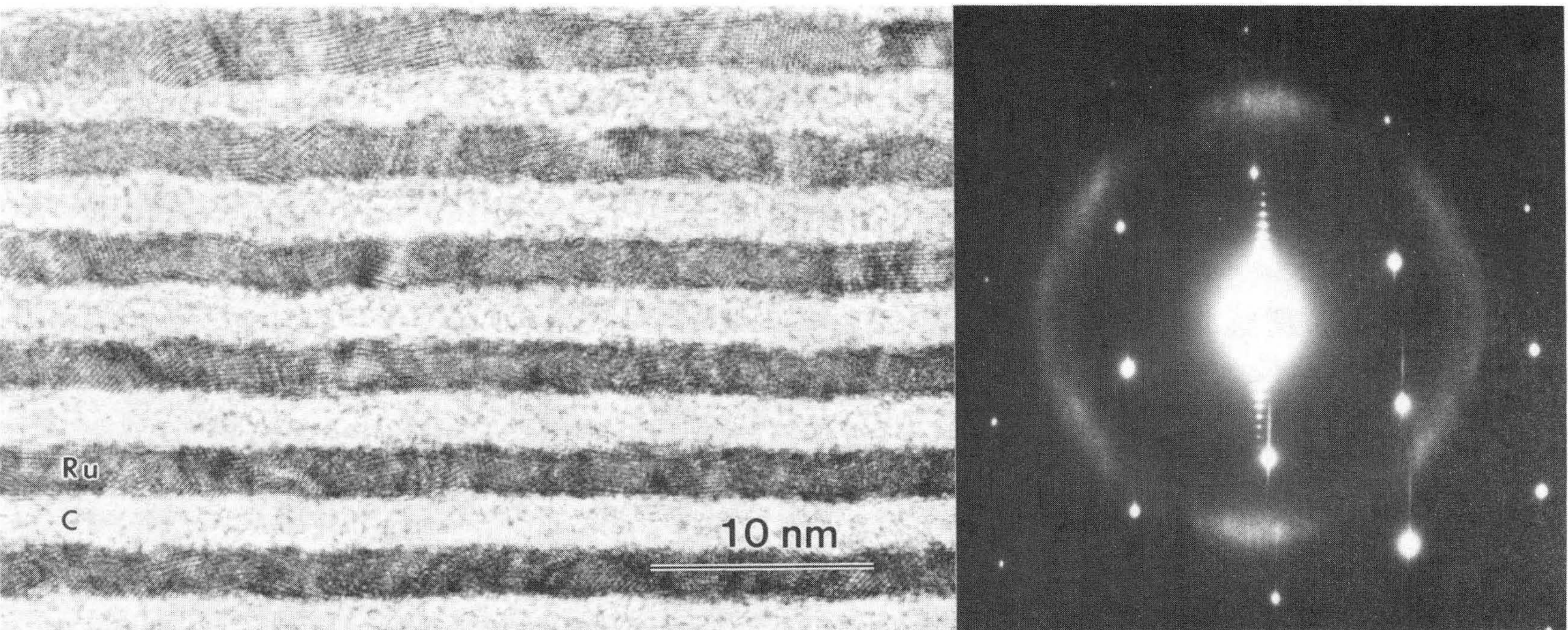

Figure 28

XBB902-1210

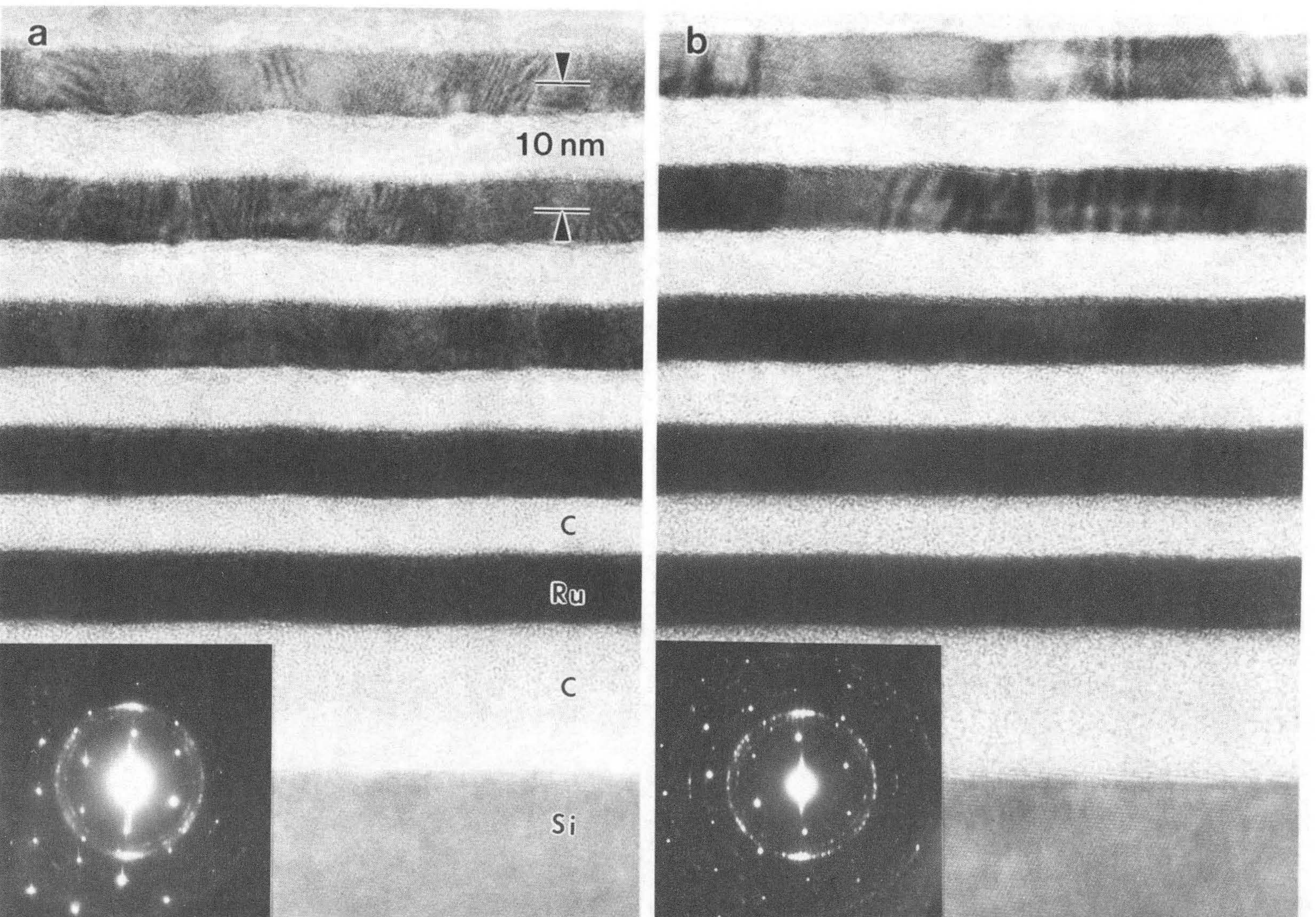

Figure 29

XBB904-2854

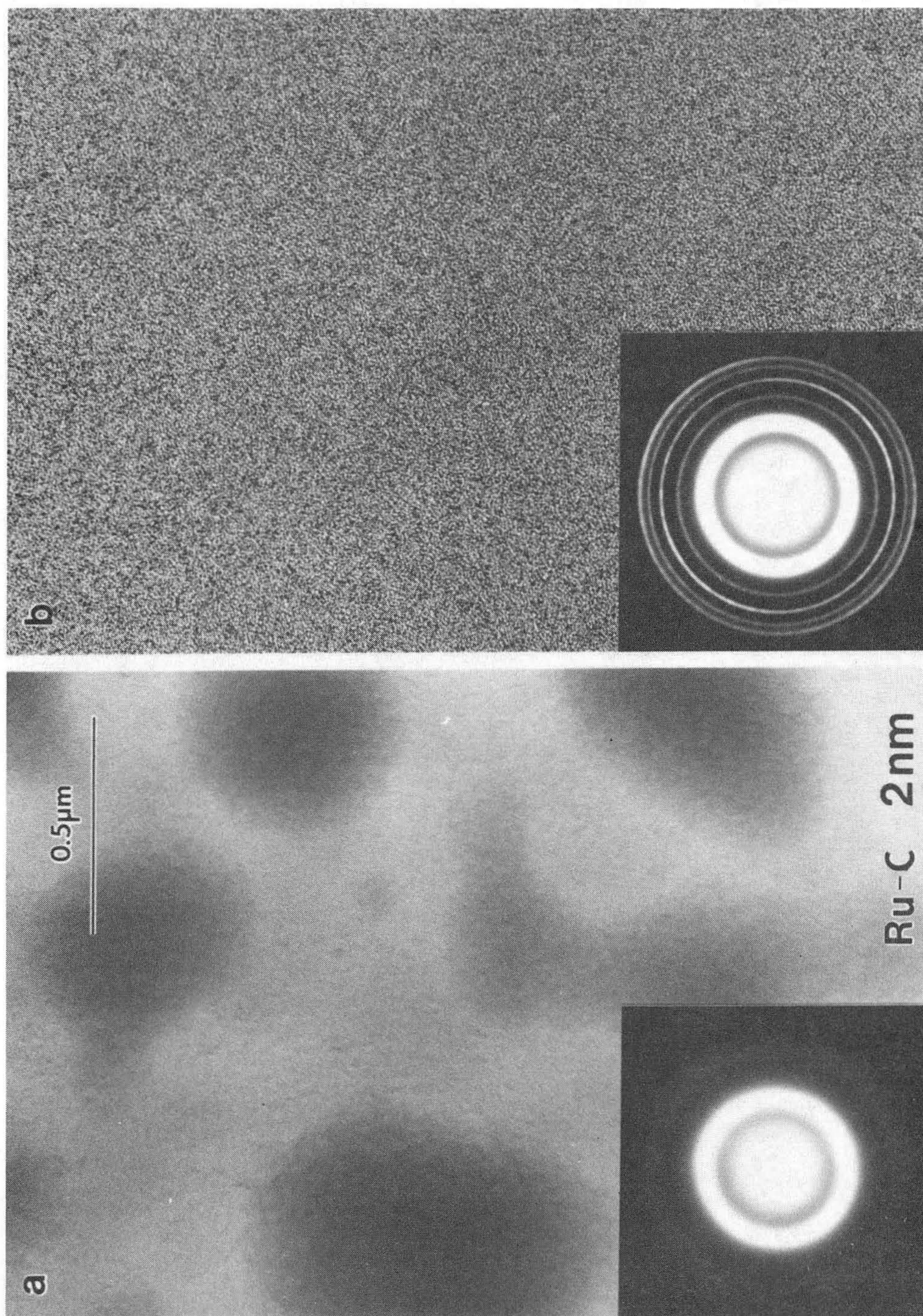

Figure 30

XBB904-3502

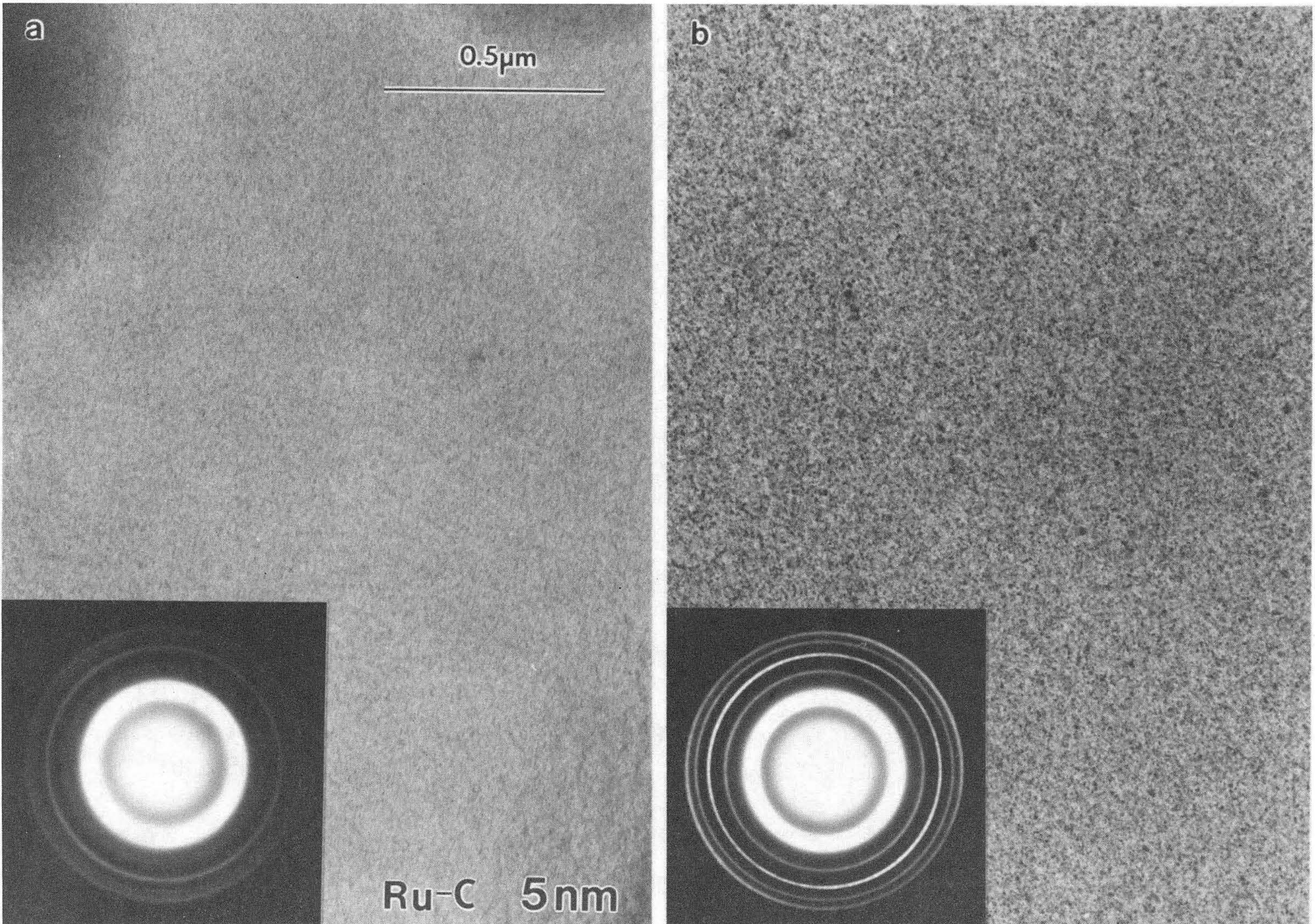

Figure 31

XBB904-3501

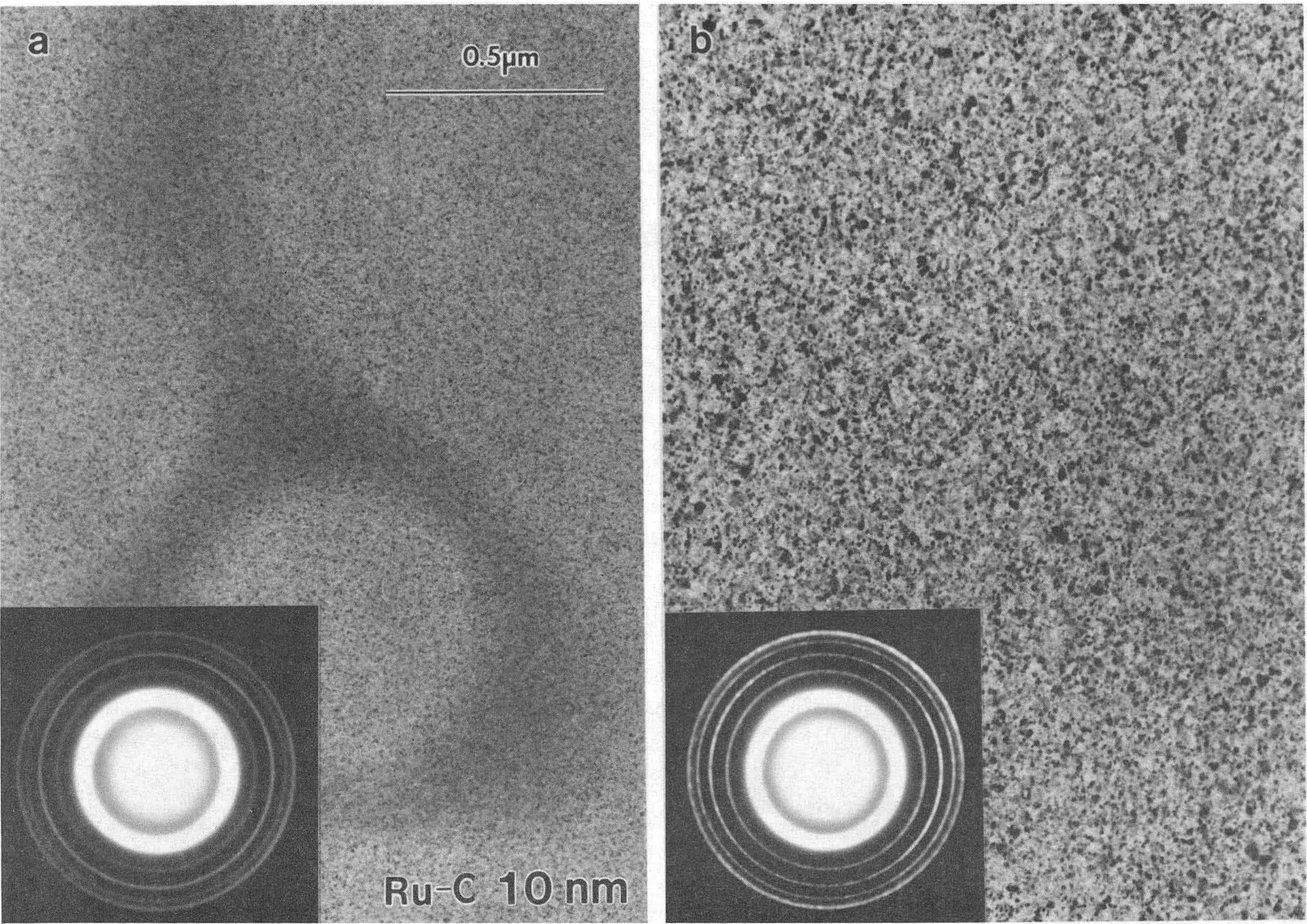

Figure 32

XBB904-2990

W - C phase diagram

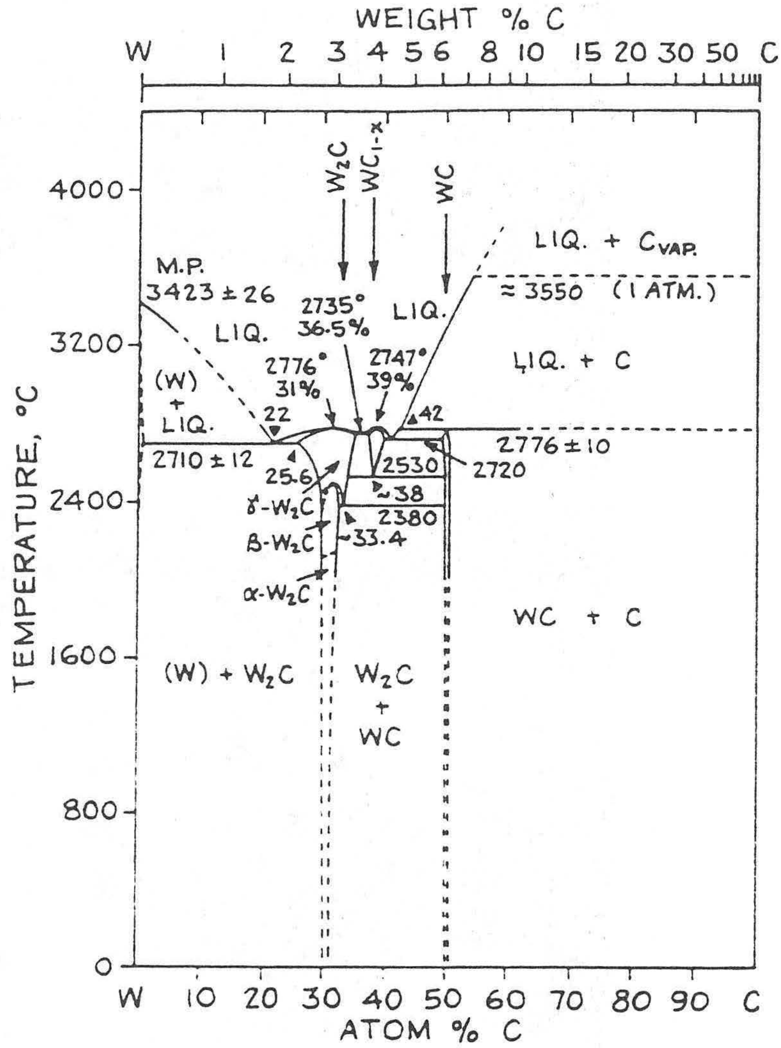

Figure 33

(from W.G. Moffatt, The Handbook of Binary Phase Diagrams, vol. 2, Genium Publishing Corporation, New York, 1987)

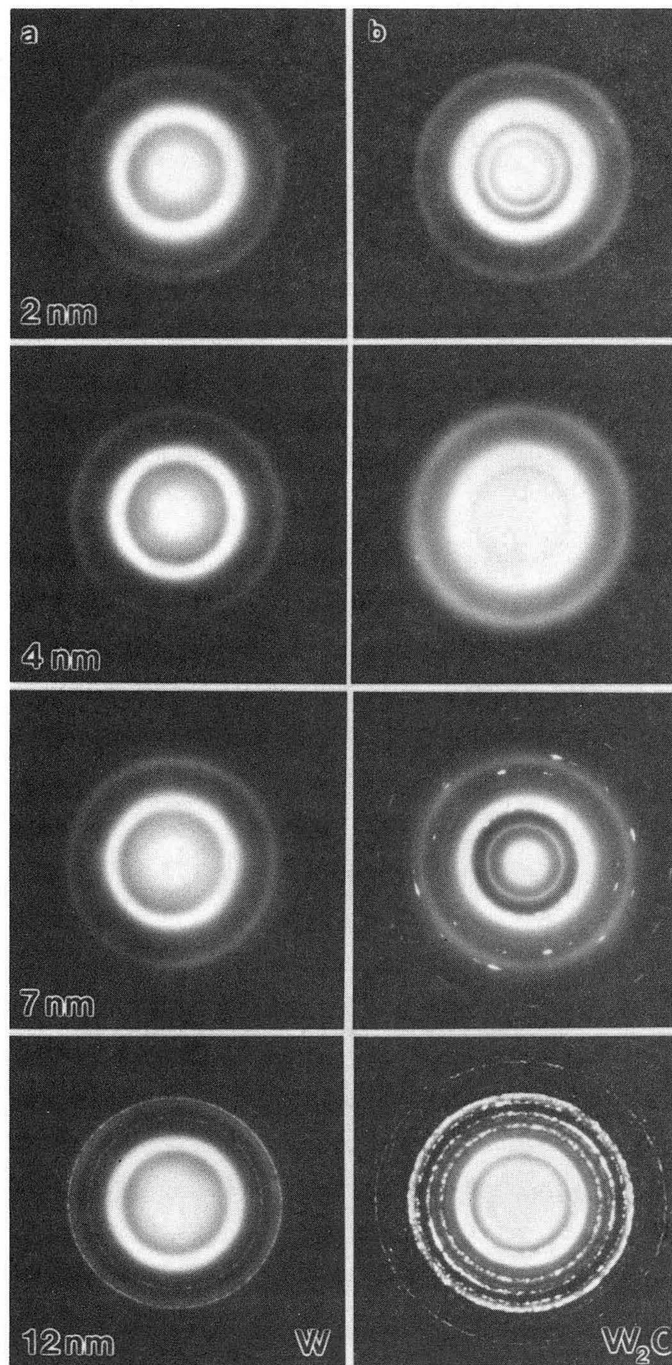

Figure 34 XBB905-3529

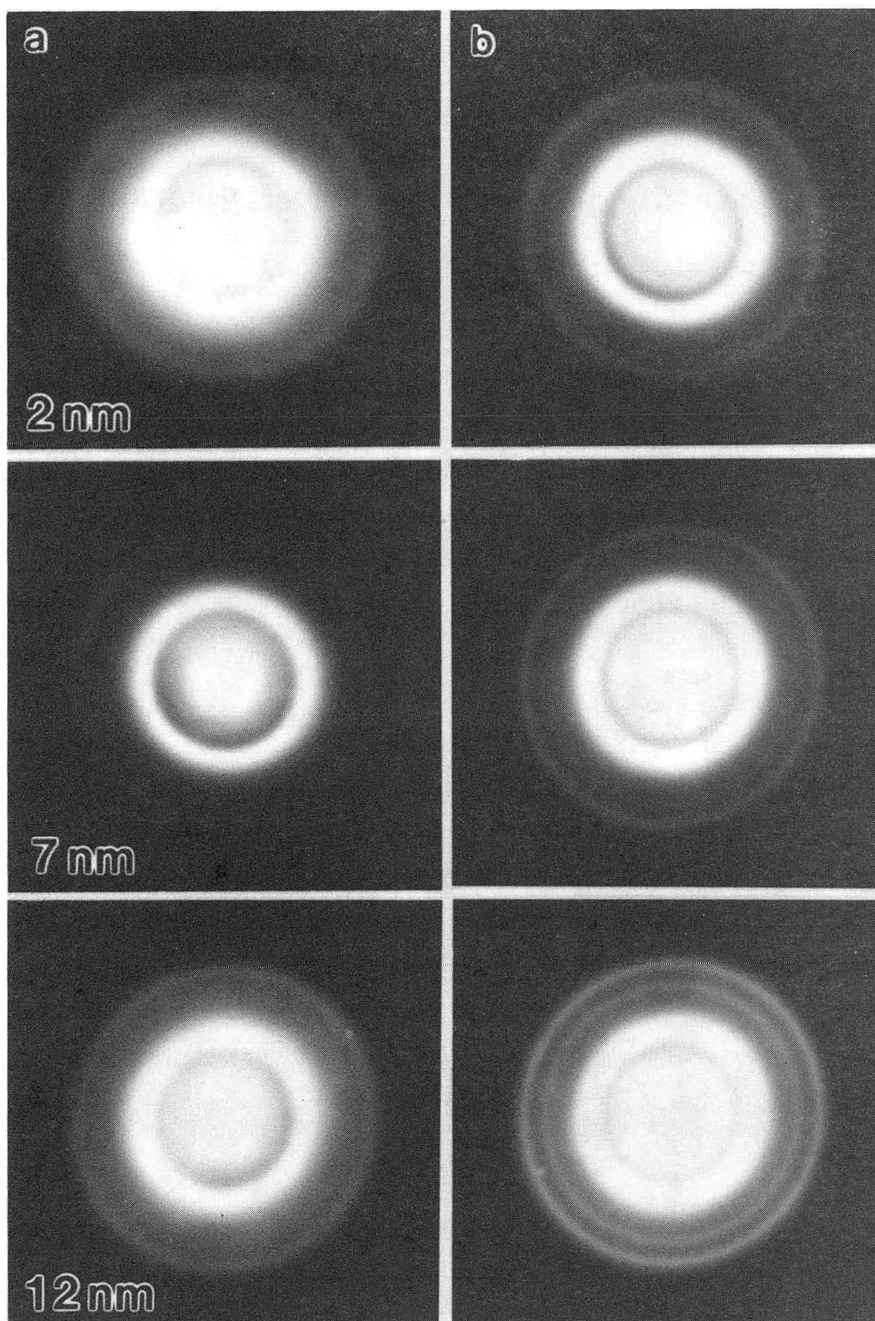

XBB905-3528

Figure 35

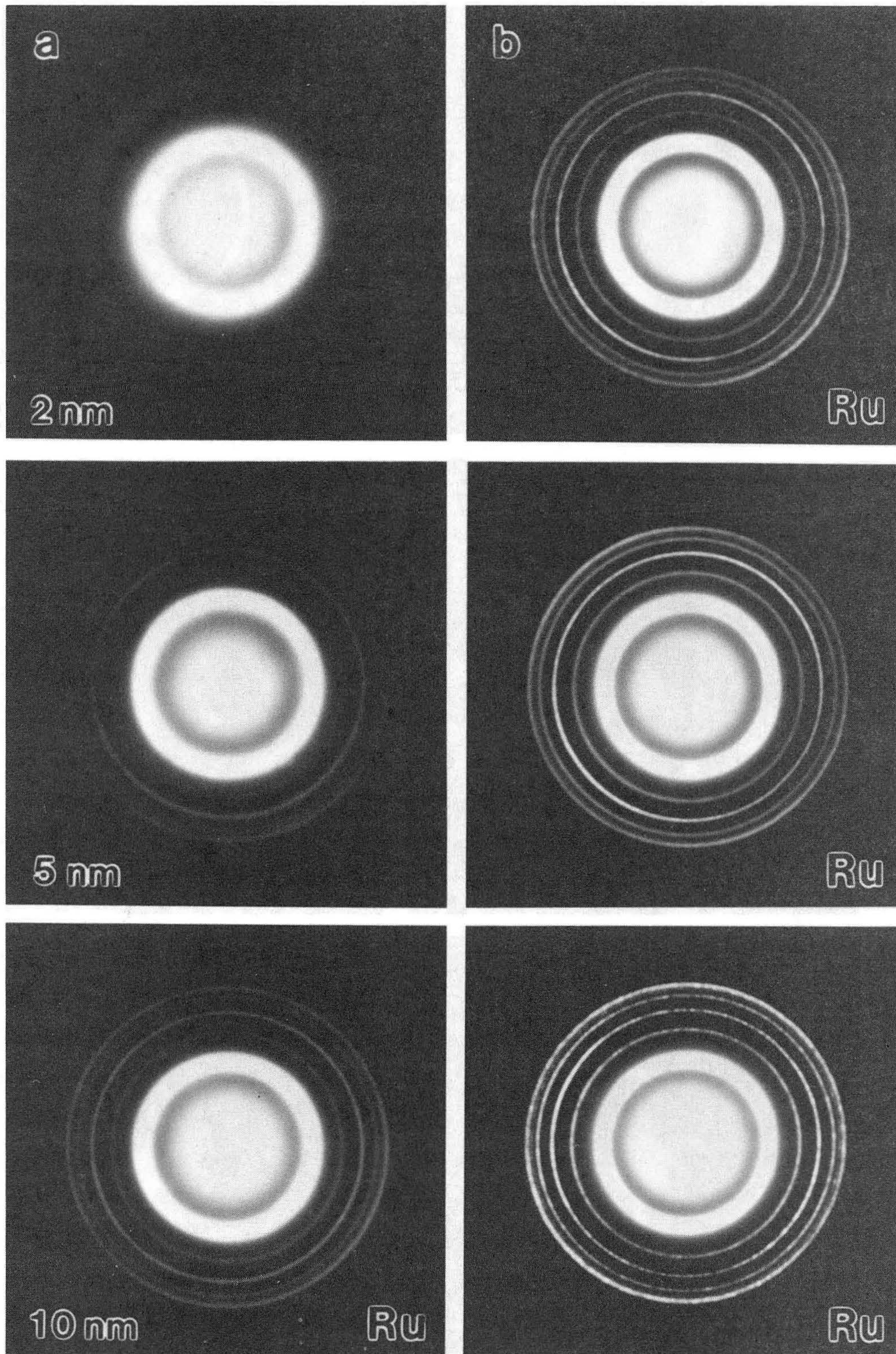

Figure 38

XBB904-2987

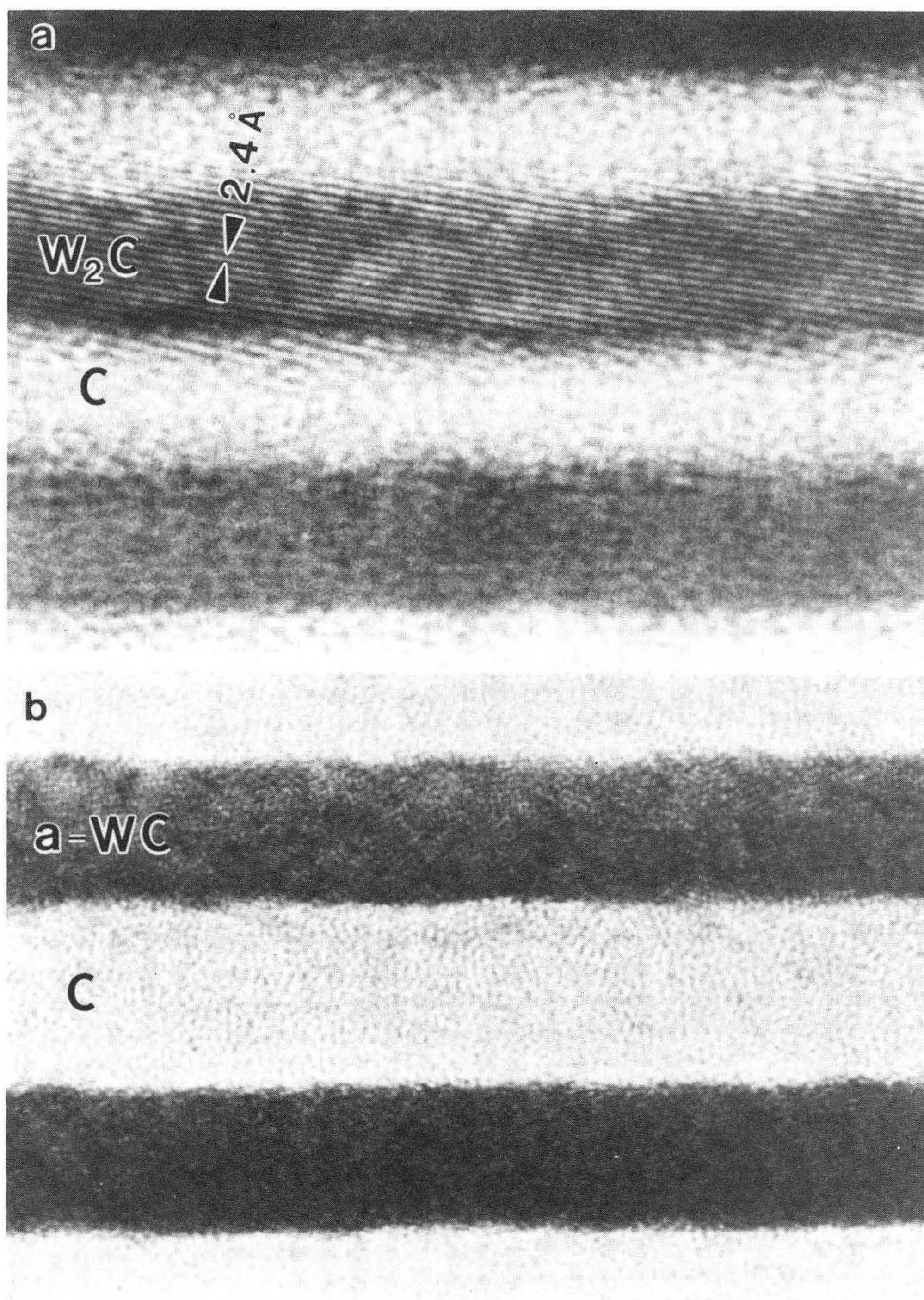

Figure 39

XBB904-3503

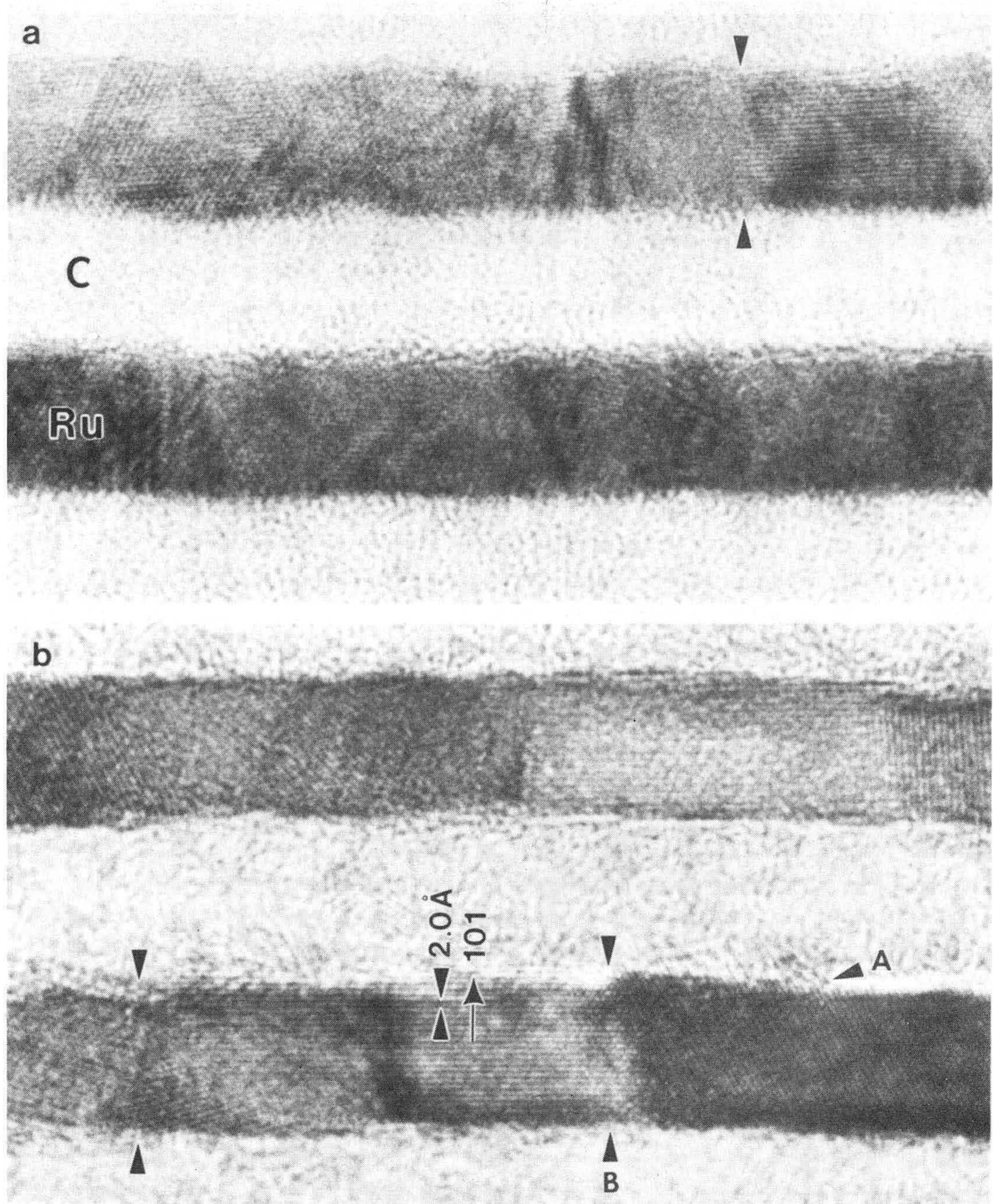

XBB904-3504

Figure 40

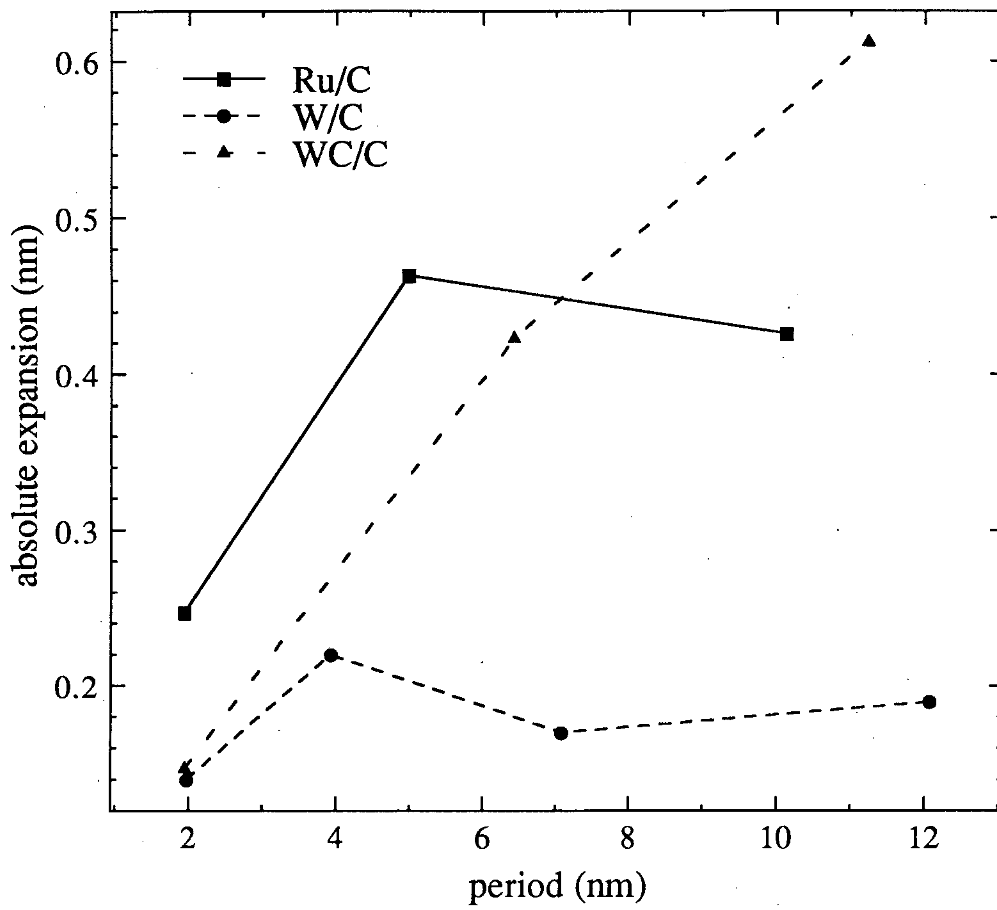

Figure 41

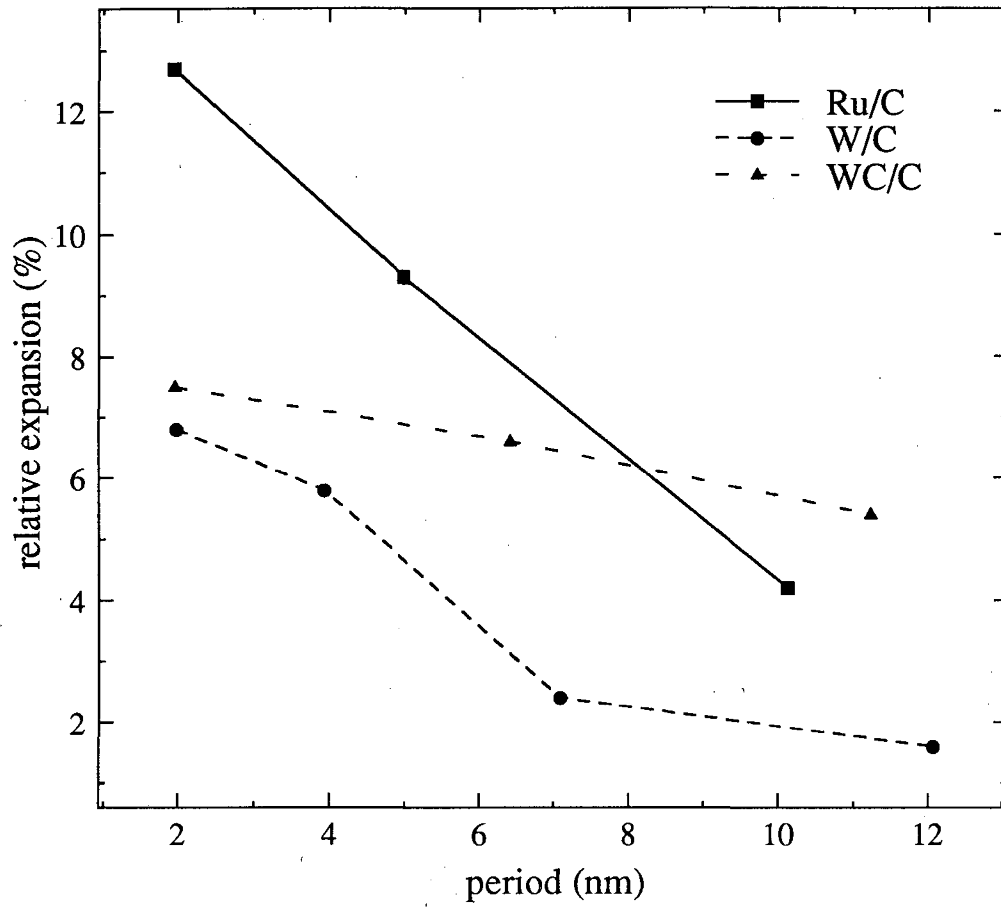

Figure 42

LAWRENCE BERKELEY LABORATORY
UNIVERSITY OF CALIFORNIA
INFORMATION RESOURCES DEPARTMENT
BERKELEY, CALIFORNIA 94720